Development of novel combined nano delivery system to improve cellular uptake of weakly basic anticancer drugs and cell imaging

Dissertation
zur
Erlangung des Doktorgrades
der Naturwissenschaften
(Dr.rer.nat.)

dem
Fachbereich Pharmazie
der Philipps-Universität Marburg
vorgelegt von

Muhammad Umair Amin
aus
Gujranwala, Pakistan

Marburg/Lahn **2020**

Erstgutachter: **Prof. Dr. Udo Bakowsky**
Zweitgutachter: **Prof. Dr. Frank Runkel**

Eingereicht am: **04-02-2020**

Tag der mündlichen Prüfung am: **17-03-2020**

Hochschulkennziffer: **1180**

Development of novel combined nano delivery system to improve cellular uptake of weakly basic anticancer drugs and cell imaging

Thesis

Submitted in the fulfilment of the requirements of degree of

Doctor of Natural Sciences (Dr.rer.nat.)

equivalent to

Doctor of Philosophy (Ph.D.)

To

The Faculty of Pharmacy,

University of Marburg by

Muhammad Umair Amin

from

Gujranwala, Pakistan

Marburg/Lahn **2020**

First Evaluator: **Prof. Dr. Udo Bakowsky**

Second Evaluator: **Prof. Dr. Frank Runkel**

Eingereicht am: **04-02-2020**

Tag der mündlichen Prüfung am: **17-03-2020**

Hochschulkennziffer: **1180**

EIDESSTATTLICHE ERKLÄRUNG

Ich versichere, dass ich meine Dissertation

“**Development of novel combined Nano delivery system to improve cellular uptake of weakly basic anticancer drugs and cell imaging”**

selbständig ohne unerlaubte Hilfe angefertigt und mich dabei keiner anderen als der von mir ausdrücklich bezeichneten Quellen bedient habe. Alle vollständig oder sinngemäß übernommenen sind Zitate als solche gekennzeichnet.

Die Dissertation wurde in der jetzigen oder einer ähnlichen Form noch bei keiner anderen Hochschule eingereicht und hat noch keinen sonstigen Prüfungszwecken gedient.

Marburg, den 04.02.2020

.....

(**Muhammad Umair Amin**)

STATUTORY D E C L A R A T I O N

I declare that this doctoral thesis

"**Development of novel combined Nano delivery system to improve cellular uptake of weakly basic anticancer drugs and cell imaging"**

has been written entirely by myself except unless stated otherwise by reference or acknowledgement. The research was carried out at the Department of Pharmaceutics and Biopharmaceutics, University of Marburg, at the campus Ketzerbach-63 (old location) and Robert-Koch-Straße-4 (new location) under the supervision of Professor Udo Bakowsky.

This thesis has not been submitted in any form elsewhere for a higher degree

Marburg, 04.02.2020

.....

(**Muhammad Umair Amin**)

Acknowledgement

I would like to express my gratitude to all those people who are very important to me and helped me a lot during my PhD timeframe. I just want to mention that without their help it was difficult to achieve what I have planned.

My deepest appreciations and thanks to my supervisor, Prof. Udo. Bakowsky for his utmost support and guidance throughout my PhD. I am really grateful to him for sharing his knowledge and suggestions during scientific discussions which helped me to cope up all the challenges related to my research. Sometimes the process was painful, but outcome was always beneficent.

I like to acknowledge my group leader Dr. Jana Brüßler, who was my immediate access point for discussions. She was always available whenever I need her assistance. I am thankful to Dr. Shashank Pinnapireddy for his help in cell culture experiment and Dr. Jens Schäfer for his technical assistance. I am also thankful for the support provided by Mrs. Eva Mohr, Julia Michaelis, Mrs. Doris Reissenweber. I would like to extend my thanks to Prof. Dr. Bernhard Brüne, Dr. Dominik Fuhrman, Dr. Christian Wölk and Michael Hellwig for their support at different stages of my doctoral work.

I am thankful to my friends Sajid Ali, Muhammad Yasir Ali, Imran Tariq for their willingness and sincerity to help me out in all the difficult times. I want to extend my thanks to all my past and current research group colleagues specially Benjamin Sebastian Seitz, who helped me directly or indirectly throughout my stay in this institute. I am grateful to my officemates for sharing such a nice time together.

Most importantly, I am highly indented to my parents and family members, my wife and foremost my daughter Haniya, who are always with me through thick and thin. They encouraged and motivated me to move forward and it is worthy to mention that without their support everything is not possible for me to be here.

Die vorliegende Arbeit entstand auf Anregung und unter Leitung

von

Herrn Prof. Dr. Udo Bakowsky

am Institut für Pharmazeutische Technologie und Biopharmazie,
der Philipps-Universität Marburg, Deutschland

Table of Contents

List of Figures

List of Tables

1 Introduction

Cancer being a second major cause of death all over the world, is most devastating disease and remains deadliest and of serious concern. According to World Health Organization (WHO) 9.6 million deaths in 2018 were due to cancer[1] and by 2020 it is a prediction that there would be 15 million new cases across the globe. According to an estimation, behind one death out of six, cancer is the major reason.[2] The limiting factor to control the cancer death is non-selective delivery of chemptherapeutics to tumor tissues, resulting in unwanted systemic exposure of anticancer drugs, causing side effects to healthy tissues and resistance of cancer cells. Therefore, the delivery of anticancer drug to target site is required to avoid undesired effects. Development of a drug delivery system is considered as a suitable tool, which can overcome these limitations and provide more satisfactory results by delivering the drugs to the target site.[3] Such drug delivery systems (DDS) have been designed to modify the pharmacokinetic and physiological properties of drug molecules.[4] For an ideal drug delivery system, it is necessary that it exhibits high drug loading capacity, biocompatibility, prolonged circulation time, protection from hydrolysis and enzymatic degradation, avoiding premature leakage, delivering higher doses at target site, controlled drug release, biodegradability and chemical stability.[5]

1.1 Nanotechnology

Nanotechnology means development of nanomaterials for the better delivery of drugs. In last few decades, recent developments in nanomaterials has opened up new areas in the treatment of cancer. Nanotechnology has addressed many of the limitations of conventional drug delivery system by increasing the target specificity, avoiding side effects and enhanced efficacy of the therapy.[6,7] Nanocarriers due to size in nanometre range have higher surface area and show very satisfactory physicochemical properties. Nanomaterials have tendency to enhance the bioavailability with prolonged circulation time and release the drug in a controlled manner.[3]

As drug carrier nanomaterials have tendency to cross biological barriers, and easily enter tumors due to localized leaky vasculature. Poor lymphatic drainage of tumor enhances the retention time of nanomaterials. Nanostructures can be prepared either by physical methods such as evaporation, laser ablation and arc discharge or by chemical methods. The latter is considered more effective as it can produce nanostructures in more controlled manner and enables different shapes, sizes and functionalization to be attained by chemical reactions.[8]

A variety of nanocarriers is available which include organic and inorganic nanomaterials. Organic nanostructures involve polymeric nanoparticles, lipid micelles, protein nanoconstructs, carbon dots, carbon nanotubes, graphene and nonodiamonds. On the other hand, inorganic nanomaterials include silica nanoparticles, quantum dots, super magnetic iron oxide nanomaterials, gold and silver nanoclusters. All these nanostructures have unique properties and certain modifications can even change the application and significance. Changes in shape and size can produce different results because interaction between nanomaterials and proteins is greatly dependent upon size and surface.[9,10]

1.1.1 Inorganic Nanomaterials

By last few years, inorganic materials have emerged as a new class in development of drug delivery systems and have become very important in the field of nanotechnology. Nanocrystals and nanowires are inorganic materials, which mainly involve metals and metal oxides. Inorganic nanotubes of different metals have also shown important applications in various research areas. Recent developments in the field of inorganic hybrid nanoparticles has opened up new dimensions as drug delivery systems in nanomedicine.[8,11] A lot of efforts have been made to produce new biocompatible and biodegradable inorganic nanostructures due to their versatility and functionalization in advanced drug delivery systems. Due to higher adsorption capability, biocompatibility and low density, amorphous silica and fumed silica are potential moieties in biomedical applications. The safety approval of silica in human clinical trial by the Food and

Drug Administration (FDA) made them most potential and promising candidate among inorganic nanomaterials.[12,13]

Silica is one of the most abundantly available material in nature from higher plants to single celled organisms. As compared to other inorganic oxides, silica is considered as safe and can be easily taken up by cells through endocytosis. Silica nanoparticles are considered very stable because they have tendency to withstand higher mechanical stress and degradation as compared to other drug delivery carriers, which require further stabilization by covalent linkers.[14,15]

1.1.1.1 Mesoporous Silica Nanoparticles

In recent past, the development of biocompatible and inorganic nano-systems has opened up new dimensions. Porous inorganic systems like silica have shown much better therapeutic effects as compared to other nanocarriers for the chemotherapeutics and gene delivery.[16] Mesoporous silica nanoparticles (MSNPs) are the advanced form of silica material and were first reported by Mobil oil scientists in 1990s.[17] Later on due the developments in nanotechnology and challenges in drug delivery systems it got utmost important as drug carrier especially in chemotherapy. MSNPs are organic templated inorganic materials where different surfactants can be used as organic templates. Figure 1 elaborates the schematic explanation for the fabrication of mesoporous silica nanoparticles. Surfactants have tendency to form round micelles by self-aggregation at critical micelle concentration (CMC) and when they are heated at higher concentration above CMC, hexagonal micelles are formed. Then silica precursors can condense at micellar surface in the presence of catalyst, to form organic-inorganic hybrid structures. To generate pores, surfactant template is removed by either calcination or extraction.[18,19]

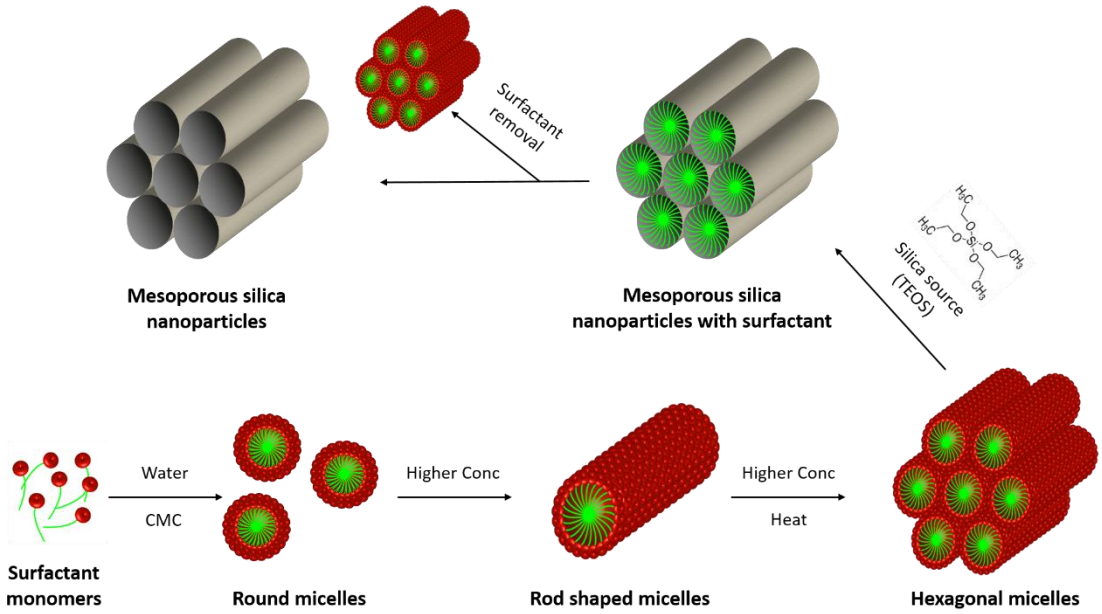

***Figure 1**: Schematic diagram elaborating the fabrication of mesoporous silica nanoparticles (MSNPs)*

As the name indicates the MSNPs consists of hexagonal pores like honeycomb structure and the name mesoporous is given because these pores are in meso-range (2 nm-50 nm). In nanomedicine, the nanoscale constructs for the encapsulation of higher concentrations of drugs, crossing of cell membrane and delivery of large doses of chemotherapeutics to tumor tissues with minimum side effects to healthy tissues, always remains challenging.[20] MSNPs have addressed many of the limitations of other nanocarriers.[16,21] As a drug delivery system, they are very attractive and suitable due to their uniqueness of porous structure, high surface area >1000 m^2/g, tuneable pore size and pore volume, high pore volume i.e. 1 cm^3/g^{-1}. These features of MSNPs assure high loading capacity for therapeutic agents and controlled release of drug.[22]

MSNPs have dual functional surfaces, including internal porous surface and external particle surface.[23,24] These surfaces can easily be functionalized to achieve better controlled release and conjugation of targeting ligand for target specificity.[25] Both hydrophilic and hydrophobic nature of MSNPs make them suitable candidate for the entrapment of wide range of drugs. Polymeric nanomaterials have a limitation of drug leakage due to high biodegradability but

MSNPs due to mechanical strength and non-toxic behaviour have become promising drug delivery system.[21,26]

The drugs can be easily loaded to MSNPs by capillary filling or adsorption, and the drug release profile can be tuned depending upon the pore structure. MSNPs are stable in both aqueous and organic solvents, contrarily to the polymeric nanomaterials which interact with organic solvents and become unstable.[27]

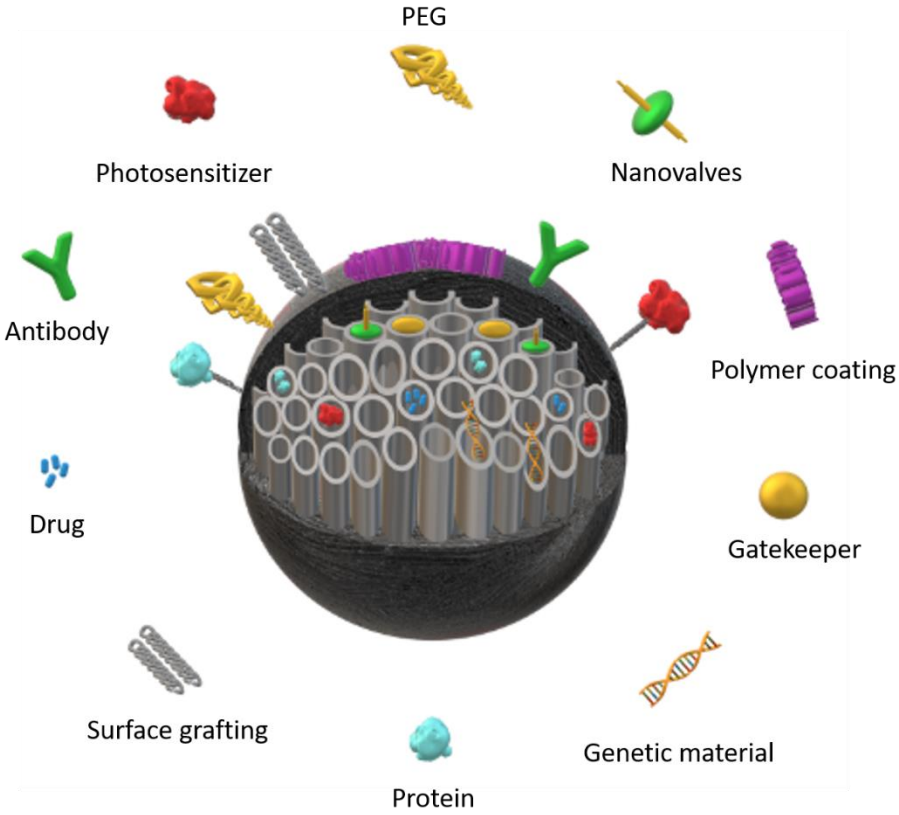

Figure 2: *Illustration of MSNPs with different modifications and loading sites*

1.1.2 Organic Nanomaterials

Organic nanomaterials have been extensively investigated for years because a wide range of organic substances are available which have very significant applications in nanomedicine. Basically, these are nanoconstructs, composing of organic substances like polymers, proteins or lipids.[28]

A variety of polymeric nanoparticles has been studied as drug delivery system because of their biocompatibility, surface modification and targeted delivery. Polymeric NPs can be of either natural or synthetic origin. Albumin, hyaluronic acid and chitosan are widely used natural polymers for nanomedicine. Among the synthetic polymers, poly acrylic acid (PAA), dendrimers, poly (lactide-co-glycolide) (PLGA), polyglycolic acid (PGA), poly lactic acid (PLA) and hyperbranched polymers remain applicable.[29-31] Mainly the synthesis methods for polymeric NPs are solvent evaporation, salting out, emulsion diffusion and nanoprecipitation. Apart from many advantages of polymeric NPs, they have some limitations as well. Polymeric degradation acidity, solvent toxicity, reproducibility and biphasic drug release are the major challenges while dealing with polymeric NPs.[32,33]

Lipid micelles are also useful carrier for the entrapment of different drugs. They are actually monolayer structures having inner hydrophobic and outer hydrophilic surface. However, they also have few limitations of lower entrapment of drugs due to small hydrophobic core and dissociation on dilution. On the other hand, liposomes are lipid bilayer structures and comparatively entrap larger amount of drugs with no direct dissociation on dilution.[6]

1.1.2.1 Liposomes

Liposomes are the most promising nanomaterials as a drug delivery carrier. Usually they are composed of phospholipids with two tail and one head region, where head group represents the hydrophilic part and tail group is fatty acid part, which is hydrophobic in nature. Liposomes formulation is based on lipid-lipid interaction and by structure, they can bifurcate hydrophilic and hydrophobic molecules. Due to highly dynamic nature, liposomes have characteristic to convert to smaller compact structure when the layer is disturbed.[34,35]

For the treatment of several diseases, liposomes remain under consideration because they can improve the therapeutic efficacy by minimizing side effects, rapid degradation and enhancing drug absorption. Liposomes show flexibility in changing the chemical composition, structure and size by method modification

and structures ranging from nanometers to micrometer scale.[36] Bilayer composition can make the liposomes either permeable and low in stability or rigid and impermeable. By surface modification, liposomes are tailored for therapeutic and diagnostic purposes along with image guided drug delivery. Liposomes, being similar to structure of cell membrane, are unique due to their low immunogenicity, degradability and good biocompatibility.[37] A representative image of liposome with hydrophilic and hydrophobic drug loading sites, is shown in figure 3. Liposomes are used as a drug carrier to enhance the cellular uptake of not only chemotherapeutics but also for the gene delivery. These outstanding features of liposomes in comparison to other nanocarriers resolve many of the issues related to drug delivery and diagnosis.[38,39]

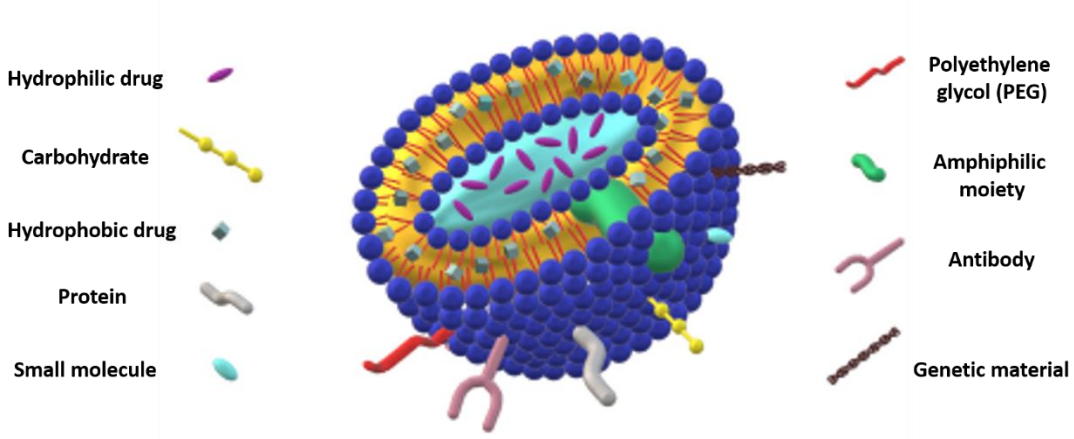

***Figure 3**: Illustration of multifunctional liposome with hydrophilic and hydrophobic moieties*

Despite of these salient features, liposomes also have certain drawbacks. One of the major limitation is opsonization of conventional liposomes by plasma protein and quick removal from circulation, but this issue can be resolved by surface modification with polyethylene glycol (PEG).[40,41] Other problems of liposomes such as leakage and stability in circulation, have already been reported, but the incorporation of cholesterol to increase the cohesiveness can minimize the leakage problem. Cholesterol increases the rigidity of lipid membrane, avoids the permeation of water soluble drugs and improves the stability.[42]

Liposomes can be classified by different factors depending upon structure, size and ionic nature. One classification is based on number of lipid layers such as multilamellar vesicles (MLVs), and unilamellar vesicles (ULVs) with further division in to large unilamellar vesicles (LUVs) and small unilamellar vesicles (SUVs). Another classification is based on the liposomal net surface charge such as neutral, anionic and cationic depending upon the composition and charges of lipids.[3]

1,2-dioleoyl-3-trimethylammonium-propane (DOTAP) is an example of cationic lipid and 1,2-dioleoyl-sn-glycero-3-phospho-L-serine (DOPS) is an anionic lipid while 1,2-dipalmetoyl-sn-glycero-3-phosphocholine (DPPC) is used as a neutral zwitterion phospholipid. The importance of cationic liposomes increased due to application in gene and protein delivery.[43,44]

Liposomes interact with cells in different ways, mainly endocytosis, with phagocytic action of reticuloendothelial system. Other mechanisms are adsorption through electrostatic interaction between lipid bilayer and cell membrane, fusion by insertion of lipid layer with cell membrane an releasing the contents in cytoplasm and lipid exchange by transferring liposomal contents to cell membrane.[45]

Few of the liposomal products are already in market. Doxil® being the first one containing doxorubicin (Dox) for the treatment of ovarian cancer and subsequently, DaunoXome®, Depocyt®, Myocet® and Mepcat® have been approved for the treatment of cancer.[34]

1.1.3 Lipid Coated MSNPs

Various studies have shown that combining two different naocarriers to form a new drug delivery system has produced promising results.[27] As mentioned above, premature leakage of the drug is very critical in case of chemotherapeutic drug delivery. To avoid premature leakage of the drug from the porous structure of MSNPs, different approaches have been adopted to provide gatekeeping effects. These include nanoparticles, polymers, organic

molecules and supramolecular assemblies, which can regulate the release of drug in a controlled manner at the target site. Some of the others, reported delivery systems, with either gatekeeping features or external stimuli response, have shown their effectiveness in non-aqueous solvents and limited application in physiological conditions.[46]

Despite of liposomal salient features, safety of highly toxic drug during circulation remains a major concern. Approach of coating liposomes on MSNPs enhance the stability of liposomes. Figure 4 is representing drug loading and lipid coating of MSNPs. On one hand we can load higher amounts of drugs in pores of MSNPs due to larger surface area and on other hand lipid layer can also be used to load another drug.[47] Both liposomes and MSNPs have very distinguishing features and by combining them very fruitful results can be obtained.[48] Lipid coated MSNPs can enhance the biocompatibility and improve cellular uptake by tumor cells.[42]

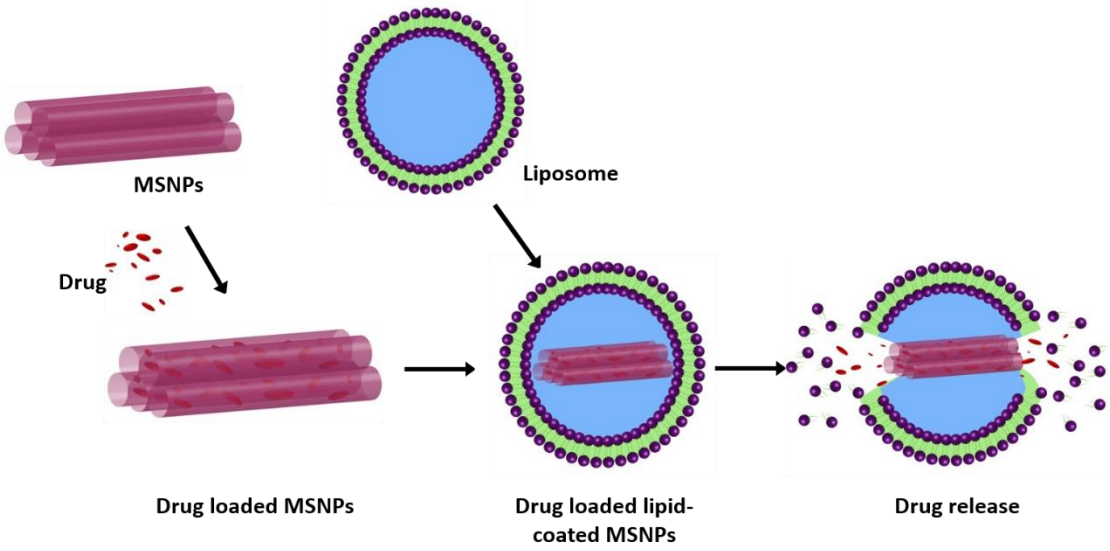

***Figure 4**: Representation of drug loading and lipid coating to mesoporous silica nanoparticles*

Lipid coated MSNPs have proved to be an ideal therapeutic delivery system, which synergistically improve drug loading, stability and controlled release of higher concentrations of multidrug at target site to enhance the therapeutic effectiveness. This synergetic effect of lipid coated MSNPs has already been reported as compared to non-lipid coated MSNPs.[48,49]

1.1.4 Stimuli Responsive DDS

Microenvironment of solid tumors, a well known barrier that hinders the drug delivery approaches, is very precisely investigated. To deal with these particular challenges different types of stimuli were considered as a solution to trigger the release of the drug to target site at specific time to enhance the therapeutic outcomes. In this regards, developments of smart nanoarchitectures with stimuli response are the hotspots by last few years in the field of nanotechnology.[44]

Stimuli responsive drug delivery systems not only deliver the anticancer drugs to the target site by minimizing the side effects due to lesser exposure to normal tissues but also release the drugs in desired cytotoxic concentrations.[50,51] In most of the cases tumor resistance to anticancer drug is relevant to subcytotoxic concentration exposure of drug to tumor.[20,52] However, other biological intratumoral factors are also involved.[53,54]

Various kinds of stimuli have been employed in drug delivery and can be categorized in to two main types including endo-triggered and exo-triggered. Among the endo-triggered, pH is most commonly used stimulus where the delivery of the drug is based on change in pH such as cancer and inflammation.[10] Another endo-triggering factor is hypoxia although it is most challenging factor for the delivery of drug to tumor but it can be used as an attractive therapeutic target. Few of the drug delivery systems have already been reported which showed better drug delivery in hypoxia as compared to normoxia. Enzymatic action, temperature and oxidation-reduction reactions are other examples of endo-triggering stimuli. Sometimes due to rapid changes in biological activities of tumor these endo-triggering factors can be effected.[55-57] Therefore, exo-triggering factors offer advantages due to easy handling, time and location specificity.

Main exo-stimuli are light, magnetic effect, ultrasound and external temperature.[44,58] Many light sensitive drug delivery systems release the drug after excitation by ultraviolet and visible light but it has limitation due to

inadequate tissue penetration.[59] Magnetic nanoparticles (MNPs) are of other type, which can release the drug on exposure to magnetic field[60] but certain limitations such as low drug loading capacity and target specificity need to be addressed. Thermosensitive drug delivery system is also an exo-triggering drug delivery system where drug is released from the carrier on exposure to higher external temperature in the form of laser, magnetic field or water baths.[61] Stimuli responsive drug release in a controllable manner have addressed this issue in recent developments but conversion of stimuli response from bench to bedside is very challenging due to many problems.[52,62]

Ultrasound (US) remain always very important for its applications in diagnostics but recently it has been extensively used as a triggering factor in therapeutics for drug and gene delivery. US is advantageous because of its cost effectiveness, portability, non-invasiveness and visualization of targeted area with accuracy.[63]

1.1.4.1 Ultrasound Triggered DDS

US triggered drug release has gained much more importance because it delivers the drug to the target site, such as tumor, and minimize the systemic toxicity. US responsive drug delivery is a promising method for the efficient treatment of certain cancers like liver tumors, which are accessible with US. In general US and specifically sonopration being a distinguishing feature of US, can be used in drug delivery systems. Sonoporation is a process by which microbubble mediated ultrasound cavitation can produce permanent or temporary pores in blood vessels wall and results in significant improvement in the extravascular therapeutic drug delivery. Microbubbles as hollow particles with gas can act as US contrasting agents due to their acoustic characteristics.[63,64]

1.1.5 MSNPs Based Stimuli Responsive DDS

MSNPs with a very distinguishing framework, provide a very suitable platform for the development of stimuli responsive drug delivery system. Ease of drug

encapsulation in pores, sealing or capping of pore openings is a very useful approach for delivering toxic and therapeutic dose with precise control.[65]

Stimuli response can be achieved either by chemical reactions or by physical or chemical changes in response to stimuli. Various techniques have been adopted for the preparation of MSNPs based stimuli responsive drug delivery systems. Mechanically drug release can be controlled with polymeric coating, which can close or open in specific physiological conditions of microenvironments.[66] This approach is based on the control of hydrophobicity and hydrophilicity of the polymer, in hydrophobic condition preferably polymer adhere to MSNPs surface and in hydrophilic condition, polymer swells due to interaction with surrounding fluid resulting in pore opening and release of drug.

Blocking the pore opening with nanomaterials is another approach where removal of these capping nanostructures is linked with stimuli such as lower pH of tumor, which can dissociate capping material to release the drug in controlled manner. Some of the reported delivery systems, with either gatekeeping features or external stimuli response, have shown their effectiveness in non-aqueous solvents, resulting in limited application in physiological conditions.[46] This problem can be copped up with lipid coated MSNPs where liposomes along with the gatekeeping effects have better cellular uptake activity due to the proto cellular nature.[67]

Similarly, acid-labile bonds can be used at pore opening, which hydrolyses on mildly acidic pH of endosomes.[68,69] In other stimuli responsive MSNPs systems, UV light or near infrared (NIR) light can be employed as a stimulus for the cleavage of linkers or generation of reactive oxygen species (ROS) for site specific actions.[70,71] Heat sensitive, thermosensitive, magnetic responsive, enzyme stimuli responsive, redox sensitive and US triggered drug delivery system based on MSNPs have already been reported for tumor targeting. Due to excellent textural properties stimuli responsive drug delivery has entered in an advanced step where use of multiple stimuli can better perform in tumor cell environmental conditions to be more specific and high precision for higher therapeutic effects with minimum systemic side effects.[10,72]

Capillary filling of MSNPs porous structure with liquid and then converting it to bubbles would be a good idea to entrap lower boiling point substances. Perfluoropentane, as an established ultrasound contrasting agent with boiling point 28ºC, is an ideal candidate to be loaded inside the pores. Perfluoropentane is used to stabilize nanobubbles in US diagnostics and due to hydrophobicity it remains undissolved in the blood. This nature of perfluoropentane has tendency to exhibit much longer lifetime on a hydrophobic surface. Hydrophobicity of MSNPs with larger surface area assures its candidature to entrap interfacial liquid inside the pores for longer time as compared to lipid entrapped microbubbles.[24]

After entrapment of liquid perfluoropentane in porous structure, due to low boiling point, it can easily be converted to vapours, which exist in the form of bubbles and creates a large volume of gas inside the pores. Figure 4 illustrates stimuli responsive drug delivery system constructed of lipid coated mesoporous silica nanoparticles with perfluoropentane as an ultrasound responsive material. Advances in sonochemistry proved that ultrasound waves could produce either some physical effects through thermal and mechanical induction or chemical effects by inducing chemical reactions or combination of both. Induction of thermal and/or mechanical effects by ultrasound waves can be helpful in conversion of low boiling point liquid to bubbles, disruption of these bubbles and exerting pressure on the carrier to release the drug.[73,74]

Lipid coating of MSNPs, as a gatekeeper at pore opening of MSNPs, provides an intact barrier against the premature release of the drug and liquid inside pores in inert conditions[75] but application of ultrasound waves on such carriers plays an important role on thermal sensitive liposomes via thermal effects leading to opening of the MSNPs pores. So the combined energy of mechanical and thermal effects on vaporization of liquid inside pores and lipid coating enhance the release of the drug.[76]

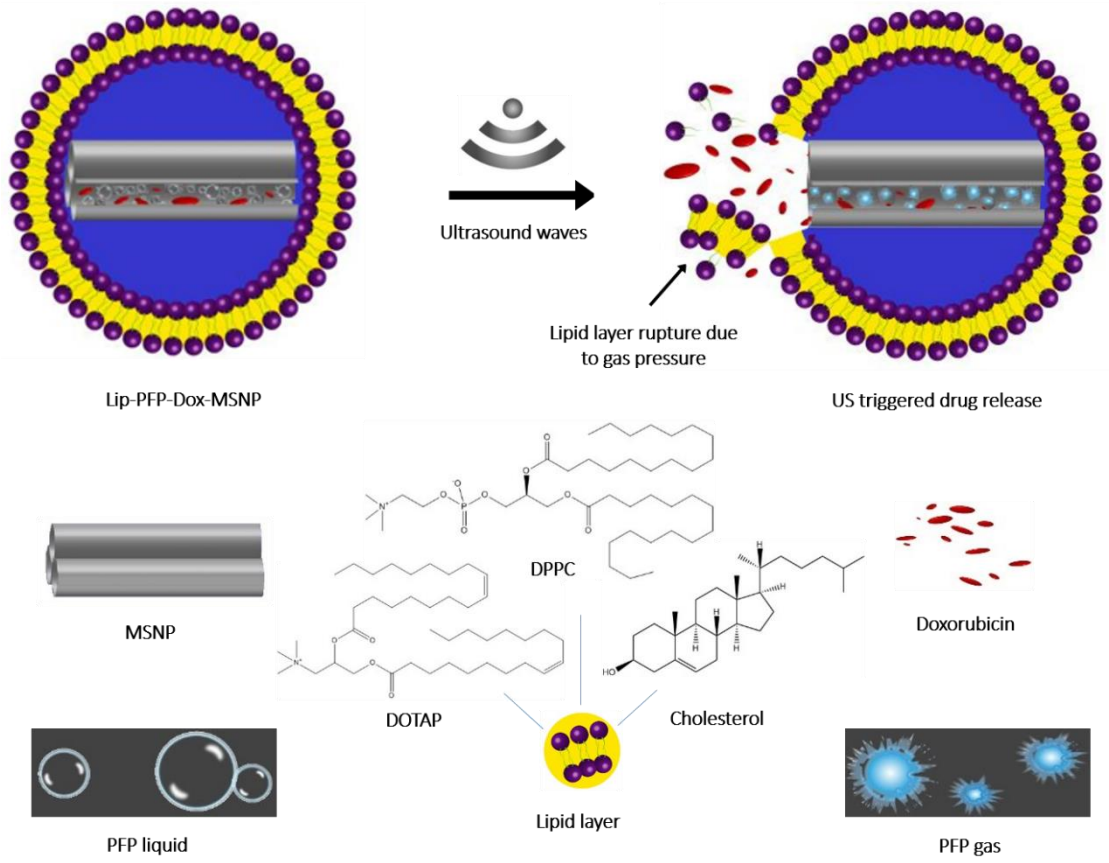

***Figure 5**: Schematic representation of ultrasound triggered release from lipid coated mesoporous silica nanoparticle*

1.2 Ultrasound

Ultrasound being a remarkable approach in biomedicine, has emerged as an important tool which has shown many applications including, release of the drug from carriers, effects on opening of blood brain barrier, thermal therapies and many others.[74,77-79] As an exogenous stimulus, ultrasound is very advantageous because of noninvasiveness, cost effectiveness and non-ionizing features. Moreover, the penetration depth can also be adjusted according to frequency and exposure duration, resulting in more specific local outcomes and minimizing the adverse effects.[80] Ultrasound can produce two different kinds of biological effects such as thermal and mechanical. Cavitation is most commonly used mechanical effect of ultrasound in enhanced drug delivery of various therapeutics.[81] Mainly, the use of cavitation nuclei to reduce

the acoustic pressure, results in destruction of gas bubbles. These nuclei can be either gas bubbles,[82] gas stabilizing solid nanoparticles[83,84] or droplets.[85]

Ultrasound can be used not only for triggered release of the drug but also for the tracking of drug carriers in the body. It is evident that US with mechanical index (MI)<0.5 is used for prolonged imaging because at this acoustic energy the bursting of contrasting bubbles is lesser but MI>0.5 causes the destruction of ultrasound contrasting agents like perfluoropentane and results in the diffusion of gas into the surrounding area. An instantaneous bursting of perfluorocarbons with MI 1.4 has also been reported.[86,87] This agent destruction is considered as a limiting factor for imaging but this limitation can be converted to beneficence, and triggered release of drug from carrier can be achieved at a desired site. The release of the drug from carrier is due to mechanical and thermal effect of the ultrasonic waves.[88] However it is very difficult to identify either alone in biological applications. The thermal effect of US irradiation is evident, which has been used for the diagnostic and therapeutic purposes such as reduction in joint stiffness, blood flow changes, muscle spasm and many others. US due to its hyperthermic effects with combination of either radiotherapy or chemotherapy, is very useful in cancer treatment.[89] Although intensity of thermal effects depends upon many factors but significant hyperthermia effects to various tissues has been reported.[90,91]

1.3 Hypoxia

Hypoxia is a condition where the tissues are deprived of oxygen, resulting in low oxygen tension and is a common feature of solid tumors.[92] It is established that hypoxia is responsible for tumor progression and metastasis, including breast cancer metastasis.[93] In cancer therapy, being a negative factor, hypoxia has a strong association with enhanced malignancy because of resistance to chemotherapy and ionized-radiation.[94-96] There is a strong evidence that hypoxia inducible factor and alteration in tumor metabolism linked with carbonic anhydrase enzyme IX and XII, can play a vital role in tumor metastasis and progression.[93]

1.3.1 Carbonic Anhydrase IX (CA-IX) Enzyme

Carbonic anhydrase IX (CA-IX) is a protein located in cell membrane of cancer cells and which is rarely expressed in normal tissues but overexpressed under hypoxic conditions.[97,98] Carbonic anhydrases are zinc metalloenzymes consisting of 15 different isozymes, which exhibit different cellular localization, catalytic activities and distributions in tissues. Few of isozymes such as carbonic anhydrase I, II, III, VII and XIII are associated with cytosol and others such as IV, IX, XII and XIV reside in cellular membrane. The major activity of carbonic anhydrase enzymes is to catalyze reversible reaction between water and carbon dioxide to produce bicarbonates and proton.[99,100]

$$CO_2 + H_2O \leftrightarrow HCO_3^- + H^+$$

Carbonic anhydrases play an important role in pH control and CO_2 homeostasis, biosynthetic reactions based on HCO_3^- and CO_2, electrolyte secretions and CO_2 transportation between lungs and tissues. By recent studies, it is revealed that hypoxic conditions of solid tumors trigger various gene expression, carbonic anhydrase IX is one of them. The over expression of carbonic anhydrase IX in hypoxic tumor is associated with poor prognosis and tumor aggression, resulting in radio and chemotherapy resistance.[100-103]

CA-IX transports intracellular CO_2 to extracellular environment after converting it to carbonic acid and proton. An over expression of CA-IX results in extracellular acidic environment which has already been reported by different cell lines in hypoxic conditions. In recent times CA-IX being endogenous marker for different tumors, has been under investigation to overcome the challenges related to chemical markers administration and invasive techniques before biopsy.[92,104,105] As homeostatic activity, CA-IX enzyme maintains the intracellular pH (pH_i) neutral to slightly basic and extracellular pH (pH_e) acidic.[106] An illustration of different mechanisms involved in pH regulation, with different extracellular proton transporters, is shown in figure 6.

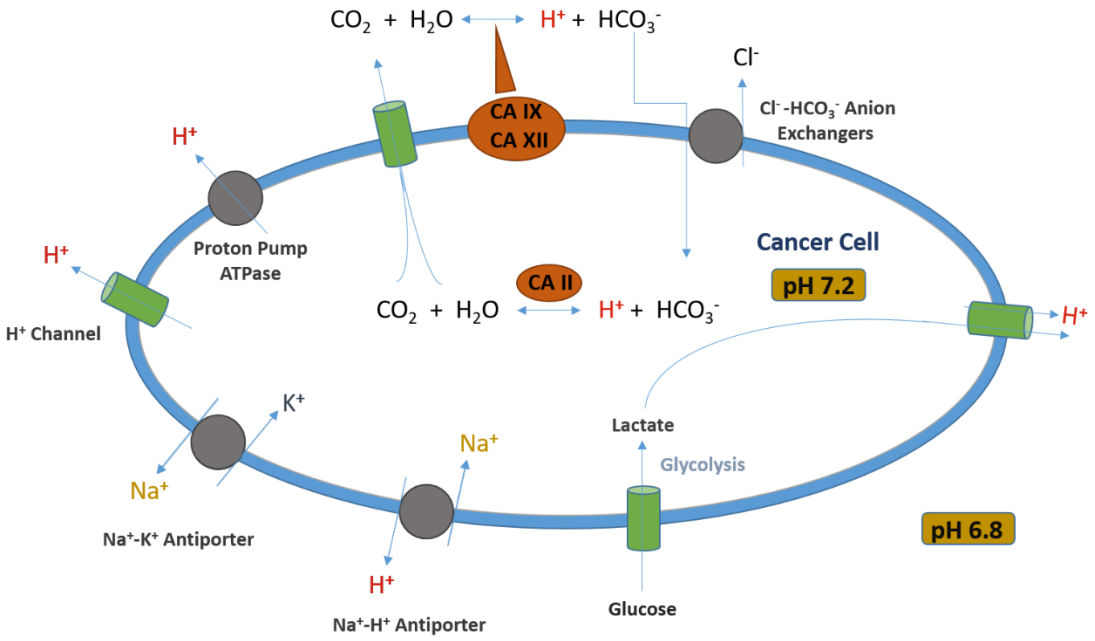

***Figure 6**: Ionic exchange and pH regulation mechanisms of cancer cells*

Most chemotherapeutics are weak electrolytes and their uptake to the cells is normally by passive diffusion but extracellular acidic environment results in ionization of such drugs. The permeability of plasma membrane to ionized substances is very low due to ion trapping and consequently lesser cellular uptake of drugs.[107] According to this ion trapping model, weakly basic drugs such as doxorubicin, daunorubicin and mitoxantrone are highly accumulated in extracellular acidic environment with lower toxicity due to limited uptake of the drug. However, weakly acidic drugs such as chlorambucil and melphalan can easily be taken up to intracellular neutral or relative higher pH environment.[108]

Different approaches have been adopted to alter internal and external pH of solid tumors, for different anticancer drugs to enhance their therapeutic effects. Extracellular pH enhancement was found with improved cytotoxic effects of weakly basic drugs such as topotecan and paclitaxel.[109] A delay in tumor growth with doxorubicin, after treatment with sodium bicarbonate solution to enhance extracellular pH, has already been reported. Carbonic anhydrase inhibition has shown synergistic effects in combination with chemotherapeutic agents.[110,111] Figure 7 is an illustration of an advanced drug delivery carrier with carbonic

anhydrase enzyme inhibitor loaded in lipid layer and doxorubicin in mesoporous silica for co-delivery. Carbonic anhydrase IX inhibition by antibodies or specific inhibitors, on one hand can enhance the effects of weakly basic drugs and on the other hand reduce the metastatic phenotype due to control of pH balance in tumor cells.[112]

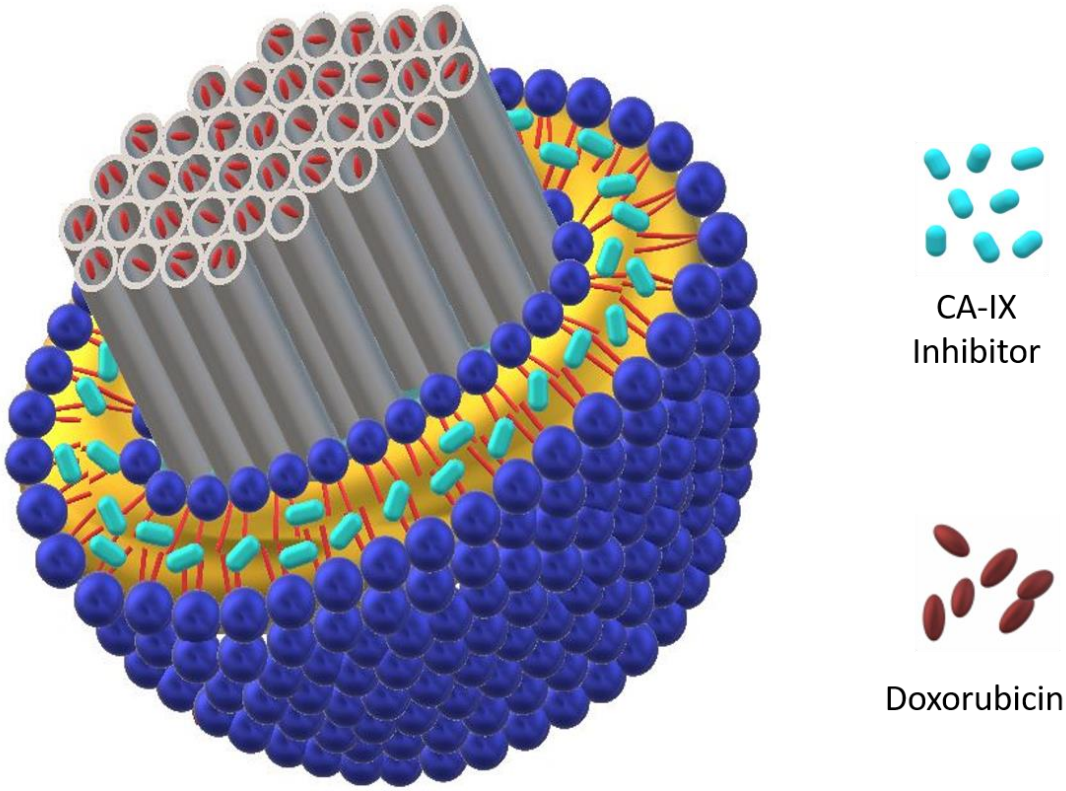

***Figure 7**: Representation of lipid coated mesoporous silica nanoparticle designed for co-delivery of carbonic anhydrase-IX inhibitor and doxorubicin*

1.4 Aims and Objectives

The purpose of this study was to develop a drug delivery system, which exhibits biocompatibility, high loading capacity, no premature leakage, site-specific drug delivery and good cellular internalization. Nanoconstructs were comprised of mesoporous silica nanoparticles, coated with lipid layer to deliver weakly basic drugs like doxorubicin with higher internalization in tumor cells. Specifically, by combining it with carbonic anhydrase IX inhibitor under hypoxic conditions to avoid ionization of drug for better cytotoxic effects. Furthermore, an ultrasound responsive smart delivery system was developed for targeted release, where the release of the drug was dependent on ultrasound.

The important aspects covered under this work are as follow

- Fabrication of mesoporous silica nanoparticles with larger surface area and development of lipid coated mesoporous silica nanoparticles to encounter lower drug delivery and premature drug release
- Physicochemical characterization for size, surface charge and surface area and morphological assessment with electron microscopy.
- *In-vitro* drug release evaluation and cytotoxic studies with a comparison of lipid coated and bared mesoporous silica nanoparticles for cellular internalization.
- Development of ultrasound responsive lipid coated mesoporous silica nanoparticles for triggered release and *in-vitro* stability evaluation
- Comparison of *In-vitro* cytotoxic effects and cellular uptake studies
- Incorporation of carbonic anhydrase-IX inhibitor into lipid coated mesoporous silica nanoparticles with doxorubicin to determine synergistic *in-vitro* cytotoxicity effects under hypoxic conditions to overcome chemoresistance

2 Materials & Methods

2.1 Materials

List of Materials

Agarose	Merck KGaA, Germany
APTES	Sigma Aldrich Chemie GmbH, Germany
CA-IX (H-11) sc-365900	Santa Cruz Biotechnology, Inc, Germany
Carbon coated copper grid	PLANO GmbH, Germany
Chloroform	VWR International GmbH, Germany
Chlorpromazine	Alpha Aesar GmbH & Co. KG., Germany
Cholesterol	Sigma Aldrich Chemie GmbH, Germany
Coverslip	Gerhard Menzel B.V. & Co. KG., Germany
Cuvette (DLS)	Malvern Instruments Ltd, UK
CTAB	Carl Roth GmbH & Co. KG , Germany
DAPI	Sigma Aldrich Chemie GmbH, Germany
DMEM	Biochrom GmbH, Germany
DMSO	Acros Organics B.V. B.A., Belgium
DOTAP	Lipoid GmbH, Germany
Doxorubicin	Fluorochem Ltd, United Kingdom
DPPC	Lipoid GmbH, Germany
Ethanol	Carl Roth GmbH & Co. KG , Germany
Fetal calf serum	PAA Laboratories GmbH, Germany
Filipin III	Sigma Aldrich Chemie GmbH, Germany
FITC	Sigma Aldrich Chemie, Germany
FluorSave	Calbiochem Corporation, USA
Glass slide	Gerhard Menzel B.V. & Co. KG., Germany
HCl	Carl Roth GmbH & Co. KG , Germany
Helium Gas	Praxair GmbH, Germany

AFM Probe: HQ:NSC14/AL_BS	MikroMasch, Estonia
AFM Probe: HQ:NSC16/AL_BS	MikroMasch, Estonia
MDA-MB 231	ATTC® , USA
Methanol	Carl Roth GmbH & Co. KG , Germany
MilliQ water	Millipore Corporation, USA
MTT	Sigma Aldrich Chemie GmbH, Germany
$NaHCO_3$	Carl Roth GmbH & Co. KG , Germany
NaOH	Carl Roth GmbH & Co. KG , Germany
Nitrogen gas	Praxair GmbH, Germany
Pen-strep	Sigma Aldrich Chemie GmbH, Germany
Formaldehyde	Alpha Aesar GmbH & Co. KG., Karsruhe Germany
Petri dishes	Sarstedt AG & Co.,Germany
PFP	abcr GmbH, Germany
Polycarbonate Membrane	Whatman plc, Maidstone, UK
Protein assay kit	Bio-Rad, Munich, Germany
RPMI	Biochrom GmbH, Germany
Sample cells (BET)	BEL Europe, GmbH, Germany
SKBr-3	ATTC® , USA
Streptomycin	Sigma Aldrich Chemie GmbH, Germany
Syringe	BD GmbH, Germany
Syringe Filter	Whatman plc, UK
TEA	Merck KGaA, Darmstadt, Germany
TEOS	Carl Roth GmbH & Co. KG , Germany
Triton X100	Sigma Aldrich Chemie GmbH, Germany
Tubulin (sigma)	Sigma Aldrich Chemie GmbH, Germany
Uranyl Acetate	Sigma Aldrich Chemie GmbH, Germany

12 well plate	Nunc GmbH & Co. KG, Germany
6 well plate	Sarstedt AG & Co.,Germany
96 well plate	Brand GmbH & Co. KG, Germany

List of Devices

AFM	JPK instruments AG, Berlin
Autoclave, Tuttnauer 3850 ELC	Tuttnauer GmbH, Germany
Bath Sonicator	Elma Schmidbauer GmbH, Germany
BELsorp mini II	BEL GmbH Europe, Germany
Centrifuge machine	Eppendorf Int., Germany
Centrifuge machine-Beckman J2-21	Beckman Coulter GmbH, Germany
CLSM	Carl Zeiss Microscopy GmbH, Germany
Cryo-TEM: Libra 120 Plus	Carl Zeiss Microscopy GmbH, Germany
Extruder-Avanti Mini	Avanti Polar Lipids Inc, USA
Luminometer: 96 well reader	MBG, Labtech, Germany
Freeze dryer, Christ Beta 1	Martin Christ Gefriertrocknunganlagen GmbH, Germany
FTIR- Alpha-ATR	Bruker GmbH, Germany
Incubator, CO2, HeraCell	Heraus GmbH & Co. KG., Hermany
ISciTive Hypoxic Workstation	Baker Ruskinn, UK
Laminar Flow Hood: Class II	NuAire Inc., USA
Magnetic stirrer	CAT Scientific USA
Rotary evaporator	Heidolph Instrumenst GmbH & Co. KG., Germany
STEM: JEOL 2200FS	JEOL, Ltd., Japan
TEM, JEOL 3010	JEOL, Ltd., Japan
Trans Blot Turbo blotting system (Bio-Rad)	Bio-Rad Laboratories GmbH, Germany

Ultrasound device: Ezono300	eZono AG, Germany
UV-visi spectrophotometer: UVmini-1240	Shimadzu Corp, Japan
Vario MICRO cube	Elementar Analysensysteme GmbH, Germany
Zetasizer NanoZS	Malvern Panalytical, Germany

2.1.1 MSNPs Fabrication

Mesoporous silica fabrication is based upon two parameters including the dynamics of surfactant for assembly formation in the form of micelles and condensation ability of inorganic oxides to form thermostable nanostructure.

2.1.1.1 Cetyltrimethylammonium Bromide (CTAB)

As a template agent CTAB is most commonly used surfactant in the synthesis of MSNPs. It is cationic in nature and a quaternary ammonium surfactant with molecular weight 364.45 g/mol. CTAB is a white powder with alkyl chain of 16 carbons. Its melting point is ranging from 237-240ºC. CTAB used here was > 99% pure and soluble in water with CMC value 0.92-1 mM.

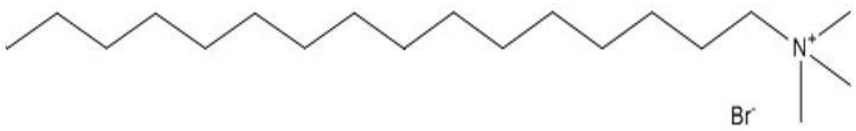

CTAB

2.1.1.2 Tetraethylorthosilicate (TEOS)

TEOS is used as a silica precursor in MSNPs preparation. Its molecular formula and molecular mass are $(C_2H_5O)_4$ Si and 208.33 g/mol respectively. TEOS is a colorless liquid with a density of 0.933 g/ml and most prevalent silicon alkoxide. It intereacts with water to produce Si-O-Si by hydrolysis and condensation. The purity of TEOS used in this work was $\geq$ 99%. Due to its anionic nature it can react with cationic template to form organic-inorganic structures.

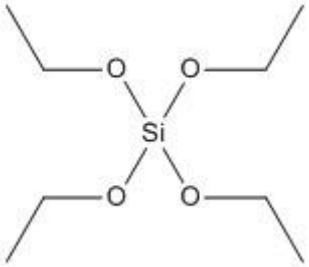

TEOS

2.1.2 Liposomal Preparation

For the liposome preparation, three different lipids were used. These lipids were >99% pure and dissolved in chloroform:methanol (2:1 v/v) at the final concentration of 10mg/ml.

2.1.2.1 DPPC

1,2-dipalmetoyl-sn-glycero-3-phosphocholine is a zwitterion, which consists of polar head group with two saturated fatty chains of palmitic acid. Its molecular weight is 734.053 g/mol with chemical formula $(C_{20}H_{40})_2$ NO_8P. The phase transition temperature of DPPC is 41ºC.

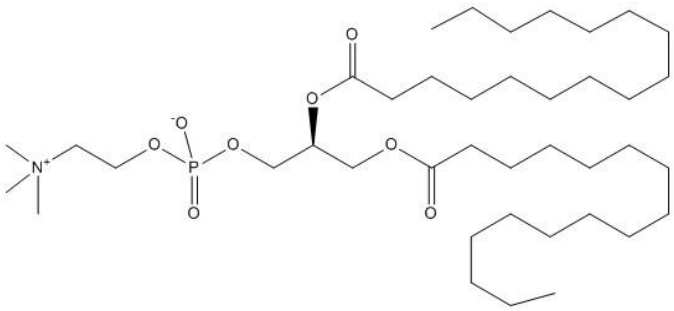

DPPC

2.1.2.2 DOTAP

1,2-dioleoyl-3-trimethylammonium-propane is a cationic lipid with unsaturated long chain fatty acids. Its transition temperature is <5ºC. DOTAP has molecular formula $C_{42}H_{80}NO_4Cl$ with molecular mass 698.542 g/mol.

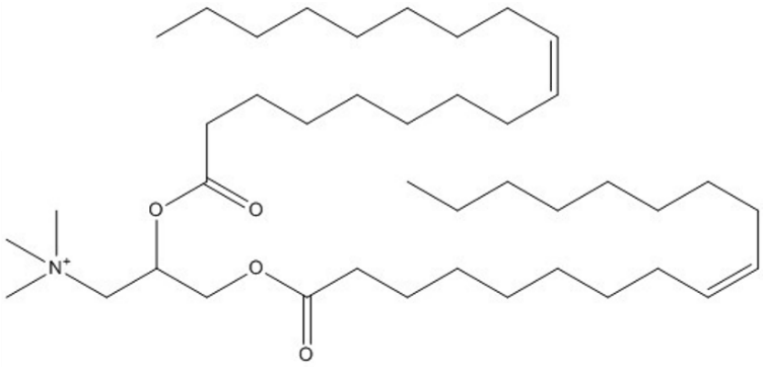

DOTAP

2.1.2.3 Cholesterol

Cholesterol is a very important part of lipid membranes and liposomes. It is used as a stabilizer, by reducing the fluidity of lipid layer resulting in modulation of drug release. Its molecular formula and molar mass are $C_{27}H_{46}O$ and 386.65 g/mol respectively.

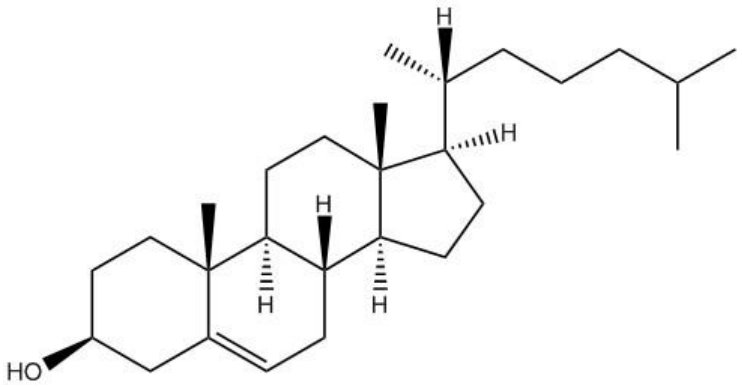

Cholesterol

2.1.3 Loading Materials

2.1.3.1 Doxorubicin (Dox)

Doxorubicin is widely used chemotherapeutic in various types of cancers especially breast cancer. It is an anthracycline and also known with name of Adriamycin. Doxorubicin shows its cytotoxic action by damaging DNA after intercalation into DNA and preventing its replication. It also inhibits progression

of topoisomerase II which has a critical role in DNA function. It is hydrophobic in nature but its hydrochloride salt is water soluble. Here we have used >95% pure doxorubicin hydrochloride as a model drug. It is red to orange powder with molecular weight of 543.52 g/mol.

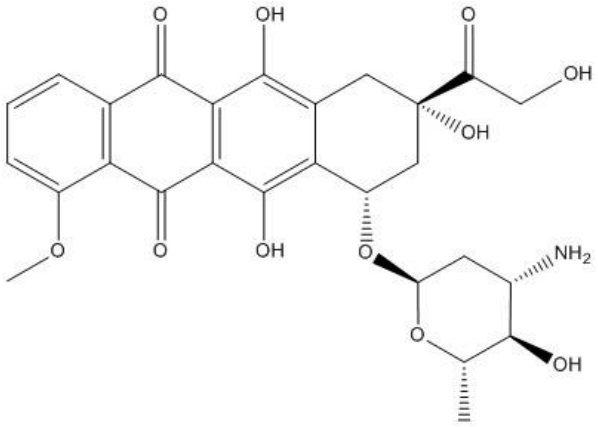

Doxorubicin

2.1.3.2 Perfluoropentane (PFP)

PFP is a fluorocarbon having molecular formula C_5F_{12} and boiling point 29ºC. Due to its ultrasound responsive nature it plays a vital role in development of ultrasound based drug delivery systems. Its molecular weight is 288.05 g/mol and density of 1.6 g/ml. PFP used in this work was 90% pure and because of lower boiling point it was stored at 4ºC.

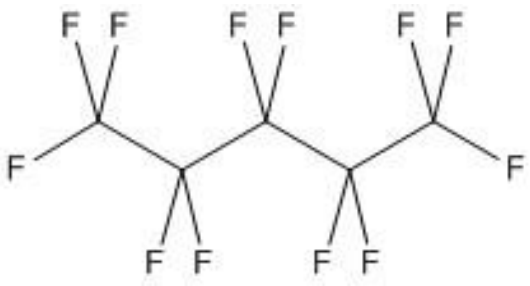

Perfluoropentane

2.1.3.3 Carbonic Anhydrase IX (CA-IX) Enzyme Inhibitor

Carbonic anhydrase IX inhibitor used in this study is a cell membrane permeable benzenesulfonamide. It is a white solid and soluble in organic solvents. The molecular formula and molecular weight of the compound are $C_{13}H_{22}N_4O_5S$ and 336 g/mol respectively. It shows specific inhibiting activity for human carbonic anhydrase isoforms such as hCA-I, hCA-II, hCA-IX and hCA-XII. Its effectiveness at lower concentrations especially for CA-IX (Ki 0.9 nM) and CA-XII (Ki 5.7 nM) is advantageous to other CA-IX inhibitors. The purity of the compound was $\geq$98% and it was stored at 4ºC.

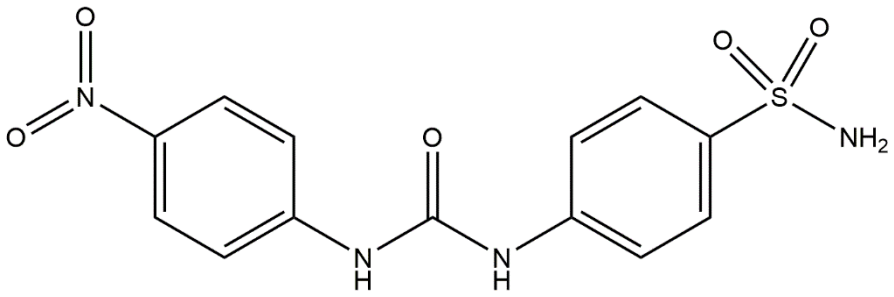

Carbonic anhydrase IX inhibitor

2.2 Experimental Section

2.2.1 Development of Carriers

2.2.1.1 Preparation of Liposomes

Liposomes were prepared with thin layer hydration technique with a slight modification of the method already been reported.[113,114] Liposomes were composed of DPPC, Cholesterol and DOTAP at molar mass ratio of 85:12:3. In brief, definite quantity of lipids dissolved in chloroform:methanol (2:1 v/v) was taken in round bottom flask and after dilution the organic solvents were evaporated subsequently under vacuum pressure. Rotary evaporator Heidolph Laborota 4000 efficient (Heidolph Instruments, Schwabach, Germany) with bath temperature 45ºC was used for reducing pressure until a thin lipid layer was formulated. After complete hydration of lipid film with PBS (pH 7.4) buffer, the mixture was sonicated in ultrasound bath at 45ºC for 15 min. For uniform size distribution the lipid mixture was extruded through a polycarbonate filter of 100 nm pore size at transition temperature.[40]

2.2.1.2 Fabrication of MSNPs

For the synthesis of MSNPs, the four main components are source of silica (TEOS), organic template as a structure directing surfactant (CTAB), catalyst bases such as sodium hydroxide (NaOH), sodium bicarbonate ($NaHCO_3$) and triethanolamine (TEA) and solvent (Water). Fabrication of MSNPs is based on hydrolysis and condensation of TEOS in the presence of water and CTAB in basic environment. CTAB is a cationic surfactant which can form hexagonal micelles by heating its aqueous solution at higher concentration than CMC. TEOS is an inorganic material, which interacts electrostatically with CTAB. In basic environment, TEOS exists as negatively charged ions and reacts with positively charged ions on cationic surfactant of hexagonal micelles. Base catalysis helps hydrolysis and condensation reaction between water, TEOS

and CTAB. MSNPs were fabricated by a modified method which has already been reported.[115]

In short a definite amount of CTAB and 350 µl of 2 M NaOH solution were added to 48 ml of purified deionized water and stirred at 350 rpm for 2 hrs at 80ºC. When the solution became pellucid and CTAB was completely dissolved in the form of hexagonal micelles, 500 µl of TEOS was added dropwise. The above mixture was stirred at same speed overnight in an inert environment at 80ºC. The molar concentrations in mmoles of CTAB:TEOS:NaOH:H_2O were used as 0.274-1.28:2.2:0.7:2667 respectively. The molar ratios of CTAB/TEOS ranging from 0.12-0.58 were used to prepare different sized particles. To check the effect of pH on MSNPs synthesis, a different catalytic base TEA was also used. Same molar ratio formulations were also prepared by using TEA and $NaHCO_3$ as catalysts instead of NaOH. The molar concentrations with TEA were as CTAB: TEOS: TEA: H_2O were used as 0.274-1.28:2.2:0.56:2667. The pH of the final solutions with NaOH and TEA were 11.04 and 8.92 respectively.

2.2.1.2.1 Surfactant Removal

The milky solution was collected and centrifuged at 16000 g for 20 min and pellet was obtained as surf-MSNPs. These surf-MSNPs were suspended in ethanol:HCl (19:1 v/v) and extraction was performed overnight at 80ºC in oil bath. MSNPs dispersion was again centrifuged at above mentioned force and time. For complete removal of surfactant, the particles were washed two times with ethanol and two times with water to obtain pure MSNPs. The particles were lyophilized and stored at -20ºC.

2.2.1.3 Surface Modified MSNPs Preparation

FITC (Fluorescein-5 isothiocyanate) and APTES (3-aminopropyl triethoxysilane) were used for the fluorescence and surface modification simultaneously. 1.1 mg of FITC and 2.4 µl of APTES were dissolved in 0.6ml ethanol under nitrogen flow and allowed to stir for 2 hr. After stirring TEOS was mixed to FITC-APTES solution and then the combined solution was added to

CTAB solution dropwise. The molar concentrations were similar as used in the simple MSNPs.

2.2.1.4 Lipid Coated MSNPs

Before extending our experiments to the coated Dox-MSNPs, we initially coated lipid to unloaded MSNPs. 70 µl of above mentioned liposomes were mixed with 1 mg of lyophilized MSNPs by pipetting. The mixture was further sonicated for 10 min and incubated at room temperature overnight. Electrostatic interaction between cationic lipid layer and anionic MSNPs surface along with liposomal surface tension resulted in the lipid coating of MSNPs. Lipid coated MSNPs were centrifuged at 16000 g for 30 min to remove the extra liposomal contents as supernatant. Pellet was suspended in purified water and lipid coating was confirmed with dynamic light scattering (DLS) and laser doppler velocimetry (LDV) by size and the shift of zeta potential.

2.2.1.5 Preparation of Dox-MSNPs

As Dox exists as a positive charge moiety at neutral pH, so it can easily be loaded in the porous structure of negatively charged MSNPs due to electrostatic interaction.[116] To evaluate the loading capacity of MSNPs 2.5 mg of lyophilized MSNPs were suspended in 6ml of purified water, sonicated for 5 min for uniform dispersion and after adding different amounts of Dox including 1.5 mg, 3 mg, 6 mg and 12 mg, suspensions were stirred overnight at 350 rpm at room temperature. Drug loaded MSNPs were centrifuged at 16000 g for 30 min and pellet was washed three times with water to remove extra Dox on surface of the MSNPs. Subsequently, the supernatants were collected and measured with UV-visible spectrophotometer. The amount of entrapped drug was then easily calculated by subtracting unentrapped drug from the total amount of drug. Finally, the drug loaded MSNPs were redispersed in water and lyophilized.

2.2.1.6 Preparation of Lip-Dox-MSNPs

To coat Dox-MSNPs with lipid layer, weighed amounts of MSNPs loaded with Dox were mixed with liposomes as mentioned above in section 2.2.1.4.

2.2.1.7 Preparation of PFP-Dox-MSNPs and Lipid Coating

The above prepared dried Dox-MSNPS corresponding to 2.5 mg MSNPs were mixed with 200 µl of ultrasound contrasting material, perfluoropentane (PFP) and sonicated for a short time at 4ºC, to enhance the capillary filling so that liquid PFP can penetrate inside the pores, and incubated in a cold environment for 24 hrs. After incubation period the extra liquid PFP outside the pores, was evaporated at room temperature and leaving behind PFP-Dox-MSNPs in dried form.

Previously optimized mass ratio of MSNPs to liposomes (1:0.7) was used to coat the liposome. After addition of definite quantity of liposomes to PFP-Dox-MSNPs the mixture was pipetted frequently and shacked well to coat the liposomes on the surface of particles to obtain Lip-PFP-Dox-MSNPs.[117] For comparative studies non-ultrasound reactive Lip-Dox-MSNPs were used as mentioned in section 2.2.1.6.

2.2.1.8 Preparation of CA-IX inhibitor Liposomes (Lip_c)

CA-IX inhibitor loaded liposomes (Lip_c) were prepared by using same method as described in section 2.2.1.1. Same molar mass ratios of DPPC, cholesterol and DOTAP were used with an addition of CA-IX inhibitor. Briefly 20 nmoles of CA-IX inhibitor dissolved in methanol were added to lipid solutions followed by same procedure in section 2.2.1.1. The final concentration of CA-IX inhibitor in liposomes was 20µM.

2.2.1.9 Preparation of Lip_c-Dox-MSNPs

For Lip_c coating of MSNPs, previously optimized molar mass ratio of MSNPs:liposome (1:0.7) was used by adopting same procedure as mentioned in 2.2.1.6. The important parameter for CA-IX inhibitor concentration was kept in mind so that even after dilution, its concentration remains higher than the minimum inhibitory concentration (K_i=0.9nM).

2.2.2 Characterization

For the characterization of MSNPs different techniques has been used. Initial characterization was done with dynamic light scattering (DLS) and Laser Doppler Velocimetry (LDV) for particle size and surface charge. Morphological studies were done with microscopic techniques like, atomic force microscope (AFM), transmission electron microscope (TEM), cryo transmission electron microscope (Cryo-TEM) and scanning transmission electron microscope (STEM). Elemental analysis and fourier transform infrared (FTIR) spectroscopy were used to characterize surfactant removal and surface modification. For surface area, pore size and pore volume Brunauer Emmett Teller (BET) was used. UV-visible spectrophotometer was used for the quantification of amount of drug loading and release profiles. Ultrasound characterization and triggered release was done with portable ultrasound device. Cell culture experiments were performed for the cytotoxic evaluation and confocal laser scanning microscope (CLSM) imaging for cellular uptake analysis.

2.2.2.1 Physicochemical Characterization

2.2.2.1.1 Dynamic Light Scattering (DLS)

Initially sizes of nanocarriers were characterized by dynamic light scattering. with the help of Zetasizer NanoZS (Malvern Panalytical, Germany). Light scattering angle was set at 173º with HeNe laser at wavelength of 633 nm. For each measurement, the formulations were diluted with 1% phosphate buffer saline (PBS) at 1:100. The adjustment of attenuator was set to automatic mode. Each formulation was measured in triplicate and each measurement consists of 15 runs. Data is presented as ZAverage of three independent formulations with standard deviation (intensity distribution). Similarly, polydispersibility index (PDI) was measured in the form of average of three independent formulations with standard deviation.

2.2.2.1.2 Laser Doppler Velocimetry (LDV)

Laser Doppler Velocity (LDV) was used for zeta potential measurements with scattered light measured at an angle of 17º with Zetasizer NanoZS (Malvern Panalytical, Germany). Same dilutions of different formulations, as mentioned above, were used for surface charge characterization. The measurements were done for three different independent formulations of MSNPs and liposomes. Each formulation was measured in triplicate and each measurement consists of 15-100 runs and is presented as average with standard deviation.

2.2.2.1.3 Elemental Analysis

We have used CTAB as an organic template and porous structure depends upon the removal of surfactant, leaving behind pores. As CTAB contains carbon, hydrogen bromine and nitrogen (Formula: $C_{19}H_{42}BrN$), the presence or absence of such elements is a good tool to analyze surfactant removal. Elemental analysis, based on combustion, was performed with vario MICRO cube (Elementar Analysensysteme GmbH, Germany) to evaluate the amount of surfactant before and after washing. Tin boats with weighed amounts of samples were subjected to combustion and finally results were collected as % age of relevant elements.

2.2.2.1.4 Surface Area Measurement

For surface area characterization along with pore size, pore volume and its distribution, gas adsorption measurements were performed with BELSorp mini II (BEL GmbH Europe, Germany). It is a quantitative process of nitrogen physiosorption by adsorption-desorption isotherm, which describes the amount of nitrogen adsorption-desorption at constant temperature as a function of nitrogen partial pressure. The Brunauer Emmett Teller (BET) is most commonly used method for the determination of surface area of porous structures by gas adsorption. Samples were pretreated at 120ºC at low pressure for 2 hrs to remove all the impurities and water contents. Then weighed amounts of pretreated samples were subjected to surface area and volume characterization. Pore size distribution was characterized by using

Barrett-Joyner-Halenda (BJH) model. Two inert gases Nitrogen and Helium were used for purging and adsorption.

2.2.2.1.5 Fourier Transform Infrared (FTIR) spectroscopy

FTIR spectroscopy of different samples was performed with Bruker-ALPHA ATR-FTIR (Bruker, Germany). For the assessment of surfactant removal, a small amount MSNPs with and without surfactants were placed on ATR crystal to get spectrum. Similarly, spectrums were obtained for the surface modified MSNPs (FITC-APTES) and lipid coated MSNPs.

2.2.2.2 Morphological Studies

2.2.2.2.1 Electron Microscopy

Electron microscope utilizes electron beam for imaging the specimen. The basic principle of electron microscopy is more or less similar to light microscope with the difference of electron instead of light. It allows to take images with much higher magnification for detailed morphological studies.

2.2.2.2.1.1 Transmission Electron Microscopy (TEM)

The TEM micrographs were taken with transmission electron microscope at 300 kV accelerated voltage (TEM JEOL 3010, 300 kV) at the Philipps University Marburg. Copper grids were used for the placement of the samples and observed under electron transmission to get the images. Due to non-conducting behavior of particles, samples were coated with a thin layer of carbon. For negative staining, lipid coated MSNPs were mixed in 1:1 v/v with 2 % uranyl acetate. After incubation for 30 min the lipid containing samples were also observed with above mentioned specifications. Another set of lipid coated MSNPs, after US irradiation, was examined at the MLU Halle Wittenberg with an EM 900 TEM (Carl Zeiss Microscopy GmbH, Oberkochen, Germany, acceleration voltage 80kV).

2.2.2.2.1.2 Cryogenic Electron Microscopy (Cryo-EM)

Cryo-TEM micrographs were taken at the MLU Halle Wittenberg. Vitrified specimens were prepared using a blotting procedure, performed in a chamber with controlled temperature and humidity using an EM GP grid plunger (Leica, Wetzlar, Germany). The sample dispersion (6 µl) was placed onto an EM grid coated with a holey carbon film (Cflat, Protochips Inc., Raleigh, NC). Excess solution was then removed by blotting with a filter paper to leave a thin film of the dispersion spanning the holes of the carbon film on the EM grid. Vitrification of the thin film was achieved by rapid plunging of the grid into liquid ethane held just above its freezing point. The vitrified specimen was kept below 108 K during storage, transferred to the microscope and investigated. Specimens were examined with a Libra 120 Plus transmission electron microscope (Carl Zeiss Microscopy GmbH, Oberkochen, Germany), operating at 120 kV. The microscope was equipped with a Gatan 626 cryotransfer system. Images were acquired using a BM-2k-120 dual-speed on-axis SSCCD camera (TRS).

2.2.2.2.1.3 Scanning Transmission Electron Microscopy (STEM)

STEM is a technique which combines both principles of scanning by scanning electron microscopy (SEM) and transmission of TEM. A highly focused beam was applied to the specimen and for scanning similar to SEM operation. Transmitted electrons are then collected to form transmission images in the form of bright field images. STEM measurements were carried out in an aberration corrected JEOL JEM 2200FS operating at 200 kV. A high angle annular dark field (HAADF) detector was used in order to retrieve image intensities proportional to atomic number of the elements in the sample.

2.2.2.2.2 Atomic Force Microscopy (AFM)

Small amount of diluted sample was placed on silica surface, fixed on a glass slide by double tape. The extra liquid was removed after the settlement of the particles and dried under air. Nanowizard 3 Nanoscience (JPK Instruments) with cantilever tips HQ:NSC14/AL_BS & HQ:NSC16/AL_BS were used to

measure the atomic force microscopy. Amplitude signals of cantilever in trace direction and height signal in retrace direction were used to obtain the images.

2.2.2.3 UV-Visible spectroscopy

UV-Visible spectroscopy is a qualitative and quantitative analysis technique, which shows a linear relationship between absorbance and concentration of the samples. In this study, we have used UVmini-1240 (Shimadzu Corp, Japan) at 482 nm and 495 nm for water and PBS pH 7.4 to find the unknown concentrations of Dox for drug loading and drug release profiles.

2.2.2.4 *In-Vitro* Drug Release

To evaluate the drug release behavior from MSNPs and Lip-Dox-MSNPs *in-vitro* drug release studies were performed. MSNPs containing 3 mg of Dox were suspended in previously activated dialysis tubes with molecular weight cut off (MWCO) value of 6000-8000 Daltons (Repligen Europe B.V. Breda, Netherlands). The tubes with 1/3 air were sealed with clips and further suspended in PBS buffer (pH 7.4) medium under air sealed environment. The medium was shaken on magnetic stirrer at 100 rpm at 37ºC. At different intervals, 3ml of the sample was taken and fresh medium was added.[118] The concentration of Dox in sample was measured with UV-visible spectrophotometer at 482 nm. The same procedure was adopted with Lip-Dox-MSNPs and amount of drug release was measured.

2.2.2.5 Ultrasound Characterization

2.2.2.5.1 Stability Studies of Lip-PFP-Dox-MSNPs

The ultrasound contrast studies were performed with the help of commercially available clinical device eZono 3000 (eZono AG, Germany) equipped with a probe having a center frequency of 3.5 MHz with MI 0.7 which are approved specifications by FDA. For ultrasound contrast characterization, we have used a self-designed model of agar phantom with a circulating set of tubes to imitate the soft tissues and blood vessels. To mimic the movements in the body, system was fitted to peristaltic pump for continuous but pulsatile movement of

fluid to one direction. Contrast can easily be visualized on the screen attached to probe and the overall layout of the model is shown in figure 8. The distance between probe and silicon tube in agar phantom model was kept 9 cm.

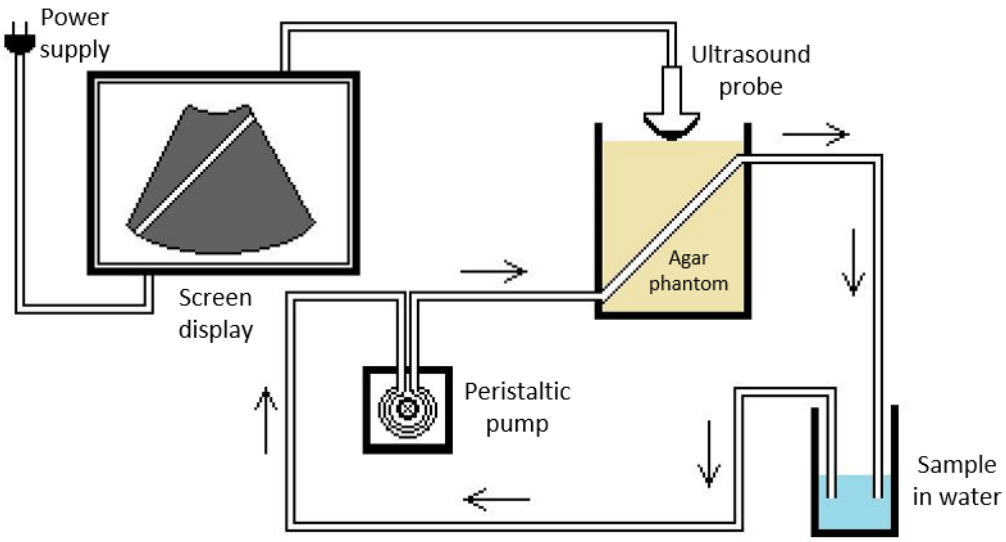

***Figure 8**. Experimental agar phantom model for US contrast evaluation of PFP loaded drug carrier.*

An amount 100 ml of PBS buffer at 37ºC was circulated in silicon tube and 100 µl of PFP loaded MSNPs sample was added to check the contrast in dynamic conditions. The stability for ultrasound contrast due to entrapped PFP inside the pores was studied for 120 hrs by adding 100 µl of sample at different time intervals.

Apart from US contrast stability, to observe the role of PFP inside the pores of MSNPs & gatekeeping effect of lipid layer on the stability and drug retention capacity of MSNPs, premature drug release test was performed under inert conditions. As our hypothesis was to trigger the release of drug by US-irradiation resulting in the conversion of liquid PFP to gaseous form so it was necessary to observe the effects of PFP on the release of drug in the absence of US radiations. Dox-MSNPs, Lipid-Dox-MSNPs and Lip-PFP-Dox-MSNPs were subjected to leakage test for 10 days. Above mentioned formulations were suspended in PBS 7.4 and incubated under static conditions at 4ºC. Samples were taken at different time intervals and amount of drug released was measured by UV-Visible spectrophotometer.

2.2.2.5.2 Ultrasound Triggered Drug Release

In vitro drug release was performed by using another self-made agar phantom having a cavity of 15 ml in the middle. In brief the middle cavity was filled with PBS buffer and a definite amount of Lip-PFP-Dox-MSNPs was added to it. The mixture was stirred at a speed of 150 rpm and was subjected to ultrasound radiations with a probe (12 MHz, MI 1.4). Samples were taken at different time intervals and same amount of fresh medium was added after each sample. After centrifugation supernatant was collected and the amount of drug release was measured with the help of UV-Vis spectrophotometer. To compare the triggering effect of ultrasound radiations, the same procedure was adopted for Dox release from Lip-Dox-MSNPs without application of ultrasound.

2.2.2.5.3 Measurement of Gas Produced by Vaporization

To confirm the availability of liquid PFP inside pores and gas production, we measured the volume of gas produced with US-irradiations in a double syringe close system connecting to each other by a two way Luer lock stopcock as shown in figure 9.[119] Briefly, 2 ml of Lip-PFP-MSNPs in purified water with final concentration of 2.5 mg/ml was contained in 10 ml Hamilton gastight syringe. After connecting to two way Luer lock stopcock, the air was removed by depressing the plunger and stopcock was closed. Another 250 µl syringe containing 20 µl of water was connected to other side of the lock to avoid any air pocket in the system. By withdrawing the plunger of large syringe to two or three times of the volume of the dispersion, vacuum was created. The plunger was held at that position for 2 min and after releasing the plunger, it returned to the volume higher than original volume. Then the amount of air produced was measured as an air pocket between plunger of large syringe and dispersion.

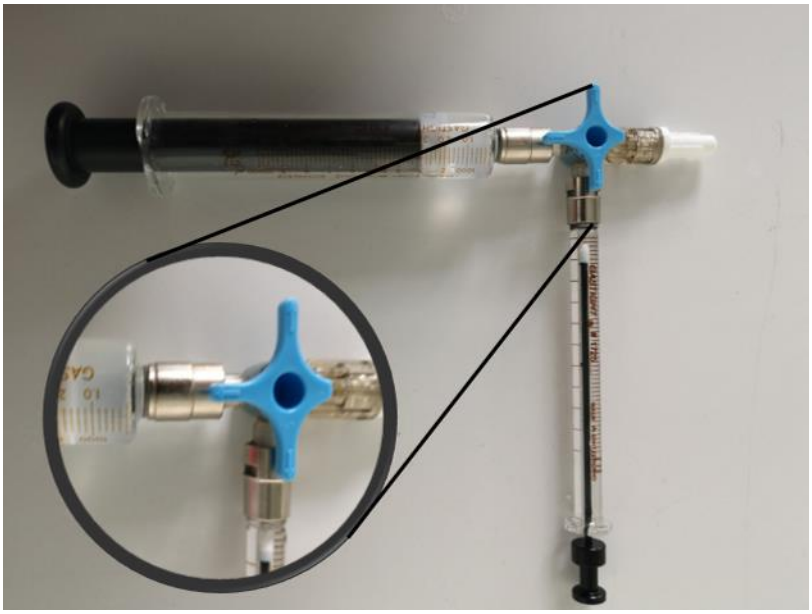

Figure 9: *A double syringe close system connected via a two-way Luer lock stopcock.*

2.2.2.6 Cell Culture Experiments

The epithelial adenocarcinoma breast cancer cells, MDA-MB 231 (ATTC, Manassas, USA) and SKBr-3 (ATTC, Manassas, USA) were used for cell culture experiments. High glucose Dulbecco's Modified Eagle's Medium (DMEM) supplemented with 10 % fetal calf serum and 10 % non-essential amino acids (NEA) was used for cultivation of the MDA-MB 231 cells. Rosewell Park Memorial Institute (RPMI) medium with 10 % fetal calf serum supplement was used for SKBr-3 cells. For optimal growing conditions, cells were provided with suitable humidity along 37ºC and 7% CO_2.

2.2.2.6.1 *In-vitro* Cytotoxicity

2.2.2.6.1.1 MTT Assay for Dox-MSNPs and Lip-Dox-MSNPs

For the cytotoxicity and cellular uptake studies, *in-vitro* cell culture experiments were performed where SKBr-3 breast cancer adenocarcinoma cells were used. Cells were incubated overnight with RPMI medium containing 10 % fetal calf serum (FCS) in 96 well plate having cell density of $1x10^4$ cells/well. After removing the medium, cells were incubated with Dox-MSNPs and Lip-Dox-

MSNPs containing specific concentrations of Dox for different time intervals including 4 hrs, 24 hrs, 48 hrs and 72 hrs. Medium was removed and fresh medium was added after specific time and incubated overnight. 3-(4,5-dimethylthiazol-2-yl)-2,5-diphenyltetrazolium bromide (MTT) dye with a final concentration of 0.6 µg/ml in fresh medium was replaced with old medium and incubated for 4 hrs. Finally, the medium was replaced with DMSO (dimethyl sulfoxide) to dissolve formazan crystals and absorbance was measured at 570 nm with plate reader (FLUOstar, BMG Labtech GmbH, Germany) to evaluate the viability of cells.

The cell viability was calculated by using following formula.

$$\% \text{ Viability} = ((Ab_{Sample} - Ab_{Blank})/(Ab_{Control} - Ab_{Blank})) \text{ X } 100\%$$

Where Ab_{Blank} was the absorbance of no cells while Ab_{Sample} and $Ab_{Control}$ were taken as treated and non-treated cells respectively. All the samples were measured in triplicate and results are given as average.

2.2.2.6.1.2 MTT Assay for US Responsive Carriers

For the cytotoxic studies and drug delivery behavior, MDA-MB 231 cells were seeded in 20 cm^2 Petri dish ($40x10^4$ cells/cm^2) in 5ml of medium and incubated for 24 hrs at 37ºC under 7 % CO_2 atmosphere. After incubation period medium was removed and Lip-Dox-MSNPs, Lip-Dox-MSNPs (US), Lip-PFP-Dox-MSNPs and Lip-PFP-Dox-MSNPs (US) having definite quantity of Dox (ranging from 200 µg/ml to 1.56 µg/ml) diluted in 5 ml of fresh medium were added to petri dishes and incubated for 4 hrs for uptake. For standard, same concentrations of pure Dox were also added to other petri dishes. All petri dishes were taken in triplicate. After incubation old medium was replaced with fresh medium and assigned petri dishes were subjected to ultrasound radiations for 5 min as shown in figure 10.

For uniform radiation, the position of petri dish was changed and after ultrasound the petri dishes were incubated overnight. 3-(4,5-dimethylthiazol-2-

yl)-2,5-diphenyltetrazolium bromide (MTT) was diluted with fresh medium having final concentration 0.6 µg/ml and old medium was replaced with it by adding 5 ml to each plate and incubated for 4 hrs. After removal of medium, DMSO was added and mixed well, to dissolve the formazan crystals. Finally, the solution from each petri dish was transferred to 96 well plate in triplicate and absorbance was measured as mentioned in section 2.2.2.6.1.1. Whole of the experiments were performed in triplicate and results were calculated as an average along with standard deviation.

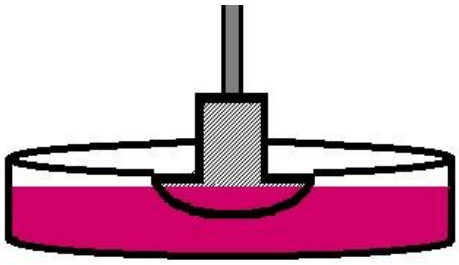

***Figure 10**: In-vitro cell culture US irradiation for triggered release*

2.2.2.6.2 Cellular Uptake Pathway Analysis

As different endocytic pathways are involved in the uptake of the same nanomaterials by different cell lines,[120] similarly certain modifications in nanomaterials result in the adaptation of different pathways for the internalization into the same cell lines. To evaluate the internalization pathway of Dox-MSNPs and Lip-Dox-MSNPs cell viability assay was performed with two different pathway inhibitors. Chlorpromazine is responsible for the inhibition of clathrin dependent endocytosis along with intracellular interference of clathrin processes. Filipin III interacts with cholesterol and ultimately inhibit the caveolea endocytic pathway.[121] Briefly, SKBr-3 cells were seeded to 96 well plates with $1x10^4$ cells /well and incubated overnight. Cells were washed with PBS buffer (pH 7.4) containing Ca^{2+} and Mg^{2+} and incubated with chlorpromazine (6 µM) and filipin III (3 µM) diluted with fresh medium for 30 min. After washing again with PBS buffer, cells were incubated with Dox-MSNPs and Lip-Dox-MSNPs containing 50µg/ml of Dox for 4 hrs and then with medium for overnight. On the following day, cells were incubated with MTT dye

for 4 hrs and absorbance of formazan crystal dissolved in DMSO was measured at 570 nm.

2.2.2.6.3 Cellular Uptake Studies

For cellular uptake studies SKBr-3 cells were seeded with RPMI medium in 6 well plates with cell density of 25×10^4 cells/cm^2 with coverslips. After 24 hrs incubation, cells were washed twice with PBS buffer. Dox-MSNPs and Lip-Dox-MSNPs diluted with medium were added and incubated for 4 hrs. After incubation, cells were washed twice with PBS buffer; later 300 µl of 4 % paraformaldehyde was added into each well and incubated for 10 min to fix the cells. After aspiration 300 µl of the nucleus staining fluorescent dye 4', 6-diamidino-2-phenylindole (DAPI) was added and incubated for 25 min. At the end, cells were washed again twice with PBS buffer and coverslip was placed on a glass slide for imaging.

Cellular uptake studies for US responsive drug delivery system was also performed where MDA-MB 231 cells were seeded with DMEM medium (cell density 40×10^4 cells/cm^2) in 20 cm^2 petri dish with cover slips in each well and incubated for 24 hrs. After incubation and washing twice with PBS buffer as mentioned above, Dox-MSNPs, Lip-PFP-Dox-MSNPs (US) and Lip-Dox-MSNPs diluted with medium were added to wells and incubated for 4 hrs. After removing, the old one, new medium was added to give US radiations for 5 min to Lip-PFP-Dox-MSNPs (US). Later on for washing, fixing, staining with DAPI and preparation of slides, same procedure was adopted as mentioned above.

The cell images were taken by using confocal laser scanning microscope (Zeiss, LSM 510, Germany). DAPI was excited by UV laser at 364 nm and emission was detected at 385-470 nm. Similarly, Dox was excited at 480 nm and FITC was excited at 495 nm. The emissions of Dox and FITC were detected at 560-590 nm and 519 nm respectively.[122]

2.2.2.7 Cell Culture Experiments under Hypoxia

In-vitro cell culture experiments under hypoxic conditions were also performed with MDA-MB 231 cells. Same medium, as mentioned above was used for cell culturing. Cells were maintained under hypoxic conditions in SciTive Hypoxic Workstation (Baker Ruskinn, Leads, UK) with1 % O_2, 5% CO_2 and residual N_2. For comparison, cells were grown in normoxic conditions with 7 % CO_2 and residual N_2.

2.2.2.7.1 Extracellular Acidification Test

As over expression of CA-IX under hypoxic conditions results in extracellular acidic environment. To investigate the effects of drug delivery system extra cellular acidification test was performed before and after exposure to formulations under hypoxia and normoxia. Cells were seeded in 6 well plates and incubated in hypoxic and normoxic conditions for 24 hrs. Later on, cells were incubated with different formulations diluted with medium for 24 hrs. The pH of each well was measured before and after treatment.

2.2.2.7.2 Immunoblotting

The over expression of CA-IX enzyme in hypoxic conditions was validated. Cells were seeded in 6 well plates with density of 25 X 10^4 cells/cm^2 and maintained under hypoxic and normoxic conditions for 24 hrs. Afterwards, media was removed and cells were washed wit PBS buffer. Later on cells were harvested and pellet was obtained, subsequently lysed with lysis buffer containing (4% SDS, 100mLTris/HCl and 150mM NaCl, pH 7.4) and stored at -20ºC. After determining total protein concentration with protein assay kit (Bio-Rad, Munich, Germany), western blot was performed for evaluation of CA-IX and HIF-1α expression. Briefly, 50µg of protein was loaded to 10% SDS gel and blotted with Trans Blot Turbo blotting system (Bio-Rad). Membrane was blocked with 5% milk in TBS-T for tubulin (sigma). For CA-IX (H-11) monoclonal antibody was used as primary antibody against CA-IX enzyme. [123,124] Similar procedure was adopted after treatment with different samples including pure

CA-IX inhibitor, Lip_c and Lip_c-Dox-MSNPs to assess the inhibition of CA-IX with 24 hrs incubation time.

2.2.2.7.3 *In-Vitro* Cytotoxicity (MTT Assay)

To evaluate the *in-vitro* cytotoxic effects of Lip_c-Dox-MSNPs cell viability assay was performed under hypoxic conditions. Briefly, MDA-MB 231 cells were seeded in 96 well plates and incubated overnight under normoxic and hypoxic conditions. The next day, after medium aspiration, formulations dissolved in medium were added. Cells were incubated for 4 hrs and 24 hrs, followed by same procedure for MTT assay under hypoxic and normoxic conditions, as mentioned in section 2.2.2.6.1.1. The amount of Dox used in each sample was 100 µg/ml and molarity of CA-IX inhibitor was 360 nM which is higher than minimum effective concentration of CA-IX inhibitor (Ki=0.9 M). Finally, the absorbance was measured with plate reader (FLUOstar, BMG Labtech GmbH, Germany) at 570 nm to evaluate the viability of cells.

Characterization	Technique used
Size distribution	Dynamic Light Scattering[125]
	Atomic Force Microscopy[126]
	Transmission Electron Microscopy[127]
Surfactant removal	Elemental analysis[128]
	Dynamic Light Scattering
	Fourier Transform Infrared spectroscopy[129]
Morphological studies	Transmission Electron Microscopy
	Cryogenic Transmission Electron Microscopy[130]
	Scanning Transmission Electron Microscopy[131]
Lipid Coating	Transmission Electron Microscopy
	Cryogenic Transmission Electron Microscopy
	Atomic Force Microscopy
Surface area, pore size and pore volume	Nitrogen sorption-desorption[132]
Drug loading and Drug release	UV-Vis spectroscopy[133]
Ultrasound contrast	eZono 3000[134]
Cytotoxicity	MTT assay[135]
Cellular uptake	Confocal Laser Scanning Microscopy[136]
CA-IX expression	Western blot analysis[137]

Table 1: *Summary table showing the techniques used for different characterizations*

3 Results & Discussion

CHAPTER 1

3.1 Fabrication of MSNPs and Characterization

3.1.1 Fabrication of MSNPs

MSNPs were prepared by a two-step sol-gel method involving hydrolysis and condensation as shown in figure 11. TEOS undergoes hydrolysis to form silanol and later condensation and polymerization between silanol-ethoxy groups or solanol-silanol result in formation of siloxane bridge which builds up entire silica structure.[138]

TEOS has an isoelectric point (IEP=pH 2) and exist as a negative charge in basic pH. This negatively charged silica source can interact with positively charged moieties such as cationic surfactants. Contrarily TEOS exists as a positive charge in pH<2 where it can interact with anionic surfactants. Here in we have adopted cationic surfactant and basic environment.

Hydrolysis :

$$Si\text{-}(O\text{-}C_2H_5)_4 + H_2O \leftrightarrow HO\text{-}Si\text{-}(O\text{-}C_2H_5)_3 + C_2H_5\text{-}OH \quad (1)$$

Condensation :

$$(H_5C_2\text{-}O)_3\text{-}Si\text{-}OH + HO\text{-}Si\text{-}(O\text{-}C_2H_5)_3 \leftrightarrow (H_5C_2\text{-}O)_3\text{-}Si\text{-}O\text{-}Si(O\text{-}C_2H_5)_3 + H_2O \quad (2a)$$

$$(H_5C_2\text{-}O)_3\text{-}Si\text{-}O\text{-}C_2H_5 + HO\text{-}Si(O\text{-}C_2H_5)_3 \leftrightarrow (H_5C_2\text{-}O)_3\text{-}Si\text{-}O\text{-}Si\text{-}(O\text{-}C_2H_5)_3 + R\text{-}OH \quad (2b)$$

Figure 11*: Two step hydrolysis and condensation method*

The size of MSNPs depends upon different factors including CTAB/TEOS ratios and pH of the medium. The pH of the solution directly effects the charge density of silica source which ultimately controls the silane hydrolysis and siloxane condensation rates.[139] We have used five different molar mass ratios where the amount of CTAB was changed but TEOS amount was fixed to 2.25 mmoles. For the basic catalytic reactions different bases like NaOH, TEA and $NaHCO_3$ were used and details are shown in table 2. For the optimization of required size different formulations were successfully prepared and they were initially characterized for size and surface charge.

Molar Ratio (CTAB/TEOS)	Components	n (mmol)	Mass (mg)
0.58	$NaOH/TEA/NaHCO_3$	0.7/0.56/0.7	28/83.5/58.8
	CTAB	1.3	473.5
	H_2O	2668	48000
0.5	$NaOH/TEA/NaHCO_3$	0.7/0.56/0.7	28/83.5/58.8
	CTAB	1.12	408
	H_2O	2668	48000
0.4	$NaOH/TEA/NaHCO_3$	0.7/0.56/0.7	28/83.5/58.8
	CTAB	0.9	326
	H_2O	2668	48000
0.3	$NaOH/TEA/NaHCO_3$	0.7/0.56/0.7	28/83.5/58.8
	CTAB	0.67	245
	H_2O	2668	48000
0.2	$NaOH/TEA/NaHCO_3$	0.7/0.56/0.7	28/83.5/58.8
	CTAB	0.45	163
	H_2O	2668	48000
0.12	$NaOH/TEA/NaHCO_3$	0.7/0.56/0.7	28/83.5/58.8
	CTAB	0.27	98
	H_2O	2668	48000

***Table 2**: Different molar mass ratios (CTAB/TEOS) with different bases (NaOH, TEA, $NaHCO_3$)*

3.1.2 Hydrodynamic Size and Surface Charge

The size of nanomaterials is most critical factor for their applications in nanomedicine. The size and surface charge of particles were characterized with DLS and LDV and results are shown in table 3. MSNPs of different sizes, ranging from 50 nm to 250 nm were prepared. The results show that using different molar mass ratios of CTAB/TEOS with different pH solutions, different size MNSPs can be produced.

The decrease of particle size by increasing the CTAB/TEOS was reported. Similar pattern starting from 0.2 to 0.5 molar ratio can be seen in our results with TEA or NaOH as shown in figure 12. It was found that molar mass ratio less than 0.1 was resulted in aggregation. This effect could be due to hydrophobic interaction between surfactants which were not part of mesostructured and adsorbed on particle surface in the form of monolayer with hydrophobic chain exposed to solution. On the other hand, the higher CTAB/TEOS ratios can produce uniformly dispersed MSNPs due to adsorption of surfactant micelles on the particle causing electrostatic repulsion.[115]

The pH value also effects the size of the particles. The pH values for the final solution of NaOH, TEA and $NaHCO_3$ were 11, 9 and 7.8 respectively. As the fabrication of MSNPs is based upon hydrolysis and condensation of TEOS and by increasing pH the hydrolysis can occur at faster rate. As a result, reduction in size was observed with increase in pH. The particle sizes of the same molar ratios with TEA were slightly higher than the sizes with NaOH.

In case of $NaHCO_3$ no significant effects in size were observed with different CTAB/TEOS ratios. $NaHCO_3$ can produce very slightly basic environment, which is very close to neutral pH. As mentioned above, the hydrolysis and condensation reactions are dependent on the pH of environmental solution and pH close to neutral pH does not have significant effects, resulting in very slow or negligible hydrolysis of TEOS.

Molar Ratio (CTAB/TEOS)	Size and Surface Charge	NaOH	TEA	$NaHCO_3$
0.58	**Size ± SD [nm]**	81.31 ± 3.11	90.29 ± 5.45	72.45 ± 0.29
	PDI	0.32	0.46	0.11
	Zet. Pot ± SD [mV]	41.10 ± 2.97	35.90 ± 0.72	41.80 ± 1.16
0.5	**Size ± SD [nm]**	69.85 ± 2.08	74.53 ± 5.42	70.86 ± 0.16
	PDI	0.27	0.39	0.05
	Zet. Pot ± SD [mV]	32.30 ± 0.32	21 ± 2.80	47 ± 1.78
0.4	**Size ± SD [nm]**	102.70 ± 2.04	108.70 ± 33.90	70.61 ± 0.444
	PDI	0.54	0.29	0.16
	Zet. Pot ± SD [mV]	32.60 ± 1.13	22 ± 0.29	38.70 ± 1.44
0.3	**Size ± SD [nm]**	115.70 ± 1.13	131.80 ± 10.88	79.3 ± 0.62
	PDI	0.21	0.27	0.21
	Zet. Pot ± SD [mV]	29.60 ± 4.30	22.20 ± 0.78	31.30 ± 0.98
0.2	**Size ± SD [nm]**	197.10 ± 3.10	232 ± 28.18	78.57 ± 0.21
	PDI	0.24	0.53	0.27
	Zet. Pot ± SD [mV]	34 ± 0.62	20.90 ± 0.22	27.50 ± 1.56
0.12	**Size ± SD [nm]**		44.65 ± 3.46	87.35 ± 0.65
	PDI	Aggregation	0.16	0.20
	Zet. Pot ± SD [mV]		12.10 ± 1.73	23.50 ± 1.26

***Table 3**: Size distribution with PDI along with surface charge of different molar mass ratios (CTAB/TEOS) with different bases (NaOH, TEA, $NaHCO_3$)*

Our results are indicating that the size of MSNPs depends not only upon CTAB/TEOS ratios but to some extent on the pH of environmental solution. Higher the molar mass ratio of CTAB/TEOS lower would be the size of MSNPs. Contrarily in inverse relation between size of MSNPs and pH up to certain level was observed which is consistent to previous findings.[140] So, the pH and CTAB/TEOS ratios in specific range are necessary to produce stable MSNPs.

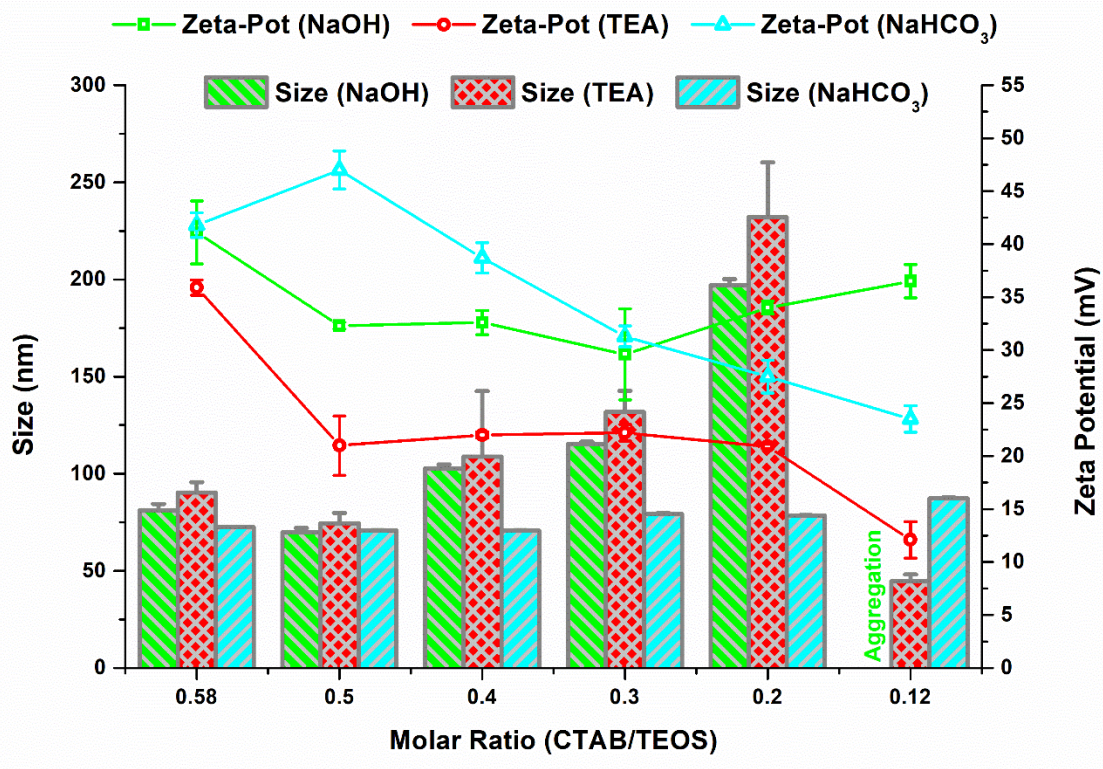

***Figure 12**: Graph showing size distribution and surface charge of different CTAB/TEOS ratios with different bases (NaOH, TEA, $NaHCO_3$)*

3.1.3 Elemental Analysis

After fabrication of MSNPs next step was the removal of surfactant template for the generation of porous structure. Here in we have adopted ethanolic extraction in acidic environment. The MSNPs were extracted for different time intervals for optimal surfactant removal. All of these samples were later characterized for elemental analysis and results are shown in table 4. As a comparison, MSNPs with surfactant template were also analysed. Here a sharp decrease in N_2, C, H and Br % ages was observed just after 5 min of extraction. So we can assume that 5 min of extraction was able to remove most of the surfactant but traces of these elements are indicating the presence of surfactant inside pores. A very slow decrease in % age of N_2, C and Br was observed from 5 min to 5 hrs. On the other hand, the % age reduction of H was very slow from 0 min to 5 hrs. This slower reduction could be due to availability of some of the water traces in the sample but it has reached to minimum after 2 to 3 hrs.

Samples		Nitrogen (%) ± SD	Carbon (%) ± SD	Hydrogen (%) ± SD	Bromine (%) ± SD
MSNPs (surf)		2.58 ± 0.06	44.30 ± 0.72	8.37 ± 0.46	19.73 ± 0.36
Extraction Time	**5min**	0.27 ± 0.02	8.83 ± 0.13	6.99 ± 0.06	3.56 ± 0.37
	10min	0.26 ± 0.01	8.19 ± 0.07	3.13 ± 0.09	3.66 ± 0.16
	15min	0.27 ± 0.01	8.81 ± 0.05	3.03 ± 0.04	3.53 ± 0.39
	20min	0.27 ± 0.02	8.52 ± 0.06	2.99 ± 0.03	5.58 ± 0.21
	30min	0.29 ± 0.02	8.08 ± 0.13	2.92 ± 0.01	5.35 ± 0.10
	40min	0.29 ± 0.02	8.25 ± 0.11	2.80 ± 0.01	3.84 ± 0.01
	50min	0.29 ± 0.02	7.10 ± 0.01	2.90 ± 0.07	3.35 ± 0.02
	1hr	0.10 ± 0.04	5.44 ± 2.40	2.06 ± 0.66	3.60 ± 0.30
	2hr	0.10 ± 0.01	3.92 ± 0.18	1.75 ± 0.01	4.59 ± 1.71
	3hr	0.09 ± 0.03	3.90 ± 0.25	1.83 ± 0.30	3.89 ± 0.69
	4hr	0.06 ± 0.03	4.04 ± 0.07	2.02 ± 0.21	3.66 ± 0.63
	5hr	0.06 ± 0.01	3.49 ± 0.17	1.78 ± 0.04	3.74 ± 0.37
	6hr	0.09 ± 0.01	3.66 ± 0.35	1.98 ± 0.04	3.94 ± 1.10
	7hr	0.10 ± 0.04	3.79 ± 0.19	1.69 ± 0.16	3.94 ± 0.22
	8hr	0.08 ± 0.01	4.20 ± 0.24	1.81 ± 0.04	4.20 ± 0.50
	23hr	0.08 ± 0.03	4.20 ± 0.17	1.90 ± 0.09	3.88 ± 0.02
	24hr	0.07 ± 0.01	4.10 ± 0.38	1.82 ± 0.18	4.02 ± 0.23

***Table 4**: Percentages by weights of nitrogen, carbon, hydrogen and bromine in MSNPs after different extraction times.*

3.1.4 Nitrogen Sorption Analysis (BET)

The role of extraction in surfactant removal was assessed with nitrogen sorption analysis because the surface area and porous structure was directly linked with availability of surfactant in pores. We have characterized same samples with different extraction times as we have analysed for elemental analysis. The results of different samples in terms of their surface area, volume, pore diameter and total pore volume are shown in table 5, where surface area and volume were obtained from BET while pore diameter and total pore volume

were obtained from BJH method. Here we can observe that MSNPs (surf) without washing has not shown larger surface area due to the fact of available surfactant template in pores with very low volume but after extraction this surfactant was removed and an increase in surface area was observed. Here, even after 5 min of extraction a larger surface area was created which is above 800 cm^2/g with volume of 191.25 cm^3/g at standard temperature and pressure (STP). The pore size of 2.43 nm in diameter with 0.84 cm^3/g also indicates the removal of surfactant. We have observed that with increasing extraction time the surface area and volume have been increased but the pore diameter remained the same for all the samples. As the data shows the maximum of the surface area and surface volume were attained with 6 hrs of extraction which are 1134 cm^2/g and 260.61 cm^3/g at STP respectively and corresponding total pore volume was 1.072 cm^3/g.

Afterward a decreasing trend was observed in surface area and volume where 7 hrs and 8 hrs extractions have shown small reduction but later on a significant reduction was observed. This significant difference might be due to the longer time extraction of MSNPs in acidic ethanol, which resulted in abrasion of particles at edges. This damage of the MSNPs has reduced the surface areas and volumes significantly, but the pore size remained the same however, the total pore volumes have been kept on reducing. These findings show that optimal extraction time is also very important for the surfactant removal without damaging the structure of MSNPs. By our results, we can assume that 6 hrs extraction time[141] is optimal duration for surfactant removal and these MSNPs were further used for other experiments.

The nitrogen adsorption-desorption isotherm of MSNPs with 6 hrs extraction time is shown in figure 13. Insight is the pore diameter measured with BJH method. Here it can be observed that adsorption-desorption isotherm is similar to type-IV isotherm with hysteresis loop where lower branch is representing addition of adsorption gas while upper branch represents withdrawal of the gas. This specific shape of hysteresis loop is directly associated with capillary condensation in the filling and emptying of mesoporous structures. These

results are clearly indicating mesoporous nature of our carriers and these finding are similar to Seyyed *et. al.*[142]

Samples		Surface Area (m^2/g)	Volume (cm^3 (STP)/g)	Pore diameter d_{peak} (nm)	Total Pore Vol (cm^3/g)
MSNPs (surf)		42.75	9.80	-	0.34
Extraction Time	**5min**	832.30	191.25	2.43	0.84
	10min	845.00	194.16	2.43	0.87
	15min	924.10	212.33	2.43	0.96
	20min	969.60	222.76	2.43	0.82
	30min	939.40	169.88	2.43	0.72
	40min	950.30	218.34	2.43	0.98
	50min	964.35	159.53	2.43	0.75
	1hr	984.60	230.81	2.43	0.81
	2hr	995.38	228.69	2.43	0.67
	3hr	918.25	210.97	2.43	0.60
	4hr	909.60	208.99	2.43	0.62
	5hr	1084.40	249.14	2.43	0.75
	6hr	1134.43	260.61	2.43	1.07
	7hr	1121.10	211.63	2.43	0.73
	8hr	1098.20	252.31	2.43	0.61
	20hr	902.70	238.48	2.43	0.81
	23hr	932.57	214.26	2.43	0.66
	24hr	913.52	209.88	2.43	0.65

***Table 5**: Surface area, surface volume, pore size and total pore volume of MSNPs after different extraction times.*

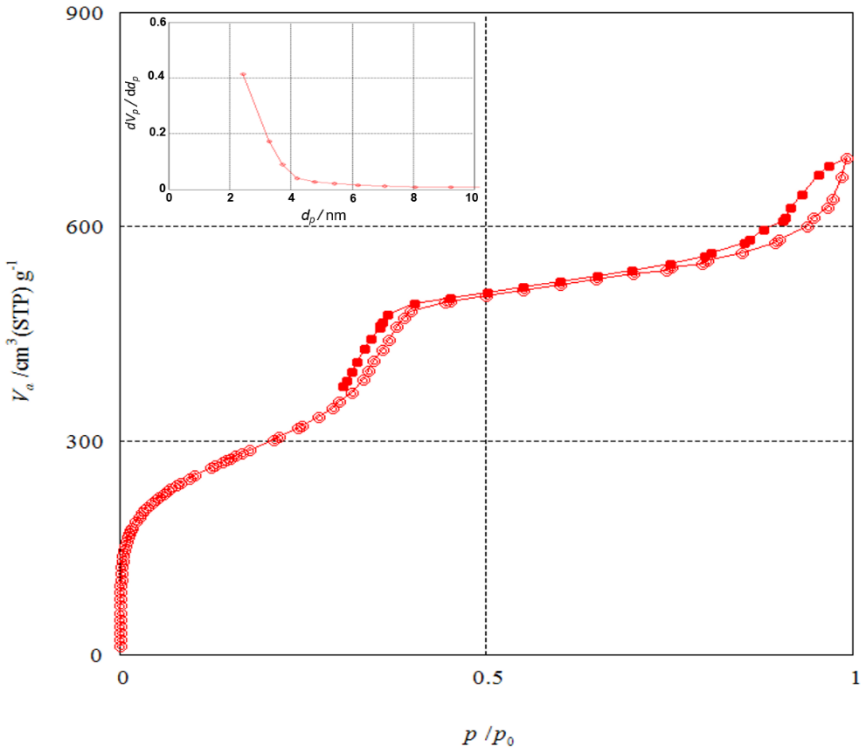

***Figure 13**: Nitrogen Adsorption-desorption isotherm with pore size of MSNPs after extraction.*

3.1.5 Fourier Transform Infrared (FTIR) Spectroscopy

The development of MSNPs and removal of surfactant was characterized by FTIR and results are shown in figure 14. CTAB surfactant typically showed two intense peaks in the region of 2800-3200 cm^{-1} which are corresponding to symmetric (2850 cm^{-1}) and asymmetric (2915 cm^{-1}) stretching vibrations of CH_2 chains. The presence of these specific peaks in spectrum of CTAB-MSNPs shows the availability of surfactant template in pores, which was later removed with extraction. In case of extracted MSNPs, the absence of these CTAB peaks indicates the removal of surfactant.[143,144]

On the other hand, FTIR spectrum of CTAB-MSNPs showed that a broad band in the region of 1000-1300 cm^{-1} is characteristic feature of Si-O-Si. The peaks at 1042 cm^{-1} and 953 cm^{-1} are typically for asymmetric vibrations of Si-O-Si and Si-OH respectively. The signals at 796 cm^{-1} are attributed to symmetrical stretching of Si-O-Si vibrations and signals at 440 cm^{-1} are due to bending vibrations of Si-O-Si. Our findings are in accordance to already reported data.[145]

FTIR Spectrum is not only showing the surfactant removal but also the formation of silica structure.

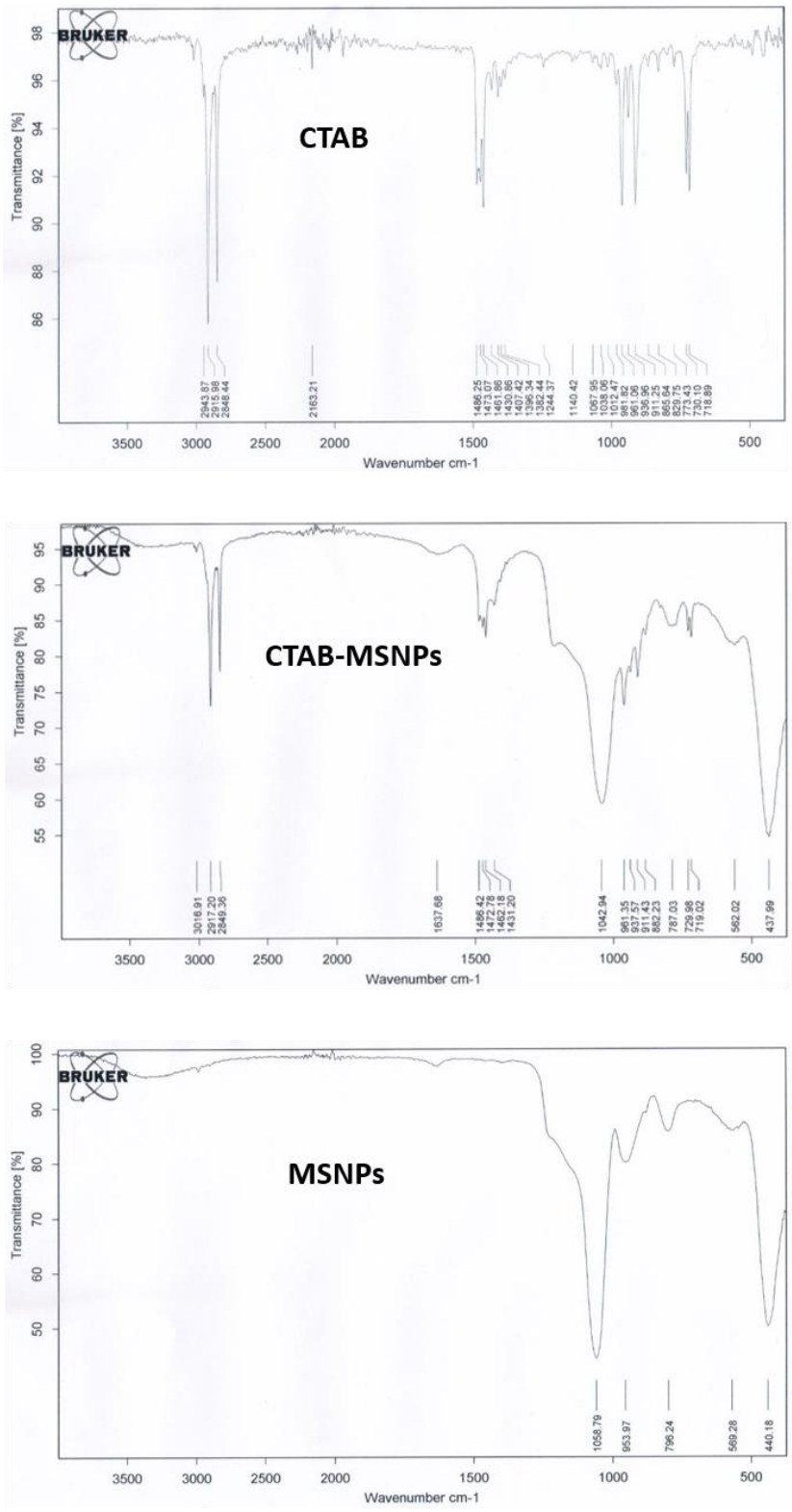

***Figure 14**: FTIR spectrums of CTAB, CTAB-MSNPs and MSNPs*

3.1.6 Morphological Studies

3.1.6.1 Atomic Force Microscopy (AFM)

For the initial characterization of morphology and size distribution, AFM investigations were performed. Although we were unable to visualize the porous structure of MSNPs but AFM images can help to realize the real size distribution. Figure 15 A is amplitude trace image of MSNPs where we can observe that MNSPs are well dispersed with no significant aggregation. The particle size was less than 100 nm which corresponds to the size distribution characterized with dynamic light scattering. Most of MSNPS were completely round in shape however, few elongated MSNPs can also be observed. Figure 15 B and 15 C are amplitude phase and 3D height traced micrographs of a single particle respectively where the shape of the particles can be visualized. We can see that particles are not completely round in shape but a little bit elongated which is in accordance to the already reported shape of MSNPs.[146] The morphology of MSNPs indicates that hexagonal array was extended more to one direction than others.

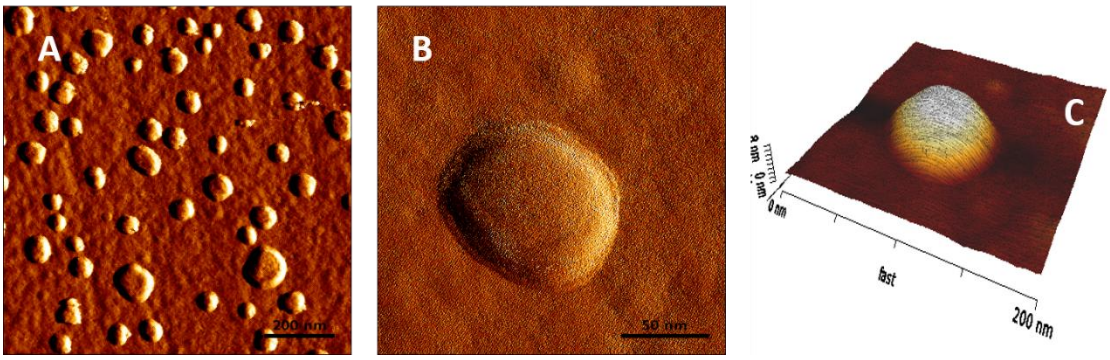

***Figure 15**: AFM micrographs of (A & B) amplitude trace and (C) height trace of MSNPs*

3.1.6.2 Transmission Electron Microscopy (TEM)

Morphological studies of MSNPs were performed with TEM and results are shown in figure 16. MSNPs were visualized before and after surfactant removal. Here the figures 16 A, 16 B and 16 C are showing the images of MSNPs with surfactants. Although the porous structure was not visualized because of presence of surfactant template but light and dark contrast could be due to

CTAB and TEOS. We can observe that particle size is less than 100 nm which is similar to that measured by DLS. Few of the MSNPS were not completely round as in figure 16 B, where face to face attachment is showing that few of MSNPs are of hexagonal shape with round edges due to porous hexagonal array which extended to the edges of the MSNPs. The dark spots around the particles in figure 16 B and C, are in the range of 2nm which might be the round micelles of CTAB. On the other hand, we can observe the porous structure of MSNPs after extraction of surfactant as shown in figure 16 D and E. The pore size was in the range of 2-3 nm, which corresponds to BJH pore size measurement. A uniform hexagonal porous structure can be observed in figure 16 E, where insights of image E (i & ii) are showing Fast Fourier Transform (FFT) and Inverse Fast Fourier Transform (IFFT) respectively. This FFT and IFFT patterns are clearly indicating hexagonal structure and further confirm the porosity of MSNPs.

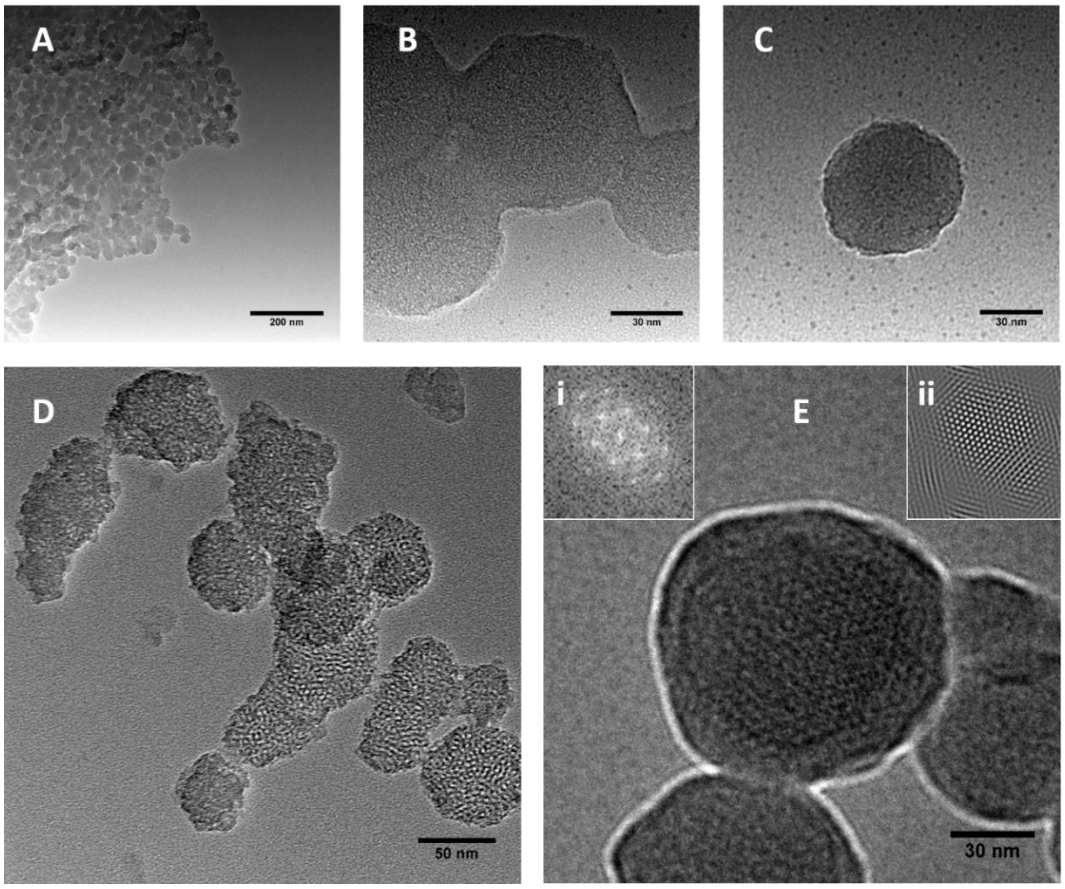

***Figure 16**: TEM images of MSNPs (A-C) with surfactant and (D&E) without surfactant where E(i) & E(ii) are representing FFT and IFFT patterns respectively*

3.1.6.3 Scanning Transmission Electron Microscopy (STEM)

The structural morphology of MSNPs was further confirmed with STEM. The dark field images were taken and micrographs are represented as figure 17. The size distribution in figure A shows that the MSNPs were in the range of 50-100 nm. These findings are similar to already reported data.[131,147] Figure 17 B shows MSNP with ordered 2D hexagonal porous structure with closely packed porous array. The shape of MSNPs was round to hexagonal with round edges. The pore size was almost 2-3 nm, which is similar to the results found by BJH pore measurement and by TEM images.

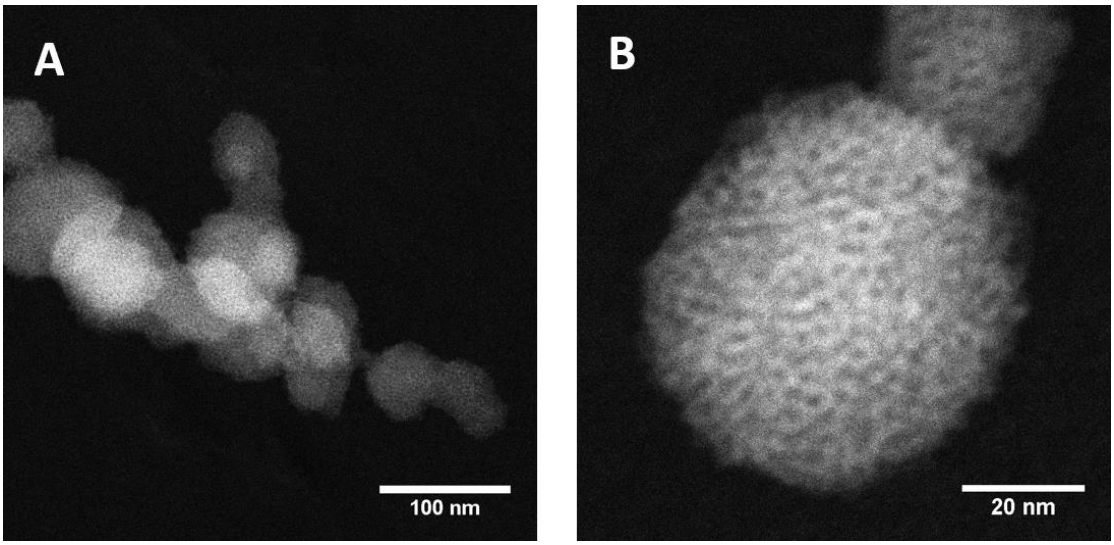

Figure 17*: STEM micrographs showing shape and porous structure of MSNPs*

3.1.7 UV-Visible Spectrophotometer

The absorption spectrum of DOX was measured with UV-visible spectrophotometer in the range of 300-700 nm. The results showed that maximum absorption peak of Dox was at 495 nm and 482 nm when dissolved in water and PBS buffer (pH 7.4) respectively. Different concentrations of Dox were prepared in water and buffer ranging from 1 µg/ml to 25 µg/ml and absorbance for each concentration was measured on corresponding wavelength. The absorbance value as a mean of triplicate was calculated and

results are presented in graphs as shown in figure 18. The drug entrapment and release profile were measured with the help of these calibration curves.

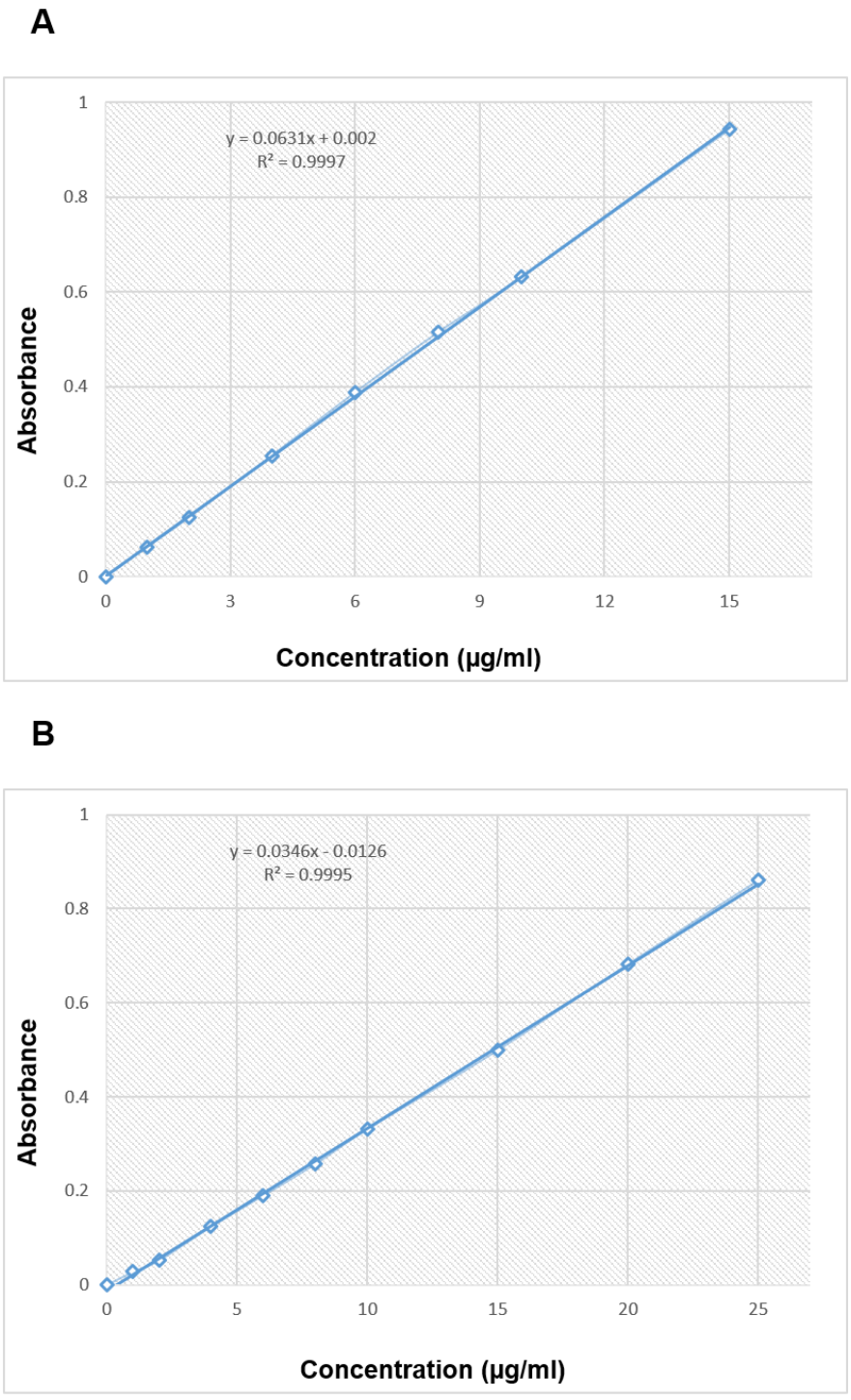

***Figure 18**: Calibration curves of Dox dissolved in (A) water and (B) PBS 7.4 pH.*

CHAPTER 2

3.2 Lipid Coated MSNPs as a Drug Delivery System

3.2.1 Liposome Preparation

Protocells in the form of liposomes were developed by thin layer hydration method, previously adopted by our research group. Different lipids were used in different molar percentages and finally DPPC, DOTAP and cholesterol with molar ratio of 85:3:12 were selected as a carrier for coating the MSNPs surface due to their relatively non-toxic effects. Another reason was higher blood compatibility in intravenous application with lower toxicity of lipid to cell membranes due to structural nature and resemblance for enhanced cellular uptake which has already been defined in previous reports.[48,49]

3.2.2 Lipid Coating of MSNPs

To optimize uniform lipid coating on the surface of MSNPs, different mass ratios of MSNPs to liposomes were used. Due to solid rigid structure, MSNPs were able to be entrapped within the softer liposomal structure due to shear applied by pipetting and vortex mixing. Selection of cationic lipid was based on the concept to develop a counter charge moiety on the surface of anionic silica for uniform coating. Apart from this, the surface tension of the liposomes has also a critical role in coating of the lipid layer on MSNPs surface. The logic behind the coating of MSNPs with lipid was to integrate the gatekeeping effect to pore opening to avoid premature leakage of the drug and to sustain the release of drug through lipid layer.[47,75]

3.2.3 Characterization

3.2.3.1 Dynamic Light Scattering (DLS)

MSNPs were initially characterized by dynamic light scattering (DLS) for size distribution and for surface charge where the particle size was in the range of 118.30 ± 2.42 nm with PDI 0.16, indicating monodisperse but broad size distribution as shown in table 6. The size distribution curve is shown in

figure 19, demonstrating particle sizes between 50 nm and 300 nm with a mode at around 100 nm. By washing MSNPs the surfactant was removed from the pores and it was confirmed by the shift of surface charge from +33.60 ± 4.67 mV to -17.03 ± 3.50 mV by Laser Doppler Velocimetry. Size distribution of MSNPs along with PDI and zeta potential are shown in table 6 and figure 19.

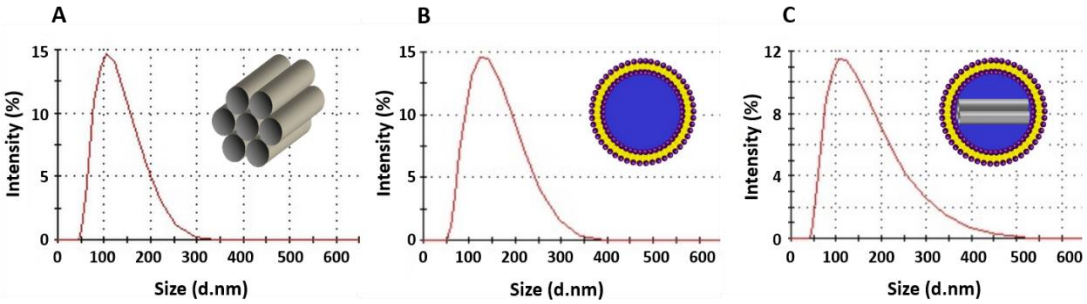

***Figure 19**: DLS measurements for Size distribution of (A) MSNPs (B) Liposomes and (C) Lip-MSNPs.*

Liposomes obtained by above mentioned method were also characterized by DLS where the measured size and zeta potential was 126.13 ± 11.77 nm and +18.16 ± 3.50 mV respectively with 0.18 PDI as in table 6. Figure 18 also shows the size distribution curve.

	Particle size ± SD [nm]	PDI	Zeta Potential ± SD [mV]	
MSNPs	118.30 ± 2.42	0.16	+33.60 ± 4.67	Before washing
			-17.03 ± 3.50	After washing
Liposomes	126.13 ± 11.77	0.18	+18.20 ± 3.50	
Lip-MSNPs	129.90 ± 10.40	0.24	+7.86 ± 2.90	

***Table 6**: Particle size, polydispersibility index (PDI) and zeta potential of MSNPs by DLS and LDV.*

DLS measurements have shown that by coating of the lipid on MSNPs, the size has been increased to 129.90 ± 10.40 nm which is almost 12 nm higher than MSNPs. Lipid coating on the surface of MSNPs resulted in a shift of charge

from negative (MSNPs) to positive side due to cationic nature of liposome. A shift of charge from -17.03 ± 3.50 mV to +7.86 ± 2.90 mV is also an indication of lipid coating as shown in table 6.

3.2.3.2 FTIR of Lipid Coating

The lipid coating of MSNPs was further ascertained with FTIR spectroscopy and results are presented in figure 20. The IR spectrum of liposomes with characteristic peaks in range of 2800-3000 cm^{-1} indicates the presence of hydrocarbons. The characteristic peaks at 2850 cm^{-1} and 2915 cm^{-1} are showing symmetric and antisymmetric stretching of CH_2 group of alkyl chain respectively. The peak at 1734 cm^{-1} is characteristic feature of ester carbonyl group of DPPC lipid.[148] On the other side the characteristic peak at 1058 cm^{-1} for MSNPs is due to asymmetric vibration of Si-O-Si groups. After lipid coating to MSNPs, similar peaks were identified which shows the lipid coating of MSNPs. This kind of IR spectrum of lipid coated MSNPs is already reported and our results are in accordance to those findings.[149]

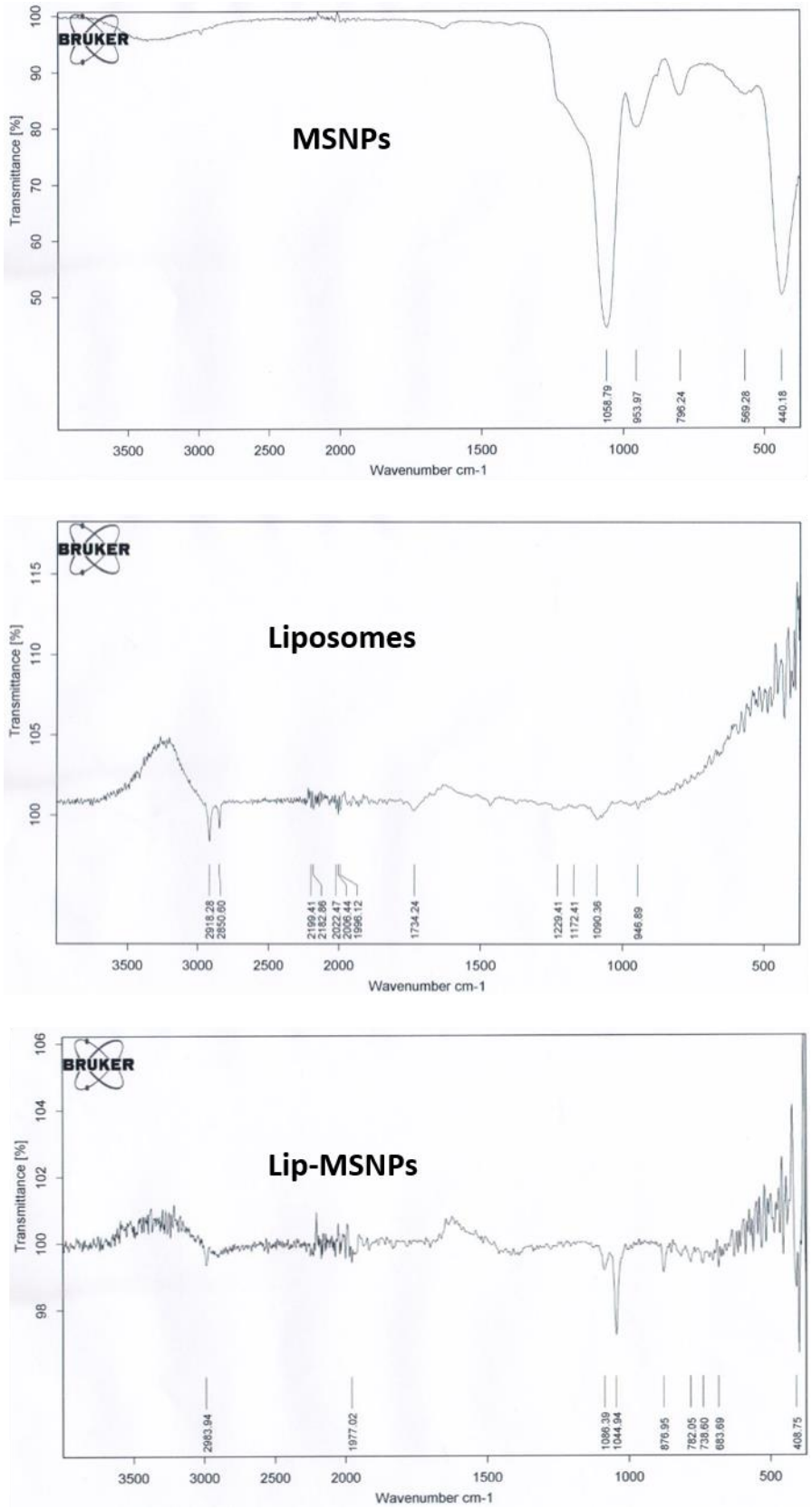

***Figure 20**: FTIR spectrums of MSNPs, Liposomes and Lip-MSNPs*

3.2.3.3 Morphological Studies with TEM and Cryo-TEM

The Cryo-TEM was performed to visualize the physical state of liposomes along with lipid coating to MSNPs. Liposomal size confirmed by CryoTEM images was in the range of 80-120 nm which is similar to the Z-average diameter measured by DLS as can be seen in figure 21 A. The liposomes are round in shape and images further confirmed the unilamelar character of the vesicles. As it was assumed that positively charged liposomes could be coated to negatively charged MSNPs. Figure 21 B is cryo-TEM micrograph of lipid coated MSNPs where a clear lipid bilayer uniform structure can be seen around MSNPs. The size of lipid layer was around 7-8 nm which is almost similar as in figure 21 A. An increase in MSNPs size from 110 nm to 130 nm was observed with lipid coating and these findings are similar to DLS size distribution. Based on literature and comparing with our findings it was established that lipid was successfully coated to MSNPs.[150] For further confirmation of lipid layer bound to MSNPs TEM micrographs were also obtained. Here negatively stained sample with 2 % uranyl acetate were visualized by TEM for good contrast as shown in figure 21 C. The thickness of outer layer shows a uniform lipid coating to MSNPs where internal core of porous structure of MSNPs is clearly observed.

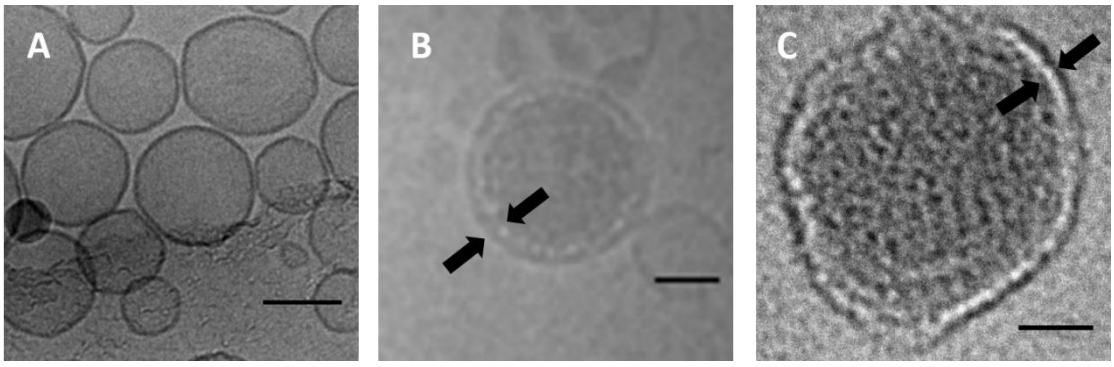

Figure 21*: Cryo-TEM images of (A) liposomes with scale bar 100 nm (B) Lip-MSNPs with scale bar 50 nm and (C) TEM image of Lip-MSNPs negatively stained with 2 % uranyl acetate with scale bar 10 nm.*

3.2.4 Drug Loading

Drug loading capacity of MSNPs was investigated by using cytostatic agent Dox as a tumor therapeutic agent. We have taken different amounts of Dox with 2.5 mg of MSNPs as mentioned in table 7. Here we have observed that the drug loading in each case was around 50 %. We can assume that due to high surface area, MSNPs have tendency to entrap large amount of drug[50,118,151] and in our studies Dox to MSNPs ratio was 1.2 mg/mg. Dox due to amine group in its structure has overall positive charge and MSNPs due to silica exhibits negative charge. Because of electrostatic interaction between Dox and MSNPs, Dox can be easily entrapped in MSNPs.[152] The high loading capacity is due to availability of large surface area of porous structure.[47] Our results have shown that larger amount of drug can be loaded in MSPNs as far as weight of MSNPs is concerned.

Dox (mg)	MSNPs (mg)	Dox/MSNPs (w/w)	Dox entrapped (mg)	%age drug entrapment
1.5	2.5	0.6	0.757	50.4
3	2.5	1.2	1.275	42.0
6	2.5	2.4	2.940	48.4
12	2.5	4.8	5.840	48.6

***Table 7**: MSNPs drug loading capacity and % age entrapment efficacy*

3.2.5 *In-vitro* Drug Release

In-vitro Dox release studies were performed to evaluate the release pattern. Here we have observed that the release of Dox from MSNPs was very slow as shown in figure 22. This sustained release behaviour of MSNPs made them suitable candidate for the delivery of chemotherapeutic drug after reaching to target site and to produce the anticancer effects for longer duration. Our data shows that % age amount of Dox release was about 7% even after 24 hrs. These findings are in accordance to Gao *et. al,* where a very sustained release

effect of drug at neutral pH has been reported.[118] We have observed from the release profile that Dox release rate from Lip-Dox-MSNPs was slower than from bared MSNPs. This relative slower release of Dox from Lip-Dox-MSNPs was due to more retention by lipid coating which prevented the release of drug. The lipid layer due to its hydrophobic nature can reduce the permeability of hydrophilic drug as a result of which lesser amount of drug release was observed. The sustained release effect due to lipid coting to MSNPs has already been reported.[75]

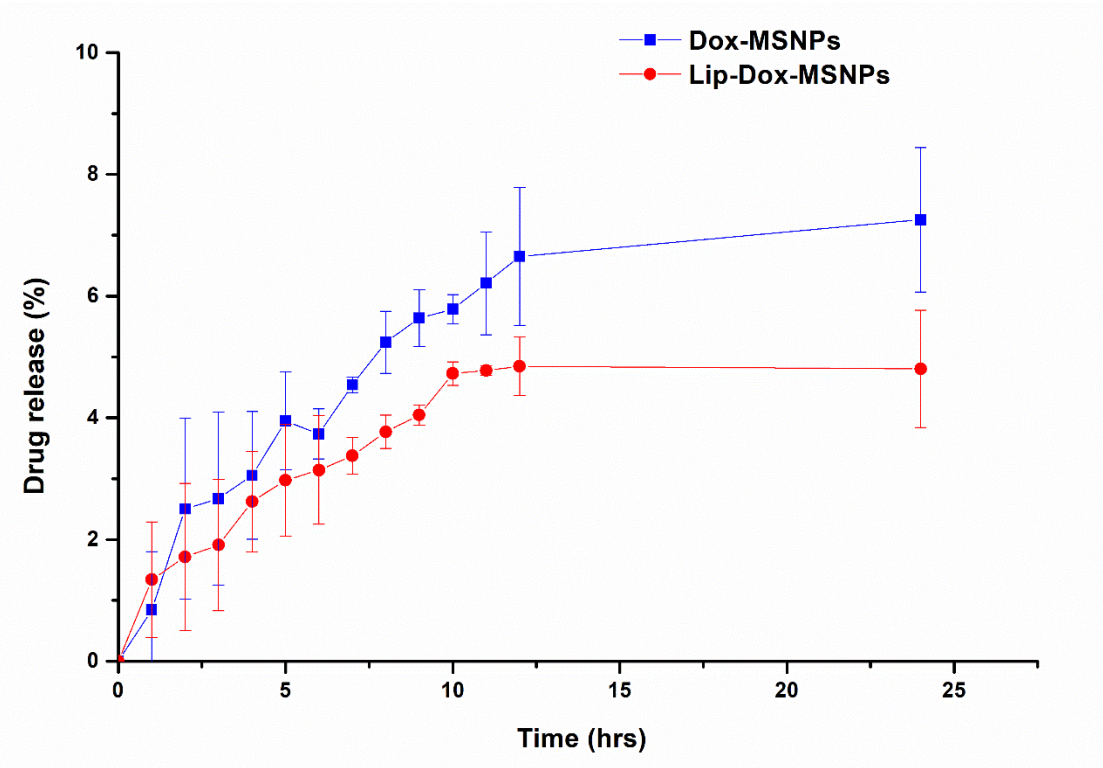

***Figure 22**: Doxorubicin release profile from Dox-MSNPs and Lip-Dox-MSNPs*

3.2.6 Drug Leakage Test

To evaluate the gatekeeping effect of lipid layer for Lip-Dox-MSNPs, drug leakage test was performed. The purpose of this test was to study the stability of drug delivery system under inert conditions. The results are shown in figure 23, where we can observe that the release of Dox from Dox-MSNPs was faster as compared to Lip-Dox-MSNPs. The amount of drug released after 10 days from Lip-Dox-MSNPs was around 6 % whereas in case of Dox-MSNPs it

was about 20 %. This faster release from Dox-MSNPs is due to absence of lipid layer which is playing a role as a gatekeeper to the pore opening. These findings are in accordance to the literature where drug leakage was minimized by lipid coating to MSNPs.[47] These results are in support to our assumption for the lipid coating to avoid or reduce premature leakage of the drug.

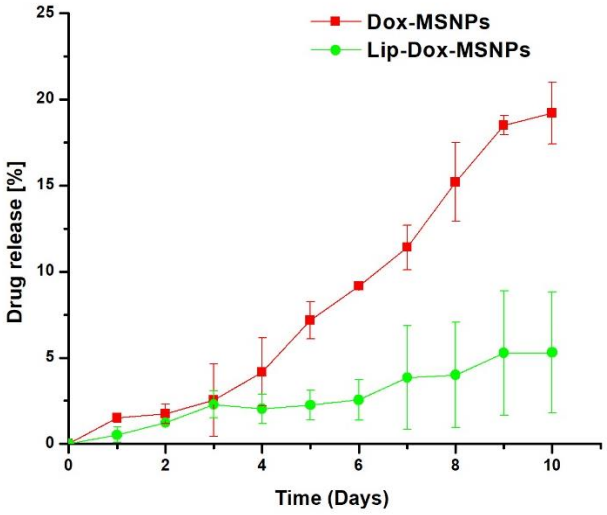

***Figure 23**: Drug leakge profile showing the release of drug from Dox-MSNPs and Lip-Dox-MSNPs under inert condition*

.

3.2.7 Cell Culture Experiments

3.2.7.1 *In-Vitro* Cytotoxicity (MTT Assay)

To evaluate cytotoxic behaviour of drug delivery system, cell viability assay was performed with MTT assay. Initially blank carriers were evaluated for their biocompatibility and inertness. The same procedure was adopted as used for drug loaded carriers. It was observed that both MSNPs and Lip-MSNPs were non-cytotoxic in nature as shown in figure 24. Here we have used just 4 hr incubation time with MSNPs and Lip-Dox-MSNPs. After evaluation of inertness of blank carriers, the study was extended to drug loaded carriers for longer incubation periods.

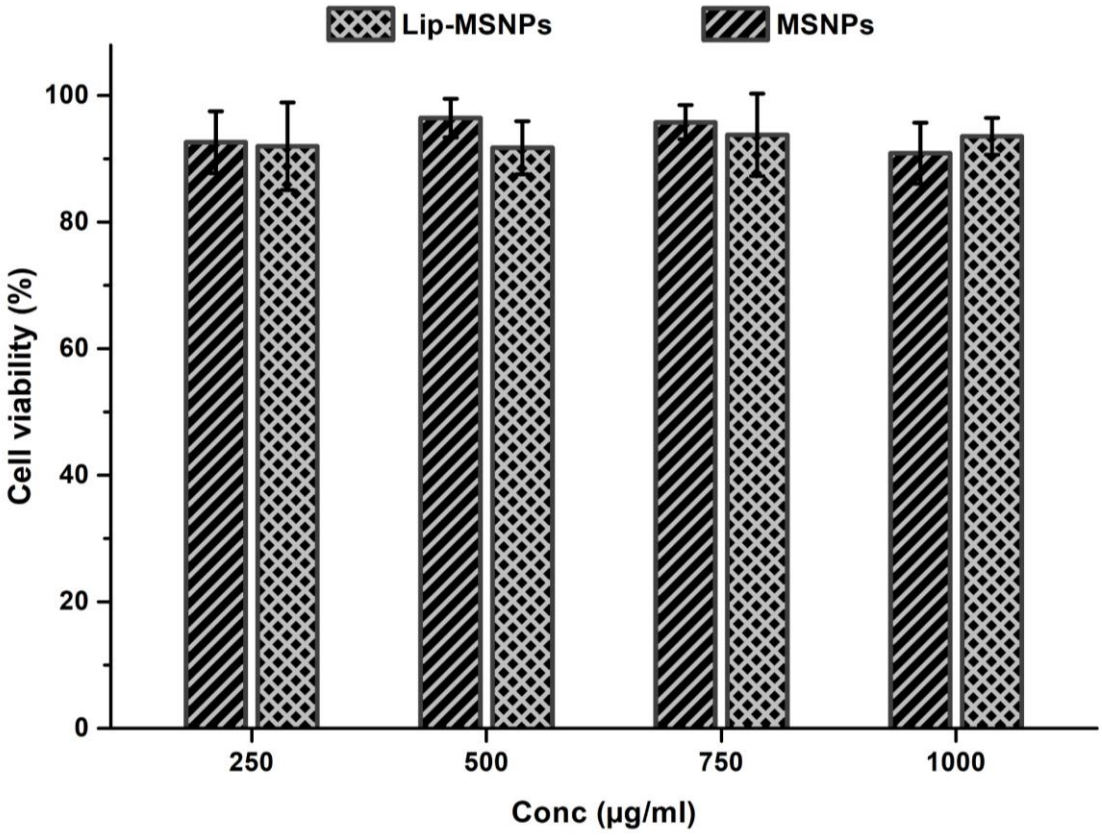

***Figure 24**: Cell viability of blank MSNPs and Lip-MSNPs*

The findings of cell viability assay have shown that after 4 hrs of incubation, Dox-MSNPs resulted in more toxicity to the cells as compared to Lip-Dox-MSNPs. But after 24 hrs, 48 hrs and 72 hrs of incubation the results were inverted and Lip-Dox-MSNPs have shown increased toxicity compared to Dox-MSNPs carriers as can be seen in Figure 25. The higher toxicity of Dox-MSNPs after 4 hrs incubation might be due to the relatively faster release of Dox from MSNPs as there was no lipid coating. On the other hand, even after higher cellular uptake of Lip-Dox-MSNPs due to lipid coating, lesser toxicity was observed due to the sustained release effect of lipid layer at the pore opening which hindered the release of drug. After 24 hrs of incubation the cytotoxicity by Lip-Dox-MSNPs was increased as compared to Dox-MSNPs and these effects are due to higher amount of drug uptake by the cells due to biocompatibility of lipid layer. Once the higher amount of carrier was available in the cells it required some time to release higher concentration of Dox as compared to Dox-MSNPs to cause more toxicity. Similar pattern of toxicity was

observed after 48 hrs and 72 hrs of incubation. Our cytotoxic studies have shown toxicity, which was not only concentration but time dependent as well.

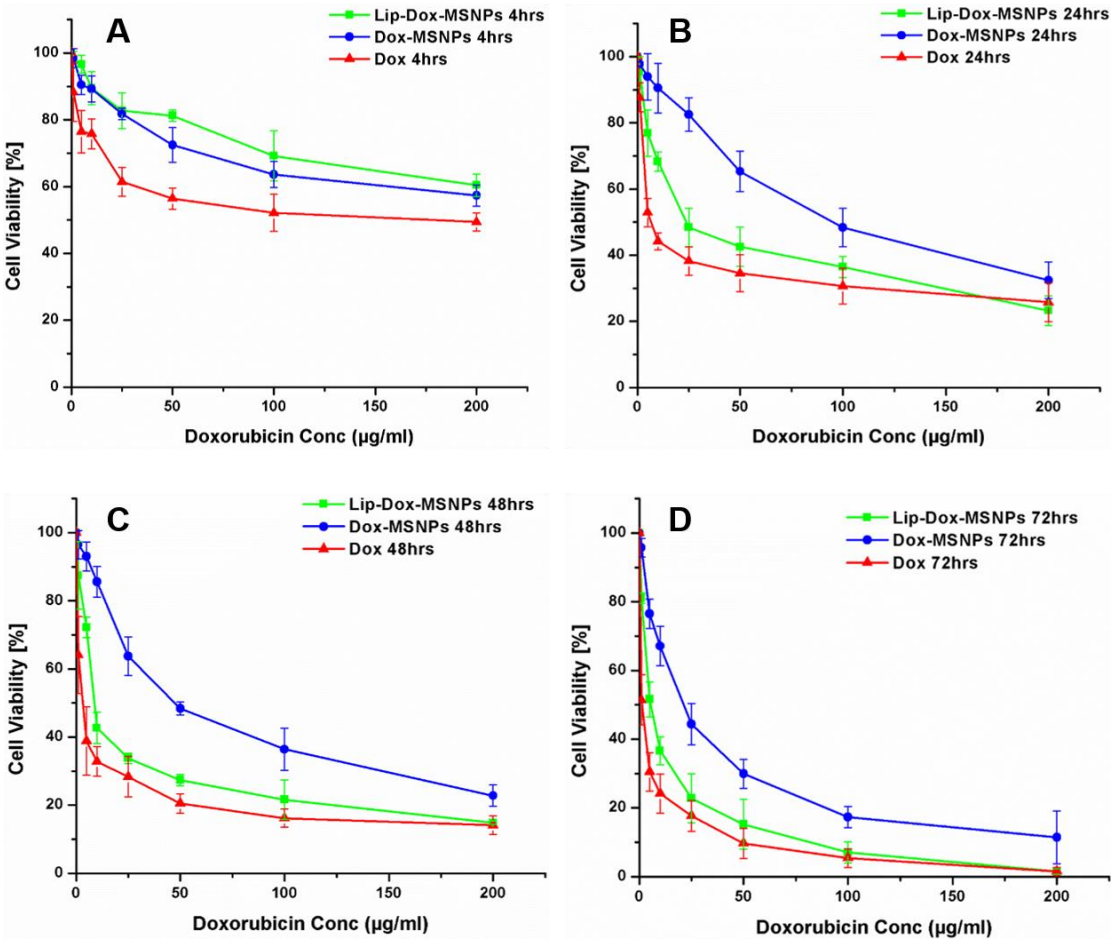

***Figure 25**: In-vitro cytotoxicity evaluation by MTT assay with SKBR-3 breast cancer cells after (A) 4 hrs, (B) 24 hrs, (C) 48 hrs and (D) 72 hrs incubation of Dox-MSNPs, Lip-Dox-MSNPs and Dox. Data is presented as mean ± SD (n=3)*

3.2.7.2 Pathway Uptake Analysis

The results of cellular uptake pathway studies are given in figure 26 which indicates that Dox-MSNPs with filipin III has shown no difference in cell viability but with chlorpromazine significant effects were observed. So we can say that Dox-MSNPs were internalized by clathrin mediated endocytosis and not by caveolea/lipid-raft mediated. In comparison, Lip-Dox-MSNPs with chlorpromazine and filipin III have shown higher cell viability, indicating involvement of both clathrin mediated and caveolea/lipid-raft mediated endocytosis. Effects of pure Dox suggest the adaptation of some other

mechanisms instead of both above mentioned pathways. These findings indicate that the internalization of Lip-Dox-MSNPs utilizes not only clathrin mediated but caveolea endocytosis pathway which is advantageous to Dox-MSNPs clathrin mediated endocytosis.

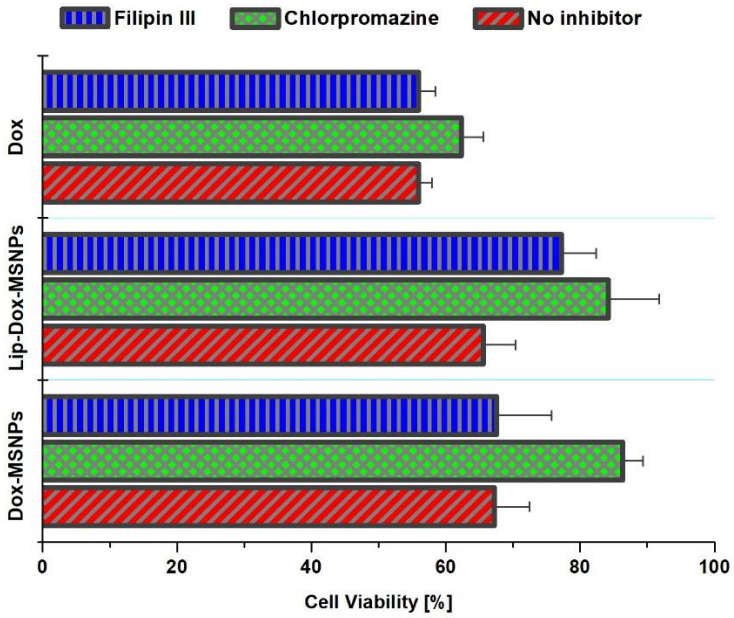

***Figure 26**: Cellular uptake pathway analysis: where MTT assay of SKBR-3 cells was performed after 30min incubation of two different pathway inhinitors including chlorpromazine (6 µM) and filipin III (3 µM) with Dox-MSNPs, Lip-Dox-MSNPs and Dox.*

3.2.7.3 Cellular Uptake Studies

Dox, a fluorescent moiety, interacts with DNA and tends to be internalized into the nucleus. To confirm the localization of Dox in nucleus of the cells, qualitative fluorescence imaging with CLSM was performed.[122] Cells were incubated with Dox-MSNPs and Lip-Dox-MSNPs containing 12.5 µg/ml of Dox for 4 hrs and after staining nucleus with DAPI, cells were fixed to glass coverslip and observed under CLSM. The microscopic images are shown in figure 27 where the localization of Dox was observed in the nuclear region along with DAPI. As postulated, stronger red intensity indicates the higher internalization of the Dox by Lip-Dox-MSNPs as compared to Dox-MSNPs. It is obvious that the higher internalization of Lip-Dox-MSNPs was due to more biocompatible protocell nature of lipid layer which enhanced cellular uptake. Although the Dox intensity of Dox-MSNPs is also indicating the delivery of drug to target site but as our

aim was to deliver the drug in higher concentrations, so Lip-Dox-MSPs were able to accomplish it. Apart from localization of Dox in the nuclear region for Lip-Dox-MSNPs, we can observe the higher intensity outside the nucleus as well. This might be due to the availability of the drug which was not completely released due to lipid layer and may require some time to get released and internalized in nucleus. These findings are supportive to our MTT assay results where after 4 hrs of incubation Dox-MSNPs have shown bit higher toxicity as compared to Lip-Dox-MSNPs and this higher toxicity would be due to relative faster release in the absence of lipid layer. Although the lipid layer has increased the cellular uptake but released the drug in a sustained manner which is also evident from 24 hrs, 48 hrs and 72 hrs toxicity results where Lip-Dox-MSNPs have shown significantly higher toxic effects to the cells.

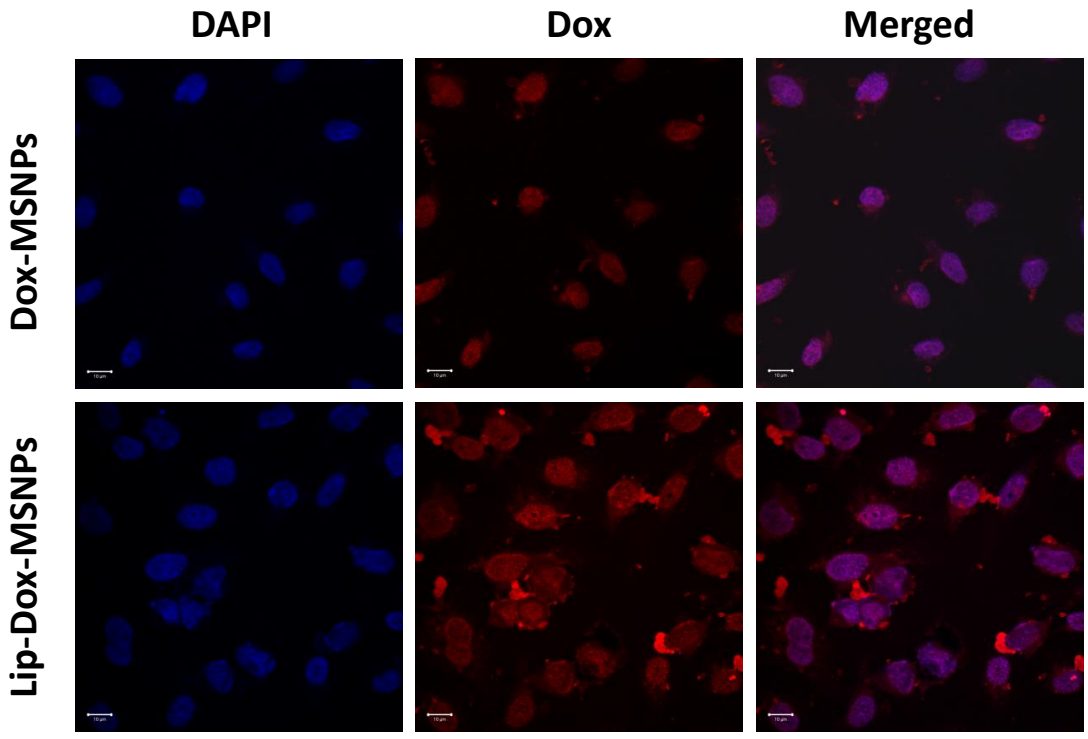

***Figure 27**: CLSM images after uptake of Dox-MSNPs and Lip-Dox-MSNPs by SKBR-3 cells where blue and red fluorescence in the nuclear region correspond to DAPI and Dox along with merged images. Higher cellular uptake of Lip-Dox-MSNPs can be visualized by higher fluorescence of Dox*

CHAPTER 3

3.3 Ultrasound Triggered Release Lipid Coated MSNPs

3.3.1 Surface Modification and Characterization

MSNPs after surface modification were characterized with FTIR spectrum and results are shown in figure 28. In comparison to unmodified MSNPs, surface modified MSNPs have shown few new characteristic FTIR peaks. These peaks are at 3354 cm^{-1} and 1631 cm^{-1} which are indicating asymmetrical NH_2 bending, which confirmed the NH_2 group existence. Although peak at 3354 cm^{-1} is not very prominent because of the OH and NH_2 group spectrum overlap. It is evident from literature that such kinds of results have been observed after surface modification of MSNPs.[153,154]

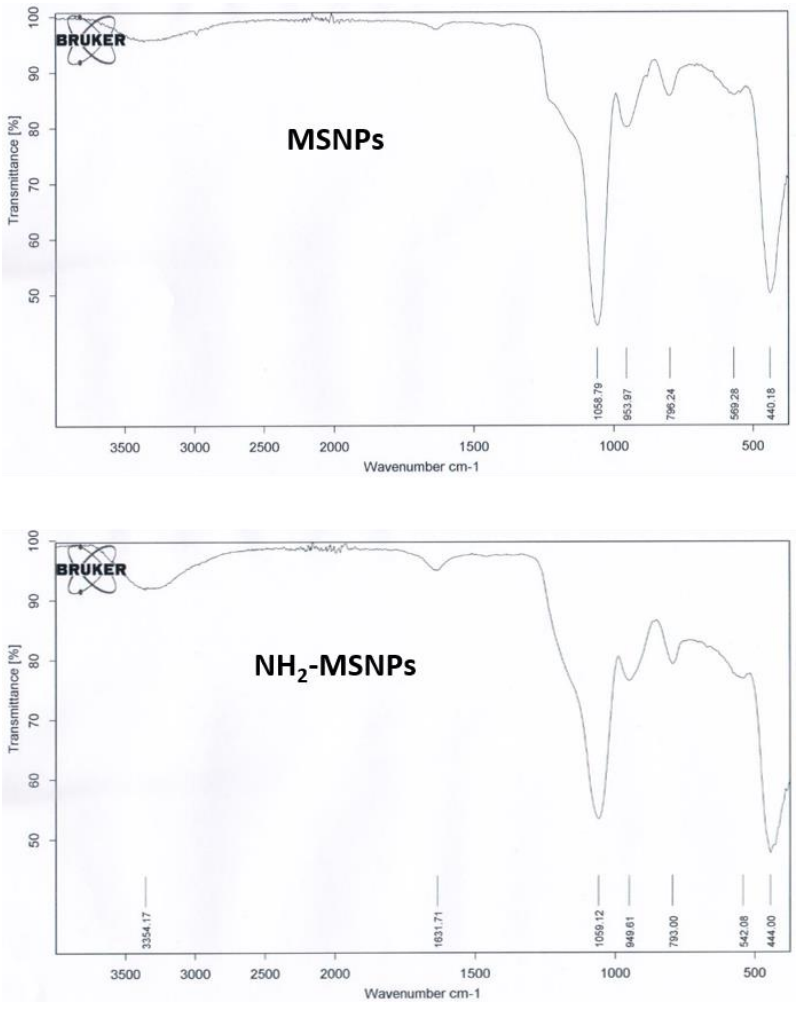

***Figure 28**: FTIR spectrums of MSNPs and surface modified NH_2-MSNPs*

Surface modification was further confirmed by surface area measurements with N_2 adsorption-desorption technique where reduction in surface area and surface volume has been observed as shown in table 8. Although the pore size remained unchanged but total pore volume was reduced.

Samples	Surface Area (m^2/g)	Volume (cm^3 (STP)/g)	Pore diameter (d_{peak}) nm	Total Pore Vol (cm^3/g)
MSNPs	1134.43	260.61	2.43	1.07
NH_2-MSNPs	935.88	215.02	2.43	1.01

***Table 8**: Surface area and surface volume of MSNPs and modified NH_2-MSNPs*

3.3.2 Preparation of Lip-PFP-Dox-MSNPs

Dox loaded MSNPS were prepared as mentioned in section 2.2.1.5. After complete washing, lyophilized Dox-MSNPs were used for the incorporation of US active PFP. Sonication at 37 kHz with 100 % power for 10 min was helpful for PFP liquid to go inside the pores of MSNPs by capillary filling which has already been reported in literature[155] The reason of using PFP is its low boiling point which is 28^{o}C. Incubating PFP with Dox-MSNPs at room temperature led to evaporation of extra liquid PFP and keeping liquid PFP inside the pores due to capillary forces, which enhance the boiling point of liquid. But combining the effect of body temperature (37^{o}C) with ultrasound can cause dislodging and vaporization of this liquid from pores and these bubbles are able to give contrast by ultrasound. PFP loading after Dox entrapment was beneficent by two ways. Firstly, the grafting and functionalization of MSNPs reduce the surface area of MSNPs for drug loading and secondly we have also observed in our experiments that pre loading of PFP to MSNPs led to evaporation of PFP during the drug loading and particle washing procedure. A very poor or negligible ultrasound contrast for such formulations has been observed. To keep PFP inside the pores, we have used dried Dox-MSNPs for incubation with PFP. Immediately after evaporation of extra liquid PFP dried PFP-Dox-MSNPs were coated with lipid layer as mentioned in section 2.2.1.4. For lipid coating we used

same ratio of lipid to MSNPs which we have already optimized with unloaded MSNPs. Lipid layer on the surface of MSNPs supposed to stay intact to keep the PFP inside the pores of carrier. These particles were resuspended in water for further experiments.

3.3.3 US Contrast Characterization and Stability

For optimization of contrast measurement, we have first observed Lip-PFP-MSNPs without drug loading before extending our studies to drug loaded Lip-PFP-MSNPs. As mentioned above for simulation and visualization of ultrasound contrast a self-made agar phantom fitted with silicon tube was used. After dispersing Lip-PFP-Dox-MSNPs in deionized water at concentration of MSNPs 1 mg/ml and 100 µl of this sample was further diluted with 100 ml of circulating medium, we have observed that our carriers are showing very good contrast even at very low concentration of MSNPs 1µg/ml. We have also performed the same experiments with non-PFP loaded but lipid coated MSNPs and found that they have not given any contrast on exposure to US waves. For stability of our Lip-PFP-Dox-MSNPs we have extended our studies for longer duration. The purpose of this study was to observe the life span of liquid PFP to be intact within pores and its effect on stability of our carriers at room temperature. To check the stability and contrast characterization we kept the carrier dispersed in purified water at room temperature and at different time intervals, including 1 hr, 2 hr, 24 hr, 48 hr, 72 hr, 96 hr and 120 hrs, 100 µl of samples were added in circulating medium and US contrast was observed with US device. Each sample has given very good contrast even after 120 hrs of span, confirming the availability of liquid PFP inside pores, and on exposure to US, conversion of this liquid to gaseous form resulting in US contrast as shown in figure 29. Our results showed that these PFP loaded MSNPs are stable in the absence of US until 5 days and can keep liquid PFP inside pores. Afterward the intensity of contrast has been reduced but still it is significant as far as the stability of US contrast is concerned.

As shown in figure 7, we worked with a circulating system to mimic blood stream, where individual sample is in circulation and in the later circulation the

intensity of contrast has been reduced leading to no contrast in the end. These results supported our hypothesis that on exposure to US waves the PFP liquid inside the pores get vaporized leading to loss of PFP in the form of gas by rupturing the lipid layer and at the end giving no more contrast. So by these experiments we can say that the lipid coated MSNPs are stable at room temperature until they are not exposed to US waves. In comparison, microbubbles have also been reported as a good US contrasting agents but their life of stability is in the range of few minutes which is a limiting factor and in contrast our drug carriers are quite stable for days and become unstable just after exposure to US waves.[69,74]

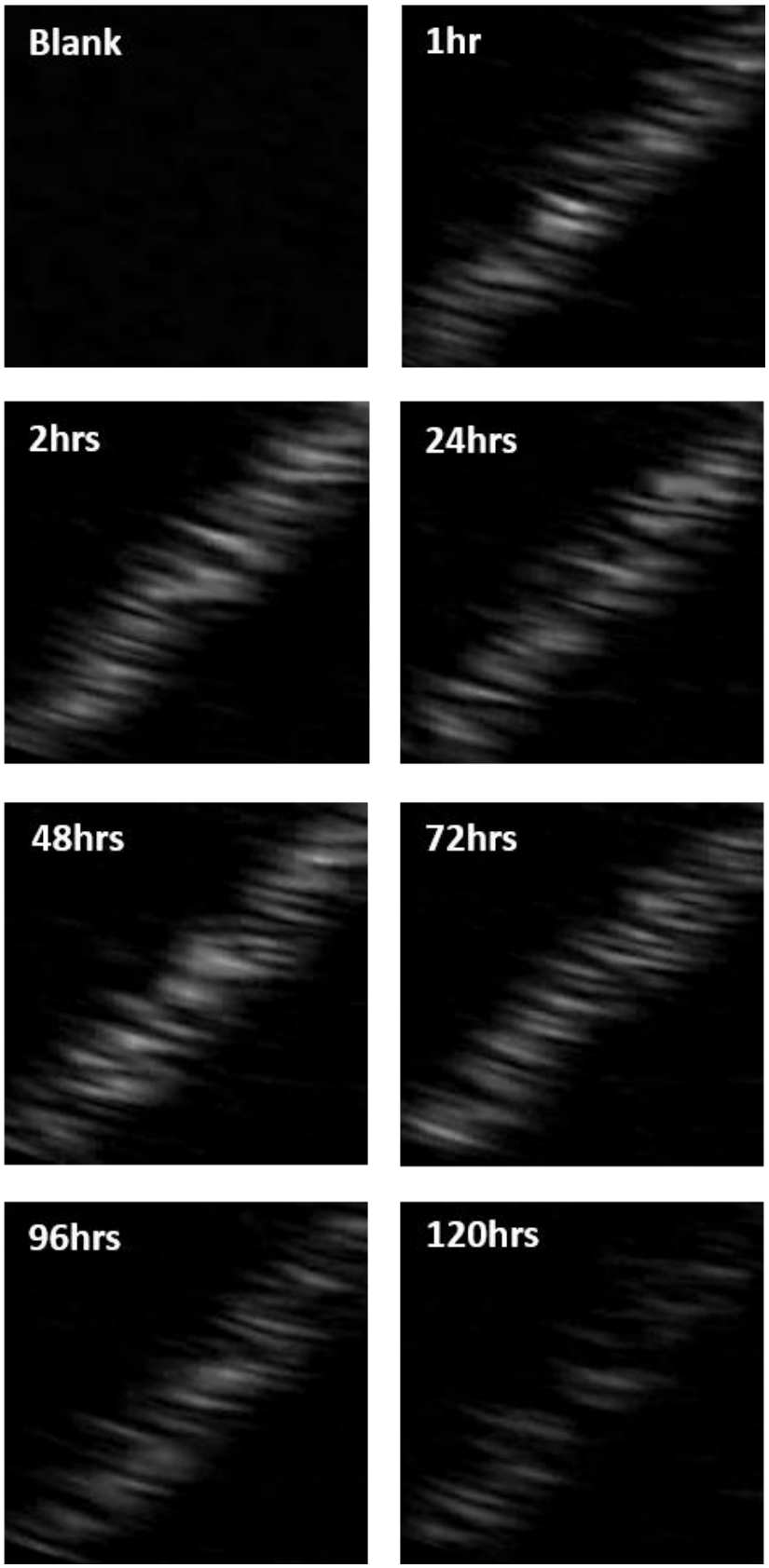

***Figure 29**: Representative images US contrast of PFP loaded Lip-MSNPs at different time intervals with 3.5MHz and MI 0.7*

3.3.4 US Triggered Release

As mentioned above drug loading of Dox was estimated by UV-spectrophotometry by comparing the concentration of Dox in the initial solution which was used for drug loading to MSNPs and the amount of unentrapped Dox in the form of supernatant after centrifugation. Based on these experiments the amount of Dox loaded in MSNPs can be easily calculated and same amount is further used for drug release profile. As per our experimental section the self-made phantom agar model was used to perform the drug release profile and for simulation purpose PBS pH 7.4 was used as a medium. For comparison we have performed drug release experiments on Lip-Dox-MSNPs and Lip-PFP-Dox-MSNPs without and with US waves respectively. In our experiments we have observed that after applying US waves the release of Dox was triggered and resulted in faster release of drug and it reached to maximum; 93 % within 3 hrs as shown in figure 30. In comparison the non-US carriers have shown slower drug release and it reached just around 10 % of total amount. We have also extended our non-US experiments for longer time and it was observed that even after 36 hrs the drug release was about 12-13 % and our findings are similar to Xin *et. al.*[50]

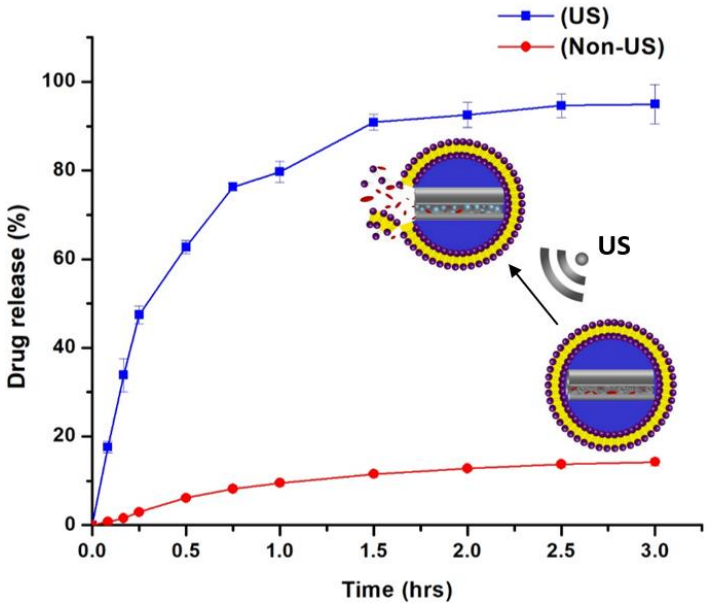

***Figure 30**: Representative image of drug release profile of Doxorubicin from Lip-PFP-Dox-MSNPs with US-irradiation versus Lip Dox-MSNPs without US-irradiation*

So it is evident from our drug release experiments that by introducing PFP in the pores and application of US waves to these carriers, the release of drug was enhanced. We can assume that thermal or mechanical energy or combination of both induces the PFP liquid to be vaporized and produce larger volume of gas. This gaseous pressure is not only responsible for the rupturing of liposomal coating but also forcing the release of the drug from pores by mechanical effects. The thermal induction of US waves on lipid layer can also enhance the rupturing effect by acoustic cavitation of lipid layer resulting in no more gatekeeping effect at pore opening.[88] Furthermore, the use of ultrasound contrasting agent upon US-irradiation can decrease the threshold of cavitation and cavitation related processes.[114]

3.3.5 Drug Leakage

In order to observe the role of PFP present in Lip-PFP-Dox-MSNPs, drug leakage test was performed. This leakage effect was compared with Dox-MSNPs and Lip-Dox-MSNPs as mentioned in section 3.2.6. The purpose of this test was to study the stability of drug inside the pores along with PFP under inert conditions. The results in figure 31 showed that the release of Dox from Lip-PFP-Dox-MSNPs was faster than Lip-Dox-MSNPs and this higher release could be due to instability of PFP inside the pores even at room temperature but this release rate was slower than Dox-MSNPs. By these results, we can assume that the availability of PFP inside the pores does not have any significant role in the release of drug under inert condition but on exposure to US-irradiation causing the triggered release, which is evident from drug release profile.

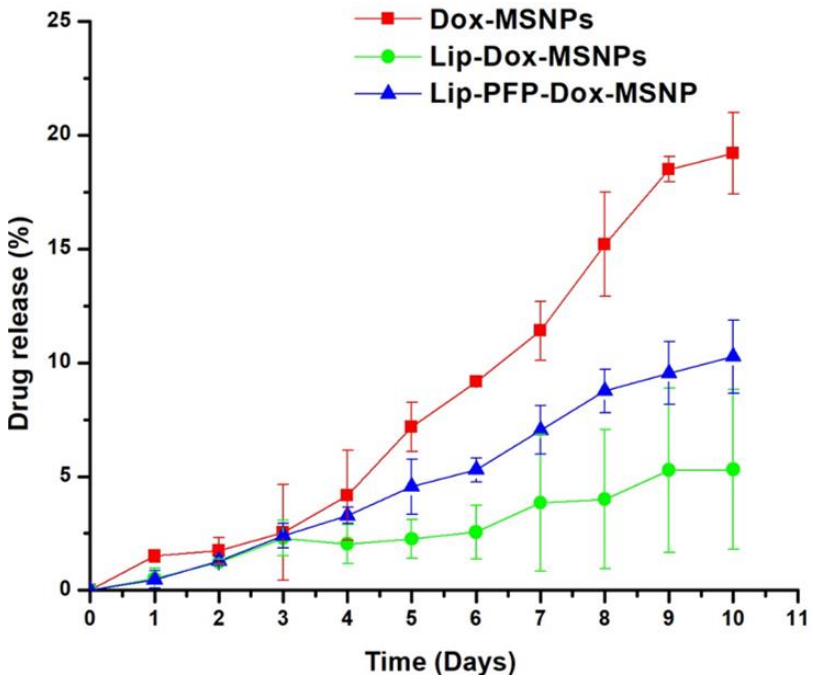

***Figure 31**: Drug release profile of Dox-MSNPs, Lip-Dox-MSNPs and Lip-PFP-Dox-MSNPs under inert conditions (non-US) with PBS buffer at 4°C*

3.3.6 Morphological Studies Before and After US

To reveal the effects of US-irradiation on PFP and lipid layer, pre and post US-irradiation TEM was performed and images are shown in figures 31 and 32. Lipid layer was stained with 2% uranyl acetate where dark and bright contrasts are representing lipid layer and MSNPs respectively. As we can see in figure 32 with black arrows, where before US, the lipid layer can be seen in the form of dark contrast around the particles in the form of uniform layer. This dark contrast is due to uranyl acetate, which made the lipid layer an electron rich area. The mesoporous character of the MSNPs cannot be seen and it maybe because of the lower magnification. In case of few particles, a lipid bilayer coating can be observed as in figure 32 B & 32 C.

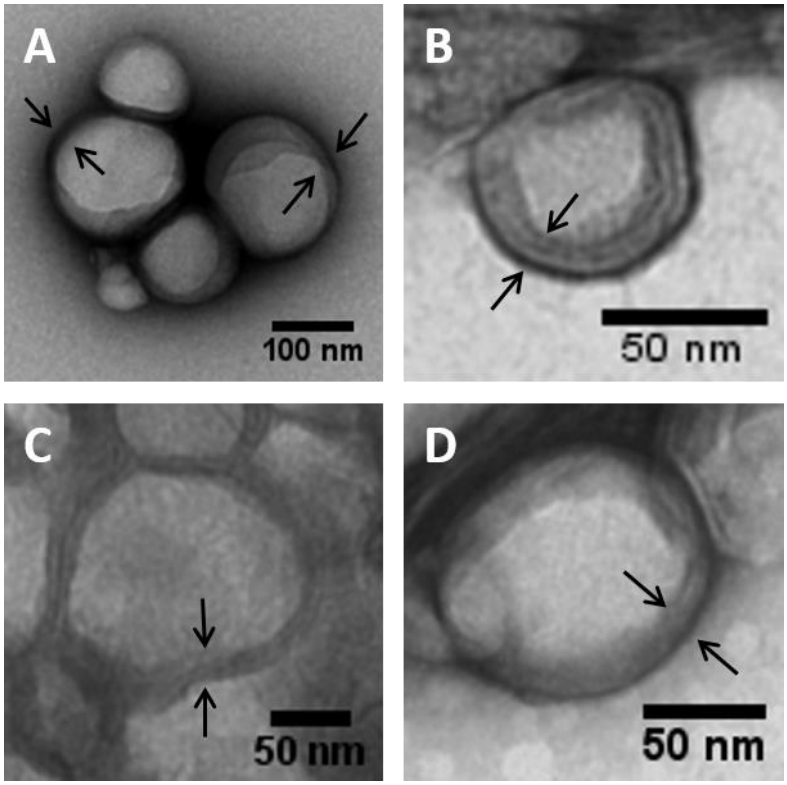

***Figure 32**: TEM micrographs of negatively stained Lip-PFP-MSNPs before US-irradiation showing uniform lipid layer around MSNPs*

To evaluate the effects of US irradiation on lipid layer the morphology of carriers was investigated with TEM and results are shown in figure 33. Here we can see that a non uniform layer around the particles, which is indicating the damage of lipid layer. The rupturing of one side of lipid layer indicates sudden exertion of gas pressure causing lipid opening from weaker side. Furthermore, this higher pressure of gas was able to damage the edges of MSNPs as well and causing the burst release of Dox. Another possibility would be the conversion of liquid PFP in to smaller bubbles sequentially attached to lipid layer and disruption of these bubbles by US, ultimately rupture the lipid layer.[88] By utilizing these reported effects of ultrasound reactive agent along with US-irradiations in our studies, we have observed the great difference of Dox release where US-triggered release of Dox is 9.5 folds higher than non-US.

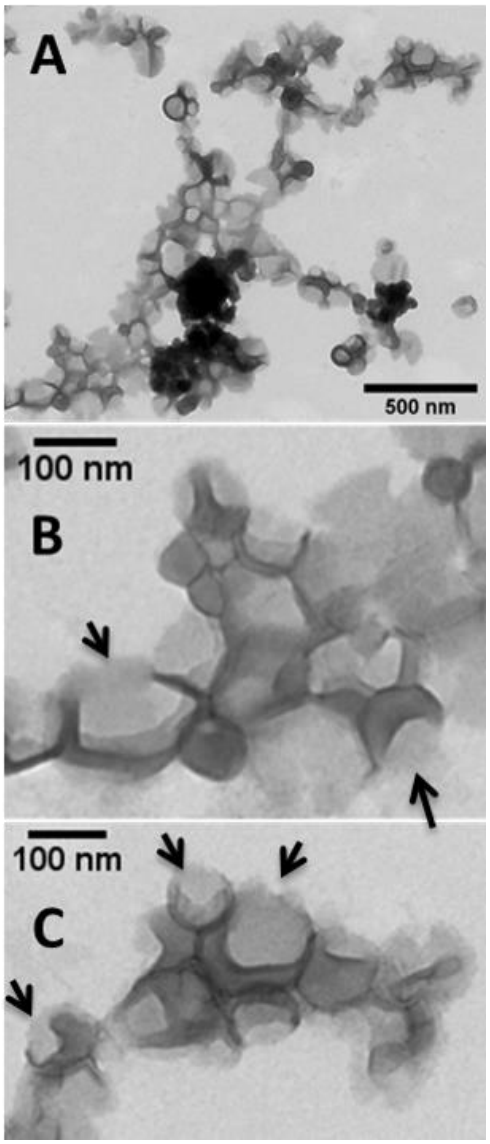

***Figure 33**: TEM micrographs of negatively stained Lip-PFP-MSNPs after US-irradiation showing bursting effects of lipid layer around MSNPs*

3.3.7 Measurement of Gas Produced by Vaporization

The amount of gas produced by liquid PFP was measured with a double syringe Luer lock system as mentioned in experimental section. Under US-irradiations, 2 ml of Lip-PFP-MSNPs dispersion containing 5 mg of MSNPs was able to produce 800 µl of gas which was significantly higher than amount of gas produced in liposomes.[119] Although the entrapped volume of PFP inside pores was much lesser but still it has produced such a large volume of gas. That would have only be possible if liquid PFP is present and converted to gas

because the volume of gas produced by same volume of liquid would be much higher than the original volume of liquid. On the other side in either case of absence of liquid PFP or presence of gaseous PFP inside pores, the amount of gas produced would be very low. These results strengthen our hypothesis of presence of liquid PFP inside pores, which on US-irradiations was converted to gas and ruptured the lipid coating.

3.3.8 Cell Culture Experiments

3.3.8.1 Carrier Inertness

To evaluate the biological compatibility of our system, cell viablility assay was performed with drug unloaded carriers. MDA-MB 231 (breast cancer adenocarcinoma) cells were incubated overnight with DMEM containing 10 % FCS in 5 ml petridish at $50x10^4$ cells/cm^2. For this study we have divided our carriers in 4 different categories including MSNPs, Lip-MSNPs, Lip-PFP-MSNPs (Non-US) and Lip-PFP-MSNPs (US). The purpose of this study was to evaluate the toxic effects of not only MSNPs and Lip-MSNPs but also the effects of US waves and PFP on the cells. Different concentrations (250 µg/ml, 500 µg/ml, 750 µg/ml and 1000 µg/ml of MSNPs) of all above four formulations in triplicate were incubated for 4 hrs keeping US-irradiated cells as blank. After removing the formulation, fresh medium was added to petri dishes and Lip-PFP-MSNPs (US) was exposed to US by using eZono device for 5 min for each plate. MTT assay was performed after overnight incubation and it has been observed that all the above mentioned formulations have not shown significant cellular toxicity. Maximum of toxicity produced by Lip-PFP-MSNPs (US) and Lip-PFP-MSNPs (Non-US) was about 7 % even at highest concentration of 1000 µg/ml of MSNPs. Although we have used lower concentrations of MSNPs in our drug-loaded carrier experiments. So we found that all our carriers, with good biocompatibility and safety, are suitable for further experiments without causing toxicity to cells and our results regarding safety of MSNPs are similar to findings in the literature.[73] Here we have used cells with medium (US) as blank and the results regarding inertness of our carriers are shown in figure 34 A.

Before extending our studies to drug loaded carriers it was necessary to perform cytotoxicity experiments with pure drug. For this purpose we have selected different concentrations of Dox divided in two different groups (US and Non-US) in triplicate. To evaluate the sono-sensitivity of the drug the above mentioned procedure of US application was adopted and MTT assay was performed. Here we have found that different concentrations of Dox, irrespective of US waves, have shown same toxicity as shown in figure 34 B. Hence it was observed that US waves don't have any significant effect on Dox cytotoxicity.

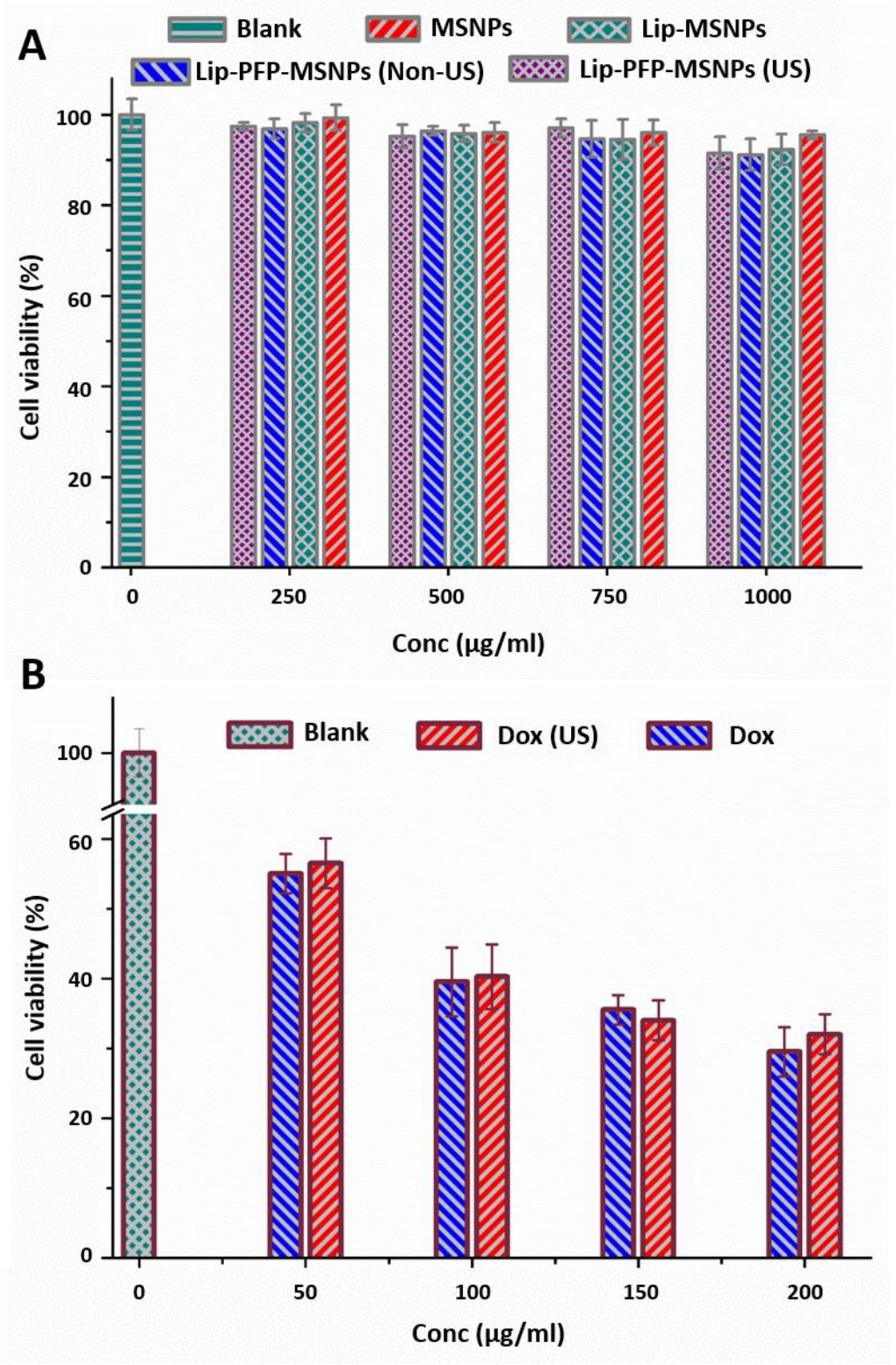

***Figure 34**: Cytotoxicity evaluation of (A) carriers (MSNPs, Lip-MSNPs, Lip-PFP-MSNPs with and without US-irradiation) and (B) Dox with and without US-irradiation (5 min, 12 MHz, MI 1.4) by using MTT assay with different concentrations. In both cases US-irradiated cells with medium were taken as blanks*

3.3.8.2 MTT Assay

After evaluation of inertness of our empty carriers and non-significant effect of US waves on Dox toxicity we have extended our studies to drug loaded carriers. In this part of study, we have divided our formulations in two main categories based on PFP (US reactive agent) incorporation. In first category, there was no PFP incorporation and it consists of two subdivisions (US and Non-US). Similarly, second category was based on the presence of PFP with further subdivisions (US and Non-US). All these formulations were subjected to cell viability assay by using the same protocol mentioned above with pure Dox as positive control. After 4hr incubation, the cells have taken up the carriers and on exposure to US waves, it has shown very significant effects. The results as in figure 35, showed that Lip-PFP-Dox-MSNPs (US) had highest cytotoxicity as compared to all other formulations. This higher cytotoxicity is supporting the evidence of *in-vitro* triggered release by US-irradiations**.**

We observed that Lipid-Dox-MSNPs (Non-US) has shown minimum of toxicity and this lower effect could be due to lesser release of the drug inside the cell after 4 hr incubation. Although cellular uptake of the Dox has been enhanced by lipid coating of Dox-MSNPs but still it was not able to release full of Dox. On the other side Lip-Dox-MSNPs (US) and Lip-PFP-Dox-MSNPs (Non-US) has shown more toxicity but these effects are quite similar to each other. The relative faster release of DOX from Lip-Dox-MSNPs (US) and Lip-PFP-Dox-MSNPs (Non-US) is due to the effects of US waves and presence of PFP respectively, which have shown higher cytotoxic effects of above mentioned formulations as compare to the formulation without any PFP and US waves. We can assume that a very small part of PFP inside the pores of Lip-PFP-Dox-MSNPs vaporized and cause some of the drug to release even in the absence of US waves and this release was higher than release of Dox in Lip-Dox-MSNPs resulting in more toxicity. Similarly, the higher cytotoxicity of Lip-Dox-MSNPs (US) as compare to toxicity of Lipid-Dox-MSNPs (Non-US) could be due to higher release of drug from the carrier by US waves. Although the exact reason of these results is not known and we can assume that higher release of the drug is because of some vibrational movements of porous structure due to energy provided by mechanical effects of US waves. The toxicities of Lip-Dox-

MSNPs (US) and Lip-PFP-Dox-MSNPs (Non-US) are lesser than the toxicity produced by Lip-PFP-Dox-MSNPs (US) because in later we have incorporated PFP, vaporized by thermal and mechanical effects of US waves. US waves, with FDA approved MI 1.4 and frequency of >10 MHz for clinical purposes, have tendency to penetrate to the surface tissues[86,156] and after the uptake of our carriers by the cells, it has produced some significant results. The PFP inside pores of carrier, being prone to be disturbed by US-irradiation, can trigger the release of the drug inside cells.[86,87] As a result, Lip-PFP-Dox-MSNPs (US) have shown more toxicity as compared to all other three formulations. Hence, it is revealed from cytotoxic studies that by combining effects of PFP inside the pores of MSNPs and US waves together, the release of drug has been enhanced in *in-vitro* tumor cells and it can produce more cytotoxic effects.

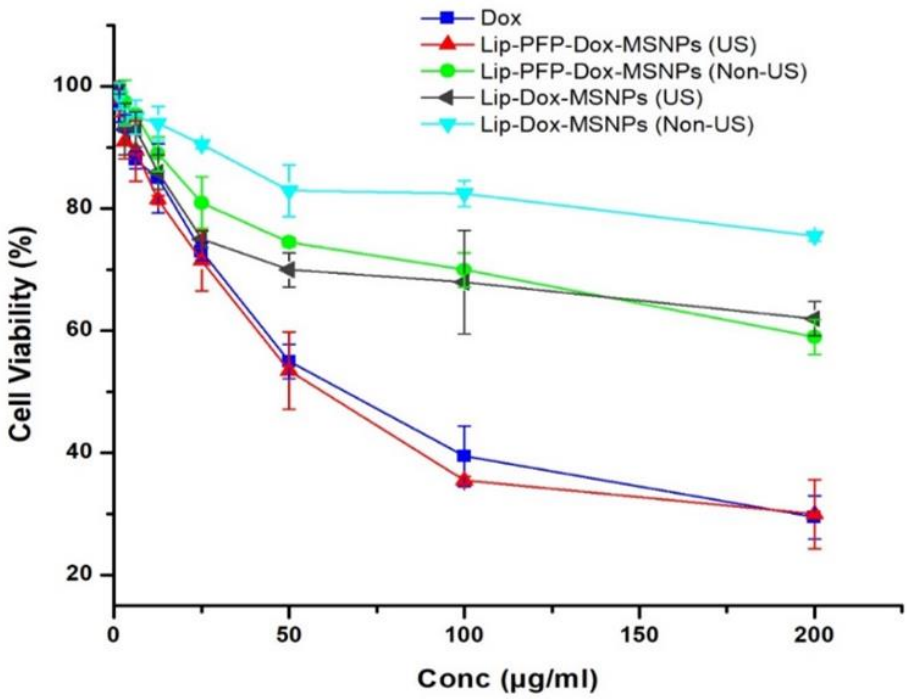

***Figure 35**: In vitro cytotoxicity studies by MTT assay, showing effects of Dox loaded carriers to MDA-MB-231 cells. A comparative cytotoxic effects of US-irradiated (5 min, 12 MHz, MI 1.4) and non-US, Lip-Dox-MSNPs and Lip-PFP-Dox-MSNPs where the US-irradiated Lip-PFP-Dox-MSNPs showed more toxicity as compared to other groups*

3.3.8.3 Cellular Uptake Studies

To strengthen our hypothesis that the release of the drug was enhanced by US waves after internalization of our carrier in cells, we have performed cellular uptake studies to observe these cells under fluorescence microscope and results are shown in figure 36. Higher cellular uptake of lipid coated MSNPs has already been reported by researchers where lipid layer, due to its biocompatibility, enhanced the delivery of the drug carriers.[49,157] For uptake studies and internalization, we have used three different formulations including Dox-MSNPs, Lip-Dox-MSNPs and Lip-PFP-Dox-MSNPs (US). In this case, we have used lower concentrations of Dox to avoid the toxicity effects as the incubation period was 4 hrs. After giving US waves and fixation of cells, nuclei stained cells were observed under CLSM for the localization of green and red fluorescence as in figure 36. Red fluorescence is characteristic of Dox and green of FITC labelled MSNPs and here we observed that localization of green fluorescence in the cytoplasmic region has shown the efficient uptake of carrier by the cells. Internalization of MSNPs is more in Lip-Dox-MSNPs (Non US) and Lip-PFP-Dox-MSNPs (US) as compare to Dox-MSNPs and this is due to the lipid coating of MSNPs which has enhanced the cellular uptake. Dox localization in the cells is also showing the uptake pattern as mentioned above. If we observe the release pattern of Dox in the cells Dox-MSNPs has shown the lesser release than lipid coated formulations. The results have shown that the drug release was enhanced in Lip-PFP-Dox-MSNPs and this release is because of triggering effect of US waves. So this intracellular release pattern is supportive to *in-vitro* release studies where we got enhanced release effects triggered by US waves.

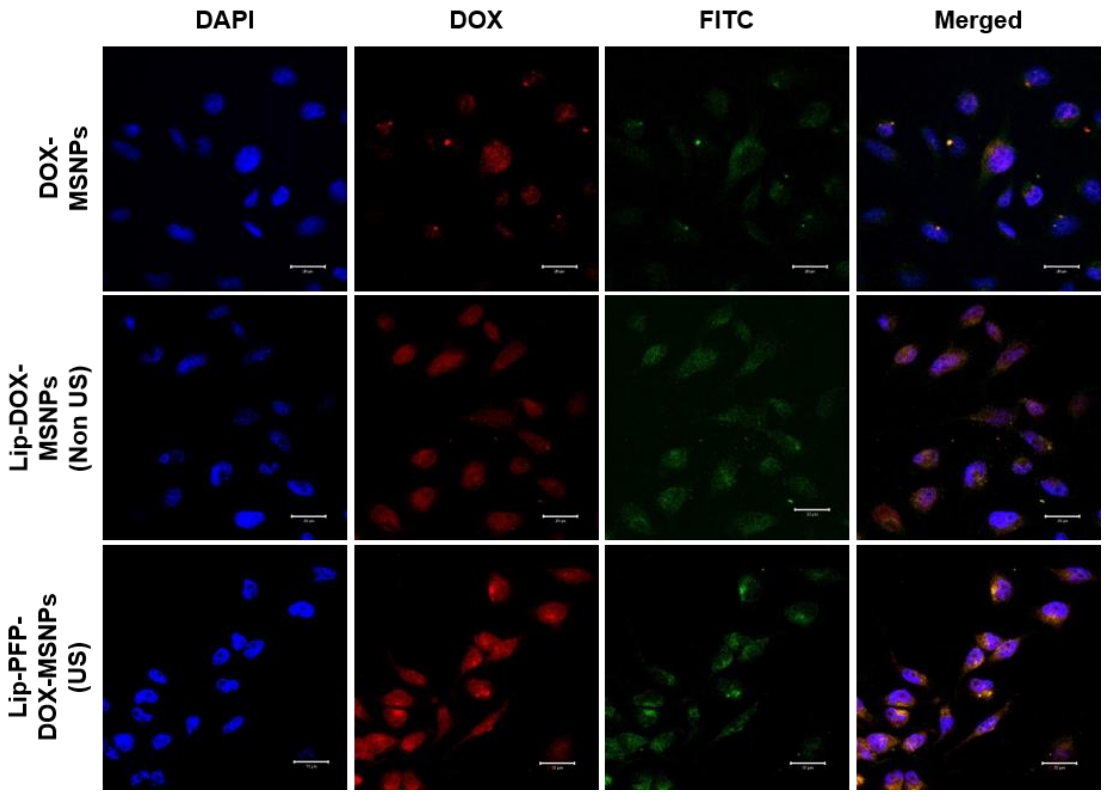

***Figure 36**: Cellular uptake studies by confocal microscopic images of MDA-MB-231 cell line after 4hr incubation at 37°C with FITC (green) labelled Dox-MSNPs, Lip-Dox-MSNPs (Non-US) and Lip-PFP-Dox-MSNPs (US), showing internalization of Dox (red) in nuclear region which was stained with DAPI (blue) with scale bar of 20µm. Higher internalization of Dox with Lip-Dox-MSNPs showed higher cellular uptake due to lipid coating and even higher internalization and triggered release Dox in Lip-PFP-Dox-MSNPs is due to presence of lipid layer and US-irradiation*

CHAPTER 4

3.4 Co-Delivery of CA-IX inhibitor and Dox in Hypoxia

3.4.1 Preparation of Lip_c

Liposomes as carriers for CA-IX inhibitor, were prepared by thin layer hydration method and same molar mass ratios of DPPC:Chloesterol:DOTAP (85:12:3) were used. CA-IX inhibitor as a hydrophobic agent was expected to be loaded in lipid bilayer. These CA-IX inhibitor liposomes (Lip_c) were initially characterized by dynamic light scattering for size distribution and laser Doppler velocimetry for surface charge. Initially, 2 mM of CA-IX inhibitor liposomes were prepared and the size was 309 ± 24.93 (nm) which was much higher than we required for MSNPs coating. The PDI and zeta potential for above mentioned liposomes were 0.54 ± 0.03 and 20.90 ± 0.81 (mV) respectively. Later the size reduction was observed with lower concentration of CA-IX inhibitor that was 20 µM. Here it was noticed that the size of Lip_c characterized with DLS was 109.20 ± 9.69 (nm) with PDI 0.21 ± 0.14 which was in the desired range. Although the reason for this size reduction was unclear but concentration dependent size and PDI reduction was in accordance to previous report.[158] Surface charge of Lip_c was also a critical factor to be characterized, for coating negatively charged MSNPs. The surface charge of Lip_c observed by LDV was +23.50 ± 7.51 (mV) which was also helpful for the coating of MSNPs.

3.4.2 Morphological Studies (AFM)

After liposome preparation and characterization, next step was to characterized lipid coating to MSNPs. The Lip_c coating to MSNPs was initially visualized by AFM and micrographs are shown in figure 37. Here we can see the Lip_c-Dox-MSNPs were in the range of 100-150 nm and not completely round. These non-round structures are the characteristic feature of MSNPs and these findings are similar to previous reports.[159] Uniform layers can be observed over MSNPs which is indicating the coating of lipid to MSNPs was successfully attained. As this technique involves the interaction of cantilever tip with sample and causes the damage or deformation of soft structures like liposomes. This feature of

AFM was helpful to visualize the lipid coating as indicated with arrows in figure 37 (A,C & D). These images are similar to the images previously reported for the lipid coated particles where incomplete lipid layer was observed around the particles under AFM.[160]

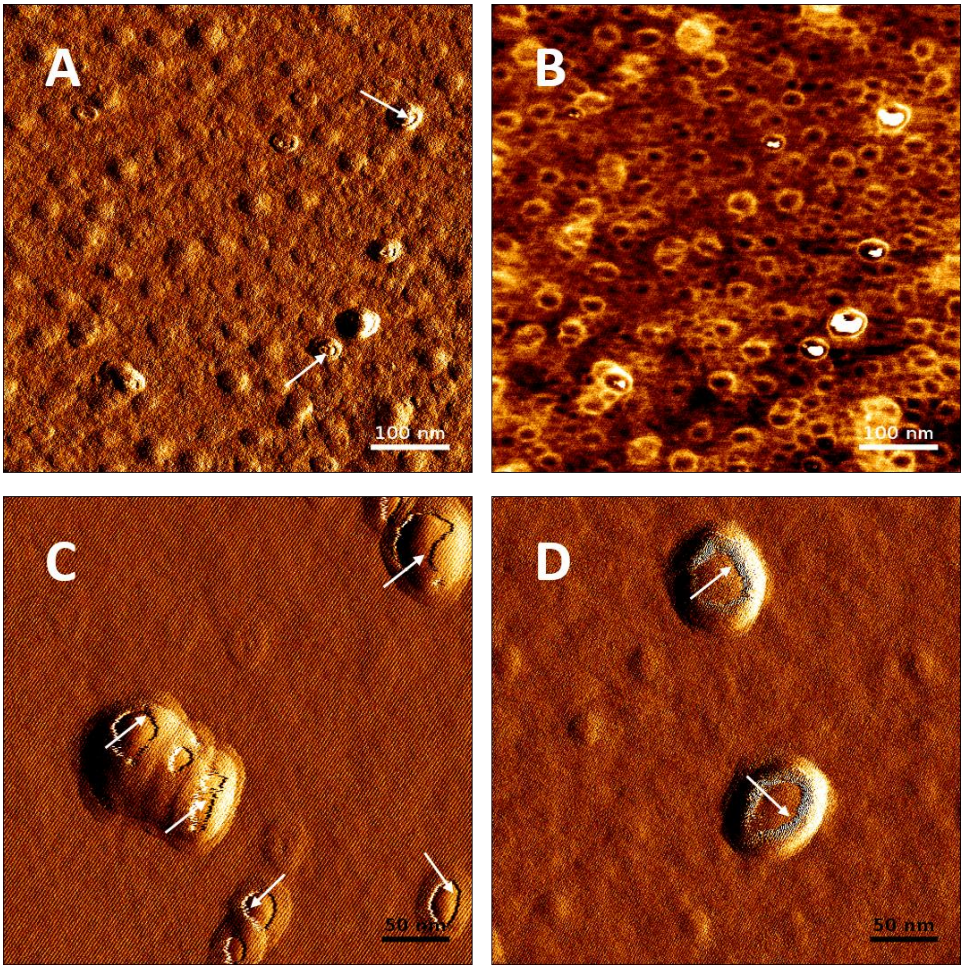

***Figure 37**: AFM images of Lip$_c$-MSNPs (A) amplitude trace, (B) phase trace (C & D) amplitude trace showing lipid coating of MSNPs.*

3.4.3 Preparation of Lip$_c$-Dox-MSNPs

As the size and surface charge of Lip$_c$ were in the same range as for blank liposomes so it was expected that Lip$_c$ can be easily loaded to Dox-MSNPs. The Dox-MSNPs prepared with mass ratio of Dox/MSNPs 0.51 were used for the development of Lip$_c$-Dox-MSNPs. For the preparation of Lip$_c$-Dox-MSNPs the same procedure was adopted by using same molar mass ratios of MSNPs:Liposome 1:0.70. As here the fixed lipid to MSNPs ratio was used so

the concentration of CA-IX inhibitor with Dox to be in effective range was necessary.

3.4.4 Cell Culture Experiments

3.4.4.1 Extracellular acidification Test

Hypoxic condition of the cells is directly associated with extracellular pH regulation, which results in reduced efficacy of chemotherapy and radiotherapy. Activity of CA-IX is one of the key factors for extracellular acidic environment. To evaluate the effects of CA-IX inhibitor on the extracellular acidic pH, cells were treated with different formulations containing CA-IX inhibitor under hypoxic and normoxic conditions.[161] As results shows in figure 38 that by inhibiting CA-IX enzyme in hypoxia, an increase in extracellular pH has been observed. This effectiveness in pH change is only possible in hypoxic conditions where enzyme is overexpressed and activated in lower oxygen supply.[123] The data indicated that under hypoxia, CA-IX was activated but with the treatment of CA-IX inhibitor the extracellular acidosis has been reduced. We also observed that there was no significance change in extracellular pH under normoxic conditions even after treating with CA-IX inhibitor. This also indicates that the inhibition of CA-IX enzyme is linked with its overexpression in hypoxic conditions where it maintains the balance between internal alkaline and external acidic environment.

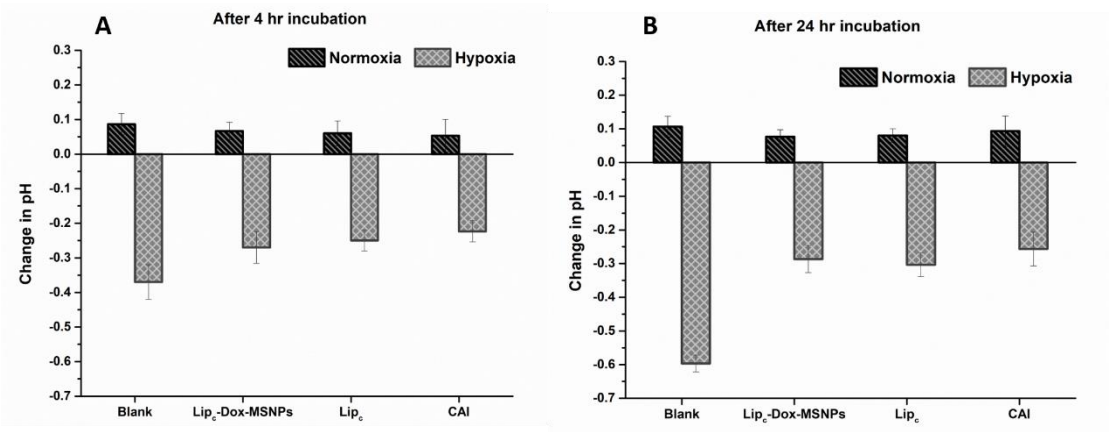

***Figure 38**: Extracellular acidification in normoxia and hypoxia before and after traetment with CAI, Lip_c and Lip_c-Dox-MSNPs after (A) 4 hr and (B) 24 hr incubation*

3.4.4.2 Western Blotting (HIF-1α and CA-IX)

To validate the over expression of CA-IX enzyme, protein expression analysis by western blot technique was performed. MDA-MB231 cells are reported to express large amounts of CA-IX enzyme under hypoxic conditions.[162] For the effectiveness of CA-IX enzyme inhibitor, it was necessary to confirm the over expression of CA-IX enzyme. HIF-1α is another indicator, normally over expressed in hypoxic conditions. The results of western blots for normoxic and hypoxic cells are shown in figure 39 and it can be observed in 39 A that both HIF-1α and CA-IX enzymes were over expressed under hypoxic conditions.[163]

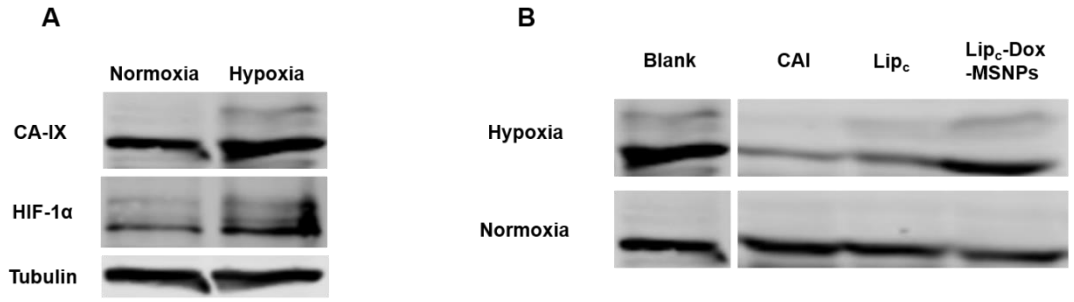

Figure 39: *Western blots of normoxic and hypoxic cells for (A) CA-IX expression and HIF-1α expression, (B) CA-IX expression after treatment*

As it can be noticed in figure 39 B, after 24 hr treatment with CA-IX inhibitor no significant effects were observed under normoxic conditions. A significant difference in CA-IX expression was observed in hypoxia between treated and non-treated samples. Cells treated with CA-IX inhibitor, Lip_c and Lip_c-Dox-MSNPs have shown lesser expressions as compared to Blank cells and these results could be due to the inhibition of CA-IX enzyme. In normoxic conditions treated and non-treated cells have shown no significant difference because CA-IX enzyme was not overexpressed. Hypoxic conditions mimic the expression of CA-IX enzyme which is necessary for CA-IX inhibitor to perform its inhibitory action.[164]

3.4.4.3 *In-vitro* Cytotoxicity Assay (MTT Assay)

Many of the chemotherapeutic agents, which are specifically designed for targeting of highly proliferating cells, fail even after reaching to hypoxic cells. The effective concentration of drugs taken up by the tumor cells is prerequisite for suitable outcomes.[165] Initially we performed our cell viability studies to evaluate cytotoxic effects of pure Dox with and without CA-IX inhibitor and Lip_c both in normoxia and hypoxia. The cytotoxic effects of Dox after 4 hr and 24 hr incubation with MDA-MBA 231 cells, pre-treated with CA-IX inhibitor and Lip_c for 4 hrs in normoxia and hypoxia, are shown in figure 40. The concentration of Dox was 100 µg/ml and for CA-IX inhibitor was 360 nM. Here we have observed that pure Dox has shown more cytotoxic effects in normoxia with 4 hr incubation period as compared to hypoxia. Similar kind of results were observed with 24 hr Dox incubation time. The lower cytotoxic effects of Dox in hypoxia are due to extracellular acidosis as we have observed in extracellular acidification test. This acidic environment cause ionization of weakly basic drug like Dox and results in lesser cellular uptake of drug. Another possibility for lesser Dox toxicity in hypoxia would be because of suppression of ROS mediated cytotoxicity of Dox in hypoxia,[166] as already reported.[167,168] Contrarily these results were different to those we got after inhibition of CA-IX. After treatment with pure CA-IX, Dox with 4 hrs incubation has shown no significant difference in cytotoxicity between normoxia and hypoxia but after 24 hrs Dox incubation it has shown better results where in hypoxia more cytotoxic effects of Dox has been observed as compared to normoxia.

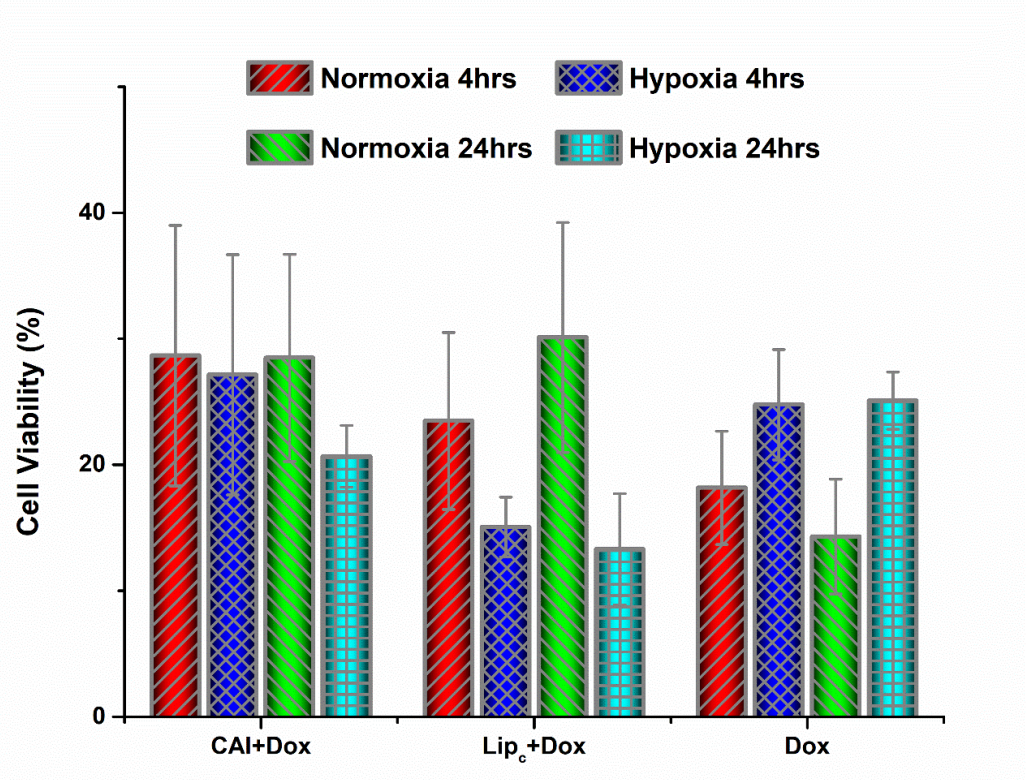

***Figure 40**: In-vitro cytotoxicity evaluation of Dox (4 hr & 24 hr incubation) with CAI and Lip$_c$ pretreated cells in normoxia and hypoxia*

When the cells were treated with Lip$_c$ before incubation with Dox, the more significant results have been observed. We found that even after 4 hr incubation in hypoxia pre-treated with Lip$_c$, Dox has shown more toxic effects as compared to pure CA-IX inhibitor in hypoxia. By these findings, it can be established that in hypoxic conditions inhibition of CA-IX enzyme is beneficent for more cytotoxic effects of Dox and these effects can be further enhanced by loading CA-IX inhibitor to liposome. The better results with liposomes, as previously reported,[169] are because of higher biocompatibility and internalization due to structure of lipid layer. After establishing this fact next step was to evaluate the cytotoxic effects of Lip$_c$-Dox-MSNPs in hypoxic environment.

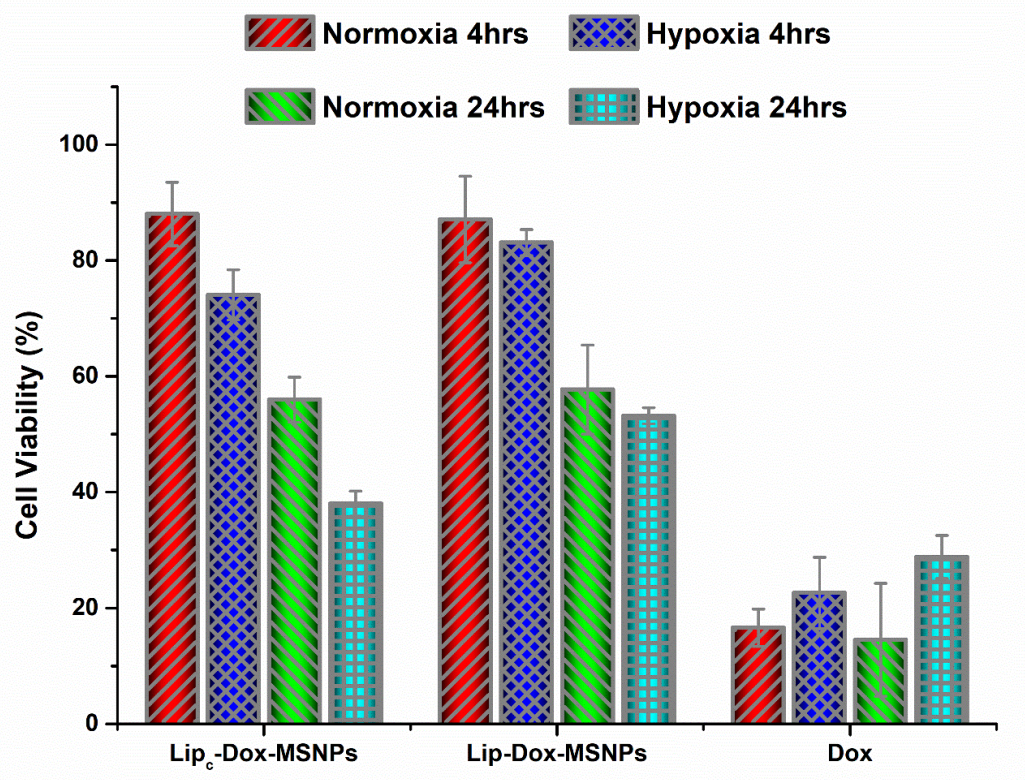

***Figure 41**: In-vitro cytotoxicity of Lip$_c$-Dox-MSNPs, Lip-Dox-MSNPs and Dox after 4 hr & 24 hr incubation in normoxia and hypoxia*

In this part of studies, as shown in figure 41, similar kind of pattern has been observed where pure Dox in hypoxia has shown lesser cytotoxic effects due to ionization and suppression of ROS-mediated toxicity of Dox, both after 4 hr and 24 hr incubation. Here the same concentrations of Dox 100 µg/ml and CA-IX inhibitor 360 nM were used. Lip$_c$-Dox-MSNPs has shown more cytotoxic effects in hypoxia as compared to normoxia both after 4 hr and 24 hr incubation. On the other hand, Lip-Dox-MSNPs has shown almost same cytotoxic effects in hypoxia and normoxia after 4 hr incubation. Along with 24 hr incubation of Lip-Dox-MSNPs have also shown same pattern in hypoxia and normoxia. As a cross comparison between Lip$_c$-Dox-MSNPs and Lip-Dox-MSNPs, in normaxia with 4 hr and 24 hr incubation, there is no significant difference but when we compare Lip$_c$-Dox-MSNPs and Lip-Dox-MSNPs in hypoxic conditions, significant difference can be observed with more Lip$_c$-Dox-MSNPs cytotoxic effects. These results are also indicating that CA-IX inhibitor can show its effects only in hypoxia when CA-IX is over expressed. Our findings are in accordance with previously established results[103,170] where the effects of Dox

in combination with CA-IX inhibition has produced better cytotoxic effects. By these synergistic effects of Lip_c-Dox-MSNPs we can assume that CA-IX inhibitor and Dox loaded drug delivery system is a suitable system for the delivery off weakly basic drug under hypoxic conditions.

4 Summary & Outlook

4.1 Summary and Outlook

In this dissertation, different types of nanoconstructs, including MSNPs and liposomes were fabricated for the development of an advanced drug delivery system which can deliver both hydrophilic and hydrophobic drugs to the tumor cells with better efficacy and biocompatibility and minimized side effects to healthy tissues. The candidature of MSNPs as nanocarriers with potential features, supported with lipid layer was explained in introduction part along with their merits and demerits. The combined effects of liposomes and MSNPs in sustained release or stimuli responsive drug delivery systems equipped with literature were highlighted. This project was mainly divided in to four major parts where nanocarriers were characterized and further evaluated for *in-vitro* analysis under different conditions such as normoxia and hypoxia.

In the first part, MSNPs of different molar mass ratios of surfactant/silica were fabricated. The parameters which can affect the particle size distribution, were evaluated. These MSNPs for their physicochemical properties were initially characterized by Dynamic Light Scattering (DLS) for size distribution and Laser Doppler Velocimetry (LDV) for surface charge. The removal of surfactant for the generation of porous structure, was evaluated with elemental analysis and surface charge. Surface area characterization of MSNPs were evaluated with nitrogen sorption desorption method, where the suface area and surface volume were influence by duration of extraction for surfactant removal. The morphological structures were characterized by different microscopies involving Atomic Force Microscopy and Electron microscopies. The morphological studies performed with AFM were in accordance to the size distribution obtained by DLS. The porous structure of MSNPs was observed with electron microscopies. Tranmission electron microscopy (TEM) has shown that the MSNPs are more or less round in shape with ordered porous structure. The pore size evaluated with TEM was the same as it was characterized with sorption-desorption pore size measurement. For further confirmation of porous structure of MSNPs, Scanning Transmission Electron Microscopy (STEM) was performed and particle size and porous distribution were evaluated.

In the work described in second chapter, a lipid coated MSNPs system was designed and characterized for further investigations. Cationic liposomes prepared with thin layer hydration technique and its coating to MSNPs was characterized with hydrodynamic size, surface charge and FTIR spectrum. Lipid coating of MSNPs were further visualized with Cryo-TEM & TEM micrographs. Higher surface area of MSNPs with higher drug loading capacity made them suitable candidate for the delivery of large amounts of drugs. *In-vitro* drug release profile has shown sustained release effects where the rate of drug release from bared drug loaded MSNPs was faster than lipid coated ones. The lipid coating to MSNPs with reduced premature drug release under inert conditions addressed the issue of premature drug leakage. In a comparative study of *in-vitro* cytotoxic profile, lipid coated MSNPs due to higher biocompatibility delivered higher concentrations of Dox and has shown more cytotoxic effects as compared to bared MSNPs. These higher cytotoxic effects with lipid coated MSNPs were further evaluated with Confocal Laser Scanning microscope where higher internalization of Dox in the cells was evident for the higher uptake of the carriers.

In the third chapter, we have successfully developed a stimuli responsive smart drug delivery system composing of lipid coated MSNPs as a carrier, Dox as a model drug, US as a stimulus and PFP as a stimuli responsive agent. By combining MSNPs with liposomes, very significant results have been produced due to the morphology and unique structure of the MSNPs along with biocompatibility and gatekeeping effects of liposomes. PFP was successfully incorporated inside the pores of MSNPs by capillary filling and very stable nanocarriers were produced. The US-irradiation, with FDA approved specifications, has produced very satisfactory triggered release effects due to rupturing of lipid layer by the gaseous pressure of vaporized PFP inside pores. *In-vitro* cell culture experiments have shown higher internalization of carrier due to biocompatibility of lipid layer and higher cytotoxic effects due to triggered release by US-irradiations. These smart nanocarriers, can be used as drug delivery system for many chemotherapeutics for site-specific triggered release of drug to enhance the efficacy and to avoid undesired side effects to healthy tissues.

The fourth chapter of this study was based on the development of a co-delivery system of carbonic anhydrase IX inhibitor and Dox, where carbonic anhydrase inhibitor loaded liposomes were coated to Dox loaded MSNPs. *In-vitro* cytotoxic experiments were performed under normoxia and hypoxia and it was evaluated that Carbonic anhydrase IX enzyme was overexpressed under hypoxic conditions. The enzyme inhibitor can be effective only when enzyme is overexpressed in hypoxia. Furthermore, the combined effects of enzyme inhibitor and Dox has produced synergistic cytotoxic effects under hypoxia due to inhibition of carbonic anhydrase IX enzyme. Better inhibition effects of carbonic anhydrase IX inhibitor loaded liposomes were observed as compared to pure enzyme inhibitor, although these findings are on the initial stage and need further to be investigated.

In future, the aim of the study will be to perform *in-vivo* evaluation of drug delivery carriers, involving biodistribution of drug and carriers in different organs. The in-vivo studies will also involve the stimuli US-responsive triggered release in animal model. As for MSNPs as drug carriers are concerned we are looking forward to develop new drug delivery system for another drug like photosensitizer. This system will be a stimuli responsive advanced drug delivery system where US would trigger the release of drug and light will activate the drug to produce cytotoxic effects. As hypoxic experiments are in early stages, so we will extend our studies in hypoxic condition for further validation of already developed system and to evaluate photodynamic effects under oxygen deprived environment.

4.2 Zusammenfassung und Ausblick

Diese Promotionsarbeit beschäftigte sich mit der Herstellung verschiedener Nanomaterialien, einschließlich mesoporöser Silikananopartikel (MSNPs) und Liposomen, um daraus ein neuartiges Arzneistoffträgersystem zu entwickeln. Das sowohl hydrophile als auch lipophile Arzneistoffe zu Tumorzellen transportieren kann und dabei, im Hinblick auf die Arzneistoffe, eine Verbesserung der Biokompatibilität, eine höhere Effektivität und weniger Nebenwirkungen auf gesundes Gewebe aufweist. In der Einleitung wurde auf die Vorzüge und Nachteile der MSNPs als Nanoträgersysteme und in Kombination mit Lipidbeschichtungen näher eingegangen. Eine genauere Erklärung der Kombinationseffekte von Liposomen und MSNPs bei Retardträgersystemen oder stimuli-responsiven Trägersystemen unter Zuhilfenahme der Fachliteratur folgte. Das vorliegende Projekt lässt sich in vier Kapitel einteilen. Hier wurden die Trägersysteme eingehen charakterisiert und auf ihre Eigenschaften unter verschiedenen *in-vitro* Bedingungen, wie z.B. Normoxie und Hypoxie, eingegangen.

Das erste Kapitel beschreibt die Herstellung der MSNPs unter Verwendung verschiedener Molmassenverhältnisse von Tensid zu Silika, zur Evaluation der die Partikelgrößenverteilung beeinflussenden Parameter. Als erste Charakterisierungsmöglichkeit der physikochemischen Eigenschaften diente dabei die Messung der Partikelgröße mit Hilfe der Dynamischen Lichtstreuung (DLS) und die Messung der Oberflächenladung durch die Lader Doppler Velocimetrie (LDV). Die Entfernung des verwendeten Tensids, um die poröse Struktur zu erzeugten, wurde durch Elementaranalyse und Oberflächenladungsmessungen bestimmt. Die Untersuchung der Oberfläche der MSNPs erfolgte mit Hilfe der Messung von Sorption und Desorption von Stickstoff, dabei wurden die gemessene Fläche und das Volumen von der Extraktionszeit des Tensids beeinflusst. Verschiedene mikroskopische Techniken, wie die Raster-Kraft- und die Elektronenmikroskopie, dienten der Charakterisierung der Morphologie der Trägersysteme. Die Ergebnisse der Größenvermessungen nach Raster-Kraft-Mikroskopie waren dabei in Übereinstimmung zu den Ergebnissen der Größenmessung mit Hilfe der DLS.

Unter Elektronenmikroskopen konnte außerdem die poröse Struktur der MSNPs beobachtet werden. Die Transmissionselektronenmikroskopie (TEM) zeigte, dass die MSNPs von mehr oder weniger runder Form waren und eine geordnete poröse Struktur aufwiesen. Die dabei gemessene Porengröße entsprach der Porengröße, die mit Hilfe der Sorptions-Desorptionsmethode bestimmt wurde. Zur genaueren Betrachtung der Porenstruktur und zur Vermessung der Porengröße und verteilung, kam außerdem ein Rastertransmissionselektronenmikroskop (STEM) zum Einsatz.

Das zweite Kapitel beschreibt das Design und die Charakterisierung lipidüberzogener MSNPs als Trägersysteme. Kationische Liposomen, hergestellt mit Hilfe der Filmbildungsmethode, und mit ihnen überzogene MSNPs wurden dabei auf ihre hydrodynamischen Durchmesser, ihre Oberflächenladung und ihr FTIR-Spektrum untersucht. Die Lipidhülle der MSNPs konnte außerdem mit Hilfe von cryo-TEM- und TEM-Aufnahmen visualisiert werden. Die große Oberfläche der MSNPs und der daraus folgenden hohen Beladungskapazität für Arzneistoffe, macht sie zu einem interessanten Kandidaten für den Transport hoher Arzneistoffmengen. Die *in-vitro* Freisetzungskurve des Arzneistoffes Doxorubicin (Dox) zeigte eine verzögerte Abgabe des Arzneistoffes, wobei die Freisetzung aus nicht überzogenen Trägersystemen schneller war, als die aus den lipidüberzogenen. Daher konnte mit Hilfe des Lipidüberzuges das Problem der frühzeitigen, ungewollten Arzneistoffabgabe unter Lagerungsbedingungen gelöst werden. Eine vergleichende *in-vitro* Studie zur Zelltoxizität konnte zeigen, dass die lipidüberzogenen MSNPs aufgrund ihrer höheren Biokompatibilität höhere Doxorubicinkonzentrationen in die Zellen bringen konnten und daher einen stärkeren zytotoxischen Effekt als die nicht überzogenen MSNPs aufwiesen. Ein Nachweis dieses verstärkten Effektes erfolgte auch mit der konfokalen Laser-Scanning-Mikroskopie. Hier zeigte sich eine stärkere Internalisation von Dox als klarer Hinweis auf eine stärkere Aufnahme der Trägersysteme in die Zellen.

Im dritten Kapitel konnte ein stimuli-responsives Trägersystemen erfolgreich entwickelt werden. Dazu dienten lipidüberzogene MSNPs als Trägersysteme,

Dox als Modellarzneistoff, Ultraschall (US) wurde als Stimulus verwendet und Perfluorpentan (PFP) war das auf den Stimulus reagierende Agens. Die Kombination von Liposomen und MSNPs ergab aufgrund der besonderen Struktur der MSNPs in Kombination mit der guten Biokompatibilität und dem Gatekeeping-Effekt der Liposomen sehr gute Ergebnisse. Der Einschluss von PFP in die Poren der MSNPs gelang durch Kapillarfüllung und es entstanden sehr stabile Nanoträgersysteme. Eine US-Behandlung mit von der FDA zugelassenen Spezifikationen löste eine sehr zufriedenstellende gezielte Freisetzung des Arzneistoffes aus. Dabei konnte ein Zerreißen der Lipidhülle, aufgrund des hohen Druckes der entstehenden Dämpfe des PFP innerhalb der Poren der MSNPs, beobachtet werden. Die durchgeführten *in-vitro* Zellkulturversuche konnten eine höhere Aufnahme aufgrund besserer Biokompatibilität bei den lipidüberzogenen Trägersystemen und einen stärkeren zytotoxischen Effekt nach gezielter Freisetzung des Arzneistoffes durch US nachweisen. Diese intelligenten Nanoträgersysteme sind für viele Chemotherapeutika einsetzbar und sorgen durch ihre gezielte Freigabe des Arzneistoffes direkt im betroffenen Gewebe für besser Effektivität des Arzneistoffes und geringe unerwünschte Nebeneffekte auf gesundes Gewebe.

Die Basis des vierten Kapitels dieser Studie war die Entwicklung eines Trägersystems für den kombinierten Transport von Doxorubicin und eines Inhibitors der Carbonischen Anhydrase IX. Dabei wurde der Inhibitor in den Lipidfilm der Liposomen eingeschlossen, die als Überzug für mit Doxorubicin beladene MSNPs dienten. *In-vitro* Untersuchungen zur Zelltoxizität wurden unter Normoxie und Hypoxie durchgeführt. Dabei wurde auch nachgewiesen, dass das Enzym Carbonische Anhydrase IX unter hypoxischen Bedingungen überexprimiert wird, sodass der Inhibitor effektive Ergebnisse erzielen kann, da er nur bei überexprimiertem Enzym seinen Effekt entfaltet. Auch konnte eine synergistische Kombination von Dox und dem Inhibitor der carbonischen Anhydrase IX unter hypoxischen Bedingungen dargestellt werden. Höhere Inhibitionseffekte gegen die Carbonische Anhydrase IX wiesen inhibitorbeladene Liposomen im Vergleich zu freiem Inhibitor auf. Diese Ergebnisse sind allerdings noch in einem initialen Stadium und bedürfen daher einer weiteren Prüfung.

Für zukünftige Studien ist es das Ziel eine *in-vivo* Evaluation des Trägersystems vorzunehmen. Dabei soll die Biodistribution des Trägersystems und des Arzneistoffes in den verschiedenen Organen untersucht werden. Die gezielte Freisetzung nach Stimulation durch US wird auch in *in-vivo* Tierversuchen geprüft. Im Bereich der MSNPs ist es das Ziel diese als Trägersysteme für andere Arzneistoffe wie zum Beispiel Photosensitizer zu entwickeln. Somit kann ein stimuli-responsives Trägersystem aufgebaut werden, bei dem die Arzneistofffreisetzung durch US und die Arzneistoffaktivierung und damit der zelltoxische Effekt durch Licht gesteuert werden kann. Eine Weiterführung der Experimente zur Hypoxie, die sich noch in einem sehr frühen Stadium befinden, sind ebenso geplant, wie weitere Untersuchungen unter hypoxischen Bedingungen für die Evaluation des photodynamischen Effektes bei Sauerstoffmangel.

5 Appendix

5.1 List of Abbreviations

WHO	World Health Organization
DDS	Drug Delivery System
FDA	Food and Drug Administration
MSNPs	Mesoporous Silica Nanoparticles
CMC	Critical Micelles Concentration
PAA	Poly Acrylic Acid
PLGA	Poly (Lactide-co-Glycolide)
PGA	Polyglycolic Acid
PLA	Poly Lactic Acid
PEG	Polyethylene Glycol
MLVs	Multilamellar Vesicles
ULVs	Unilamellar Vesicles
LUVs	Large Unilamellar Vesicles
SUVs	Small Unilamellar Vesicles
DOTAP	1,2-dioleoyl-3-trimethylammonium-propane
DOPS	1,2-dioleoyl-sn-glycero-3-phospho-L-serine
DPPC	1,2-dipalmetoyl-sn-glycero-3-phosphocholine
Dox	Doxorubicin
MNPs	Magnetic Nanoparticles
US	Ultrasound
NIR	Near Infrared
ROS	Reactive Oxygen Specie
MI	Mechanical Index

CA-IX	Carbonic Anhydrase IX
pH_i	Intracellular pH
pH_e	Extracellular pH
CTAB	Cetyltrimethylammonium Bromide
TEOS	Tetraethylorthosilicate
IEP	Isoelectric Point
PFP	Perfluoropentane
PBS	Phosphate Buffer Saline
DLS	Dynamic Light Scattering
LDV	Laser Doppler Velocimetry
Dox-MSNPs	Doxorubicin loaded Mesoporous Silica Nanoparticles
Lip-Dox-MSNPs	Lipid coated Doxorubicin loaded mesoporous silica nanoparticles
Lip-PFP-Dox-MSNPs	Lipid Coated Doxorubicin and Perfluoropentane Loaded Mesoporous Silica Nanoparticles
Lip-PFP-Dox-MSNPs (US)	Ultrasound Irradiated Lipid Coated Doxorubicin and Perfluoropentane Loaded Mesoporous Silica Nanoparticles
Lip-PFP-Dox-MSNPs (US)	Ultrasound Irradiated Lipid Coated Doxorubicin and Perfluoropentane Loaded Mesoporous Silica Nanoparticles
Lip_c	CA-IX Inhibitor Liposomes

Lip_c-Dox-MSNPs

Doxorubicin Loaded Mesoporous Silica Nanoparticles Coated with Carbonic Anhydrase IX Inhibitor Loaded Liposomes

AFM	Atomic Force Microscopy
TEM	Transmission Electron Microscopy
FFT	Fast Fourier Transform
IFFT	Inverse Fast Fourier Transform
SEM	Scanning Electron Microscopy
STEM	Scanning Transmission Electron Microscopy
Cryo-TEM	Cryogenic Transmission Electron Microscopy
FTIR	Fourier Transform Infrared
BET	Brunauer Emmett Teller
BJH	Barret Joyner Halenda
CLSM	Confocal Laser Scanning Microscope
PDI	Polydispersibilty Index
FITC	Fluorescein-5 isothiocyanate
APTES	3-aminopropyl triethoxysilane
HAADF	High Angle Annular Dark Field
MWCO	Molecular Weight Cuttoff
DMEM	Dulbecco's Modified Eagle's Medium
NEA	Non-Essential Amino Acids
RPMI	Rosewell Park Memorial Institute
FCS	Fetal Calf Serum
MTT	3-(4,5-dimethylthiazol-2-yl)-2,5-diphenyltetrazolium Bromide
DMSO	Dimethylsulfoxide

DAPI	4’, 6-diamidino-2-phenylindole
HIF	Hypoxia Inducing Factor

5.2 References

1. Bray F, Ferlay J, Soerjomataram I, Siegel RL, Torre LA, Jemal A. Global cancer statistics 2018: GLOBOCAN estimates of incidence and mortality worldwide for 36 cancers in 185 countries. CA: a cancer journal for clinicians 2018;68:394-424.

2. Tamizhazhagan V, Pugazhendy K, Sakthidasan V, Jayanthi C, Rajesh S, Manikanadan P. Social and Economic Burden of Cancer on 2020-Minireview. Cancer Research Journal 2018;6:10.

3. Wicki A, Witzigmann D, Balasubramanian V, Huwyler J. Nanomedicine in cancer therapy: challenges, opportunities, and clinical applications. J Control Release 2015;200:138-57.

4. Allen TM, Cullis PR. Drug delivery systems: entering the mainstream. Science 2004;303:1818-22.

5. Jain KK. The handbook of nanomedicine: Springer; 2008.

6. Palazzolo S, Bayda S, Hadla M, et al. The clinical translation of organic nanomaterials for cancer therapy: a focus on polymeric nanoparticles, micelles, liposomes and exosomes. Current medicinal chemistry 2018;25:4224-68.

7. Zhang Q, Liu F, Nguyen KT, et al. Multifunctional Mesoporous Silica Nanoparticles for Cancer-Targeted and Controlled Drug Delivery. Advanced Functional Materials 2012;22:5144-56.

8. Rao C, Vivekchand S, Biswas K, Govindaraj A. Synthesis of inorganic nanomaterials. Dalton Transactions 2007:3728-49.

9. Pelaz B, Alexiou C, Alvarez-Puebla RA, et al. Diverse applications of nanomedicine. ACS Publications; 2017.

10. Mura S, Nicolas J, Couvreur P. Stimuli-responsive nanocarriers for drug delivery. Nat Mater 2013;12:991-1003.

11. Sanchez C, Belleville P, Popall M, Nicole L. Applications of advanced hybrid organic–inorganic nanomaterials: from laboratory to market. Chemical Society Reviews 2011;40:696-753.

12. Simovic S, Ghouchi-Eskandar N, Moom Sinn A, Losic D, A Prestidge C. Silica materials in drug delivery applications. Current Drug Discovery Technologies 2011;8:250-68.

13. Benezra M, Penate-Medina O, Zanzonico PB, et al. Multimodal silica nanoparticles are effective cancer-targeted probes in a model of human melanoma. The Journal of clinical investigation 2011;121:2768-80.

14. Tourne-Peteilh C, Begu S, Lerner DA, Galarneau A, Lafont U, Devoisselle J-M. Sol–gel one-pot synthesis in soft conditions of mesoporous silica materials ready for drug delivery system. Journal of sol-gel science and technology 2012;61:455-62.

15. Klichko Y, Liong M, Choi E, et al. Mesostructured silica for optical functionality, nanomachines, and drug delivery. Journal of the American Ceramic Society 2009;92:S2-S10.

16. Tang F, Li L, Chen D. Mesoporous silica nanoparticles: synthesis, biocompatibility and drug delivery. Adv Mater 2012;24:1504-34.

17. Kresge C, Leonowicz M, Roth WJ, Vartuli J, Beck J. Ordered mesoporous molecular sieves synthesized by a liquid-crystal template mechanism. nature 1992;359:710.

18. Vyshegorodtseva E, Larichev YV, Mamontov G. The influence of CTAB/Si ratio on the textural properties of MCM-41 prepared from sodium silicate. Journal of Sol-Gel Science and Technology 2019:1-10.

19. ALOthman ZA. A review: fundamental aspects of silicate mesoporous materials. Materials 2012;5:2874-902.

20. He Q, Gao Y, Zhang L, et al. A pH-responsive mesoporous silica nanoparticles-based multi-drug delivery system for overcoming multi-drug resistance. Biomaterials 2011;32:7711-20.

21. Vivero-Escoto JL, Slowing II, Trewyn BG, Lin VS. Mesoporous silica nanoparticles for intracellular controlled drug delivery. Small 2010;6:1952-67.

22. Zhou Y, Quan G, Wu Q, et al. Mesoporous silica nanoparticles for drug and gene delivery. Acta pharmaceutica sinica B 2018;8:165-77.

23. Valtchev V, Tosheva L. Porous nanosized particles: preparation, properties, and applications. Chem Rev 2013;113:6734-60.

24. Jin Q, Lin C-Y, Kang S-T, et al. Superhydrophobic silica nanoparticles as ultrasound contrast agents. Ultrasonics sonochemistry 2017;36:262-9.

25. Li X, Chen Y, Wang M, Ma Y, Xia W, Gu H. A mesoporous silica nanoparticle–PEI–fusogenic peptide system for siRNA delivery in cancer therapy. Biomaterials 2013;34:1391-401.

26. Tang F, Li L, Chen D. Mesoporous silica nanoparticles: synthesis, biocompatibility and drug delivery. Advanced materials 2012;24:1504-34.

27. Lu J, Liong M, Zink JI, Tamanoi F. Mesoporous silica nanoparticles as a delivery system for hydrophobic anticancer drugs. small 2007;3:1341-6.

28. Farokhzad OC, Cheng J, Teply BA, et al. Targeted nanoparticle-aptamer bioconjugates for cancer chemotherapy in vivo. Proceedings of the National Academy of Sciences 2006;103:6315-20.

29. Wang S, Fan W, Kim G, et al. Novel methods to incorporate photosensitizers into nanocarriers for cancer treatment by photodynamic therapy. Lasers in surgery and medicine 2011;43:686-95.

30. Elzoghby AO, Samy WM, Elgindy NA. Albumin-based nanoparticles as potential controlled release drug delivery systems. Journal of controlled release 2012;157:168-82.

31. Choi KY, Chung H, Min KH, et al. Self-assembled hyaluronic acid nanoparticles for active tumor targeting. Biomaterials 2010;31:106-14.

32. Vauthier C, Bouchemal K. Methods for the preparation and manufacture of polymeric nanoparticles. Pharmaceutical research 2009;26:1025-58.

33. Kumari A, Yadav SK, Yadav SC. Biodegradable polymeric nanoparticles based drug delivery systems. Colloids and surfaces B: biointerfaces 2010;75:1-18.

34. Wakaskar RR. General overview of lipid–polymer hybrid nanoparticles, dendrimers, micelles, liposomes, spongosomes and cubosomes. Journal of drug targeting 2018;26:311-8.

35. Jone A. Liposomes: a short review. Journal of Pharmaceutical Sciences and Research 2013;5:181.

36. ElBayoumi TA, Torchilin VP. Current trends in liposome research. Liposomes: Springer; 2010:1-27.

37. Ali S, Amin MU, Ali MY, et al. Wavelength dependent photo-cytotoxicity to ovarian carcinoma cells using temoporfin loaded tetraether liposomes as efficient drug delivery system. European Journal of Pharmaceutics and Biopharmaceutics 2020;15:50-65.

38. Tariq I, Pinnapireddy SR, Duse L, et al. Lipodendriplexes: A promising nanocarrier for enhanced gene delivery with minimal cytotoxicity. European Journal of Pharmaceutics and Biopharmaceutics 2019;135:72-82.

39. Lamichhane N, Udayakumar TS, D'Souza WD, et al. Liposomes: clinical applications and potential for image-guided drug delivery. Molecules 2018;23:288.

40. Mahmoud G, Jedelská J, Omar SM, Strehlow B, Schneider M, Bakowsky U. Stabilized tetraether lipids based particles guided prophyrins photodynamic therapy. Drug delivery 2018;25:1526-36.

41. Hadjidemetriou M, Al-Ahmady Z, Kostarelos K. Time-evolution of in vivo protein corona onto blood-circulating PEGylated liposomal doxorubicin (DOXIL) nanoparticles. Nanoscale 2016;8:6948-57.

42. Pattni BS, Chupin VV, Torchilin VP. New developments in liposomal drug delivery. Chemical reviews 2015;115:10938-66.

43. Akbarzadeh A, Rezaei-Sadabady R, Davaran S, et al. Liposome: classification, preparation, and applications. Nanoscale research letters 2013;8:102.

44. El-Sawy HS, Al-Abd AM, Ahmed TA, El-Say KM, Torchilin VP. Stimuli-responsive nano-architecture drug-delivery systems to solid tumor micromilieu: past, present, and future perspectives. ACS nano 2018;12:10636-64.

45. Mishra H, Chauhan V, Kumar K, Teotia D. A comprehensive review on Liposomes: a novel drug delivery system. Journal of Drug Delivery and Therapeutics 2018;8:400-4.

46. Bernardos A, Aznar E, Marcos MD, et al. Enzyme-responsive controlled release using mesoporous silica supports capped with lactose. Angew Chem Int Ed Engl 2009;48:5884-7.

47. Liu X, Situ A, Kang Y, et al. Irinotecan delivery by lipid-coated mesoporous silica nanoparticles shows improved efficacy and safety over liposomes for pancreatic cancer. ACS nano 2016;10:2702-15.

48. Cauda V, Engelke H, Sauer A, Arcizet D, Rädler J, Bein T. Colchicine-loaded lipid bilayer-coated 50 nm mesoporous nanoparticles efficiently induce microtubule depolymerization upon cell uptake. Nano letters 2010;10:2484-92.

49. Wang D, Huang J, Wang X, et al. The eradication of breast cancer cells and stem cells by 8-hydroxyquinoline-loaded hyaluronan modified mesoporous silica nanoparticle-supported lipid bilayers containing docetaxel. Biomaterials 2013;34:7662-73.

50. Wu X, Wang Z, Zhu D, et al. pH and thermo dual-stimuli-responsive drug carrier based on mesoporous silica nanoparticles encapsulated in a copolymer-lipid bilayer. ACS Appl Mater Interfaces 2013;5:10895-903.

51. Wang S, Huang P, Chen X. Stimuli-Responsive Programmed Specific Targeting in Nanomedicine. ACS Nano 2016;10:2991-4.

52. Lopes JR, Santos G, Barata P, Oliveira R, Lopes CM. Physical and chemical stimuli-responsive drug delivery systems: targeted delivery and main routes of administration. Curr Pharm Des 2013;19:7169-84.

53. M Al-Abd A, A Al-Abbasi F, P Torchilin V. Intratumoral pharmacokinetics: challenges to nanobiomaterials. Current pharmaceutical design 2015;21:3208-14.

54. Choi I-K, Strauss R, Richter M, Yun C-O, Lieber A. Strategies to increase drug penetration in solid tumors. Frontiers in oncology 2013;3:193.

55. Thambi T, Deepagan V, Yoon HY, et al. Hypoxia-responsive polymeric nanoparticles for tumor-targeted drug delivery. Biomaterials 2014;35:1735-43.

56. Zhang R, Li Y, Zhang M, Tang Q, Zhang X. Hypoxia-responsive drug–drug conjugated nanoparticles for breast cancer synergistic therapy. RSC Advances 2016;6:30268-76.

57. Jabłońska-Trypuć A, Matejczyk M, Rosochacki S. Matrix metalloproteinases (MMPs), the main extracellular matrix (ECM) enzymes in collagen degradation, as a target for anticancer drugs. Journal of enzyme inhibition and medicinal chemistry 2016;31:177-83.

58. Levacheva I, Samsonova O, Tazina E, et al. Optimized thermosensitive liposomes for selective doxorubicin delivery: formulation development, quality analysis and bioactivity proof. Colloids Surf B Biointerfaces 2014;121:248-56.

59. Yang G, Liu J, Wu Y, Feng L, Liu Z. Near-infrared-light responsive nanoscale drug delivery systems for cancer treatment. Coordination Chemistry Reviews 2016;320:100-17.

60. Cheng R, Meng F, Deng C, Klok HA, Zhong Z. Dual and multi-stimuli responsive polymeric nanoparticles for programmed site-specific drug delivery. Biomaterials 2013;34:3647-57.

61. Torchilin VP. Multifunctional, stimuli-sensitive nanoparticulate systems for drug delivery. Nature reviews Drug discovery 2014;13:813.

62. Slowing II, Vivero-Escoto JL, Wu CW, Lin VS. Mesoporous silica nanoparticles as controlled release drug delivery and gene transfection carriers. Adv Drug Deliv Rev 2008;60:1278-88.

63. Chowdhury SM, Lee T, Willmann JK. Ultrasound-guided drug delivery in cancer. Ultrasonography 2017;36:171.

64. Yao J, Feng J, Chen J. External-stimuli responsive systems for cancer theranostic. Asian journal of pharmaceutical sciences 2016;11:585-95.

65. Zhao Y, Vivero-Escoto JL, Slowing II, Trewyn BG, Lin VS. Capped mesoporous silica nanoparticles as stimuli-responsive controlled release systems for intracellular drug/gene delivery. Expert opinion on drug delivery 2010;7:1013-29.

66. Li Z, Barnes JC, Bosoy A, Stoddart JF, Zink JI. Mesoporous silica nanoparticles in biomedical applications. Chemical Society Reviews 2012;41:2590-605.

67. Liu J, Stace-Naughton A, Jiang X, Brinker CJ. Porous nanoparticle supported lipid bilayers (protocells) as delivery vehicles. J Am Chem Soc 2009;131:1354-5.

68. Rahikkala A, Pereira SA, Figueiredo P, et al. Mesoporous Silica Nanoparticles for Targeted and Stimuli-Responsive Delivery of Chemotherapeutics: A Review. Advanced Biosystems 2018;2:1800020.

69. Wang Y, Liu G, Hu H, et al. Stable Encapsulated Air Nanobubbles in Water. Angew Chem Int Ed Engl 2015;54:14291-4.

70. Meinhardt M, Krebs R, Anders A, Heinrich U, Tronnier H. Wavelength-dependent penetration depths of ultraviolet radiation in human skin. Journal of biomedical optics 2008;13:044030.

71. Huang P, Lin J, Wang S, et al. Photosensitizer-conjugated silica-coated gold nanoclusters for fluorescence imaging-guided photodynamic therapy. Biomaterials 2013;34:4643-54.

72. De La Rica R, Aili D, Stevens MM. Enzyme-responsive nanoparticles for drug release and diagnostics. Advanced drug delivery reviews 2012;64:967-78.

73. Paris JL, Cabañas MV, Manzano M, Vallet-Regí M. Polymer-grafted mesoporous silica nanoparticles as ultrasound-responsive drug carriers. ACS nano 2015;9:11023-33.

74. Suzuki R, Oda Y, Utoguchi N, Maruyama K. Progress in the development of ultrasound-mediated gene delivery systems utilizing nano- and microbubbles. J Control Release 2011;149:36-41.

75. Zhang X, Li F, Guo S, et al. Biofunctionalized polymer-lipid supported mesoporous silica nanoparticles for release of chemotherapeutics in multidrug resistant cancer cells. Biomaterials 2014;35:3650-65.

76. Klibanov AL, Shevchenko TI, Raju BI, Seip R, Chin CT. Ultrasound-triggered release of materials entrapped in microbubble-liposome constructs: a tool for targeted drug delivery. J Control Release 2010;148:13-7.

77. Grüll H, Langereis S. Hyperthermia-triggered drug delivery from temperature-sensitive liposomes using MRI-guided high intensity focused ultrasound. Journal of Controlled Release 2012;161:317-27.

78. Escoffre J-M, Mannaris C, Geers B, et al. Doxorubicin liposome-loaded microbubbles for contrast imaging and ultrasound-triggered drug delivery. IEEE transactions on ultrasonics, ferroelectrics, and frequency control 2012;60:78-87.

79. van den Bijgaart RJ, Eikelenboom DC, Hoogenboom M, Fütterer JJ, den Brok MH, Adema GJ. Thermal and mechanical high-intensity focused ultrasound: perspectives on tumor ablation, immune effects and combination strategies. Cancer Immunology, Immunotherapy 2017;66:247-58.

80. Rapoport N, Nam KH, Gupta R, et al. Ultrasound-mediated tumor imaging and nanotherapy using drug loaded, block copolymer stabilized perfluorocarbon nanoemulsions. J Control Release 2011;153:4-15.

81. Paris JL, Mannaris C, Cabañas MV, et al. Ultrasound-mediated cavitation-enhanced extravasation of mesoporous silica nanoparticles for controlled-release drug delivery. Chemical Engineering Journal 2018;340:2-8.

82. Holland CK, Apfel RE. Thresholds for transient cavitation produced by pulsed ultrasound in a controlled nuclei environment. The Journal of the Acoustical Society of America 1990;88:2059-69.

83. Kwan JJ, Myers R, Coviello CM, et al. Ultrasound-propelled nanocups for drug delivery. Small 2015;11:5305-14.

84. Kwan J, Graham S, Myers R, Carlisle R, Stride E, Coussios C. Ultrasound-induced inertial cavitation from gas-stabilizing nanoparticles. Physical Review E 2015;92:023019.

85. Correas J, Quay S. EchoGen emulsion: a new ultrasound contrast agent based on phase shift colloids. Clinical radiology 1996;51:11.

86. Şen T, Tüfekçioğlu O, Koza Y. Mechanical index. Anatol J Cardiol 2015;15:334-6.

87. Correas J-M, Bridal L, Lesavre A, Méjean A, Claudon M, Hélénon O. Ultrasound contrast agents: properties, principles of action, tolerance, and artifacts. European radiology 2001;11:1316-28.

88. Sirsi SR, Borden MA. State-of-the-art materials for ultrasound-triggered drug delivery. Adv Drug Deliv Rev 2014;72:3-14.

89. Ter Haar G. Therapeutic ultrasound. European Journal of ultrasound 1999;9:3-9.

90. Baker KG, Robertson VJ, Duck FA. A review of therapeutic ultrasound: biophysical effects. Physical therapy 2001;81:1351-8.

91. Tang K, Niu C, Xu Y, et al. Phase-shifted paclitaxel-loaded multifunctional contrast agent for US/MR imaging and synergistic hyperthermal/chemotherapy of metastasis in lymph nodes. RSC advances 2018;8:5407-19.

92. Gieling RG, Parker CA, De Costa LA, et al. Inhibition of carbonic anhydrase activity modifies the toxicity of doxorubicin and melphalan in tumour cells in vitro. Journal of enzyme inhibition and medicinal chemistry 2013;28:360-9.

93. Lou Y, McDonald PC, Oloumi A, et al. Targeting tumor hypoxia: suppression of breast tumor growth and metastasis by novel carbonic anhydrase IX inhibitors. Cancer research 2011;71:3364-76.

94. Cosse J-P, Michiels C. Tumour hypoxia affects the responsiveness of cancer cells to chemotherapy and promotes cancer progression. Anti-Cancer Agents in Medicinal Chemistry (Formerly Current Medicinal Chemistry-Anti-Cancer Agents) 2008;8:790-7.

95. Pouysségur J, Dayan F, Mazure NM. Hypoxia signalling in cancer and approaches to enforce tumour regression. Nature 2006;441:437.

96. Pettersen EO, Ebbesen P, Gieling RG, et al. Targeting tumour hypoxia to prevent cancer metastasis. From biology, biosensing and technology to drug development: the METOXIA consortium. Journal of enzyme inhibition and medicinal chemistry 2015;30:689-721.

97. Pastorek J, Pastorekova S. Hypoxia-induced carbonic anhydrase IX as a target for cancer therapy: from biology to clinical use. Seminars in cancer biology; 2015: Elsevier. p. 52-64.

98. Mahon BP, Pinard MA, McKenna R. Targeting carbonic anhydrase IX activity and expression. Molecules 2015;20:2323-48.

99. Supuran CT. Carbonic anhydrases: novel therapeutic applications for inhibitors and activators. Nature reviews Drug discovery 2008;7:168.

100. Akocak S, Ilies MA. Next-generation primary sulfonamide carbonic anhydrase inhibitors. Targeting carbonic anhydrases 2014;1:35.

101. Neri D, Supuran CT. Interfering with pH regulation in tumours as a therapeutic strategy. Nature reviews Drug discovery 2011;10:767.

102. Muz B, de la Puente P, Azab F, Azab AK. The role of hypoxia in cancer progression, angiogenesis, metastasis, and resistance to therapy. Hypoxia 2015;3:83.

103. Shabana AM, Mondal UK, Alam MR, et al. pH-sensitive multiligand gold nanoplatform targeting carbonic anhydrase IX enhances the delivery of doxorubicin to hypoxic tumor spheroids and overcomes the hypoxia-induced chemoresistance. ACS applied materials & interfaces 2018;10:17792-808.

104. Airley RE, Loncaster J, Raleigh JA, et al. GLUT-1 and CAIX as intrinsic markers of hypoxia in carcinoma of the cervix: Relationship to pimonidazole binding. International journal of cancer 2003;104:85-91.

105. Hoskin P, Sibtain A, Daley F, Wilson G. GLUT1 and CAIX as intrinsic markers of hypoxia in bladder cancer: relationship with vascularity and proliferation as predictors of outcome of ARCON. British journal of cancer 2003;89:1290.

106. Sedlakova O, Svastova E, Takacova M, Kopacek J, Pastorek J, Pastorekova S. Carbonic anhydrase IX, a hypoxia-induced catalytic component of the pH regulating machinery in tumors. Frontiers in physiology 2014;4:400.

107. Wojtkowiak JW, Verduzco D, Schramm KJ, Gillies RJ. Drug resistance and cellular adaptation to tumor acidic pH microenvironment. Molecular pharmaceutics 2011;8:2032-8.

108. Mahoney BP, Raghunand N, Baggett B, Gillies RJ. Tumor acidity, ion trapping and chemotherapeutics: I. Acid pH affects the distribution of chemotherapeutic agents in vitro. Biochemical pharmacology 2003;66:1207-18.

109. Vukovic V, Tannock I. Influence of low pH on cytotoxicity of paclitaxel, mitoxantrone and topotecan. British journal of cancer 1997;75:1167.

110. Raghunand N, He X, Van Sluis R, et al. Enhancement of chemotherapy by manipulation of tumour pH. British journal of cancer 1999;80:1005.

111. Teicher B, Liu S, Liu J, Holden S, Herman T. A carbonic anhydrase inhibitor as a potential modulator of cancer therapies. Anticancer research 1993;13:1549-56.

112. Thiry A, Dogne J-M, Masereel B, Supuran CT. Targeting tumor-associated carbonic anhydrase IX in cancer therapy. Trends in pharmacological sciences 2006;27:566-73.

113. Endreas W, Brüßler J, Vornicescu D, Keusgen M, Bakowsky U, Steinmetzer T. Thrombin-Inhibiting Anticoagulant Liposomes: Development and Characterization. ChemMedChem 2016;11:340-9.

114. Marxer EE, Brüssler J, Becker A, et al. Development and characterization of new nanoscaled ultrasound active lipid dispersions as contrast agents. Eur J Pharm Biopharm 2011;77:430-7.

115. Yamada H, Urata C, Higashitamori S, Aoyama Y, Yamauchi Y, Kuroda K. Critical roles of cationic surfactants in the preparation of colloidal mesostructured silica nanoparticles: control of mesostructure, particle size, and dispersion. ACS Appl Mater Interfaces 2014;6:3491-500.

116. Yuan L, Tang Q, Yang D, Zhang JZ, Zhang F, Hu J. Preparation of pH-responsive mesoporous silica nanoparticles and their application in controlled drug delivery. The Journal of Physical Chemistry C 2011;115:9926-32.

117. Dengler EC, Liu J, Kerwin A, et al. Mesoporous silica-supported lipid bilayers (protocells) for DNA cargo delivery to the spinal cord. J Control Release 2013;168:209-24.

118. Gao Y, Chen Y, Ji X, et al. Controlled intracellular release of doxorubicin in multidrug-resistant cancer cells by tuning the shell-pore sizes of mesoporous silica nanoparticles. ACS nano 2011;5:9788-98.

119. Huang SL, Hamilton AJ, Pozharski E, et al. Physical correlates of the ultrasonic reflectivity of lipid dispersions suitable as diagnostic contrast agents. Ultrasound Med Biol 2002;28:339-48.

120. Schäfer J, Höbel S, Bakowsky U, Aigner A. Liposome–polyethylenimine complexes for enhanced DNA and siRNA delivery. Biomaterials 2010;31:6892-900.

121. Duse L, Agel MR, Pinnapireddy SR, et al. Photodynamic Therapy of Ovarian Carcinoma Cells with Curcumin-Loaded Biodegradable Polymeric Nanoparticles. Pharmaceutics 2019;11:282.

122. Yu C, Qian L, Uttamchandani M, Li L, Yao SQ. Single-vehicular delivery of antagomir and small molecules to inhibit miR-122 function in hepatocellular carcinoma cells by using “smart” mesoporous silica nanoparticles. Angewandte Chemie International Edition 2015;54:10574-8.

123. Rami M, Dubois L, Parvathaneni N-K, et al. Hypoxia-targeting carbonic anhydrase IX inhibitors by a new series of nitroimidazole-sulfonamides/sulfamides/sulfamates. Journal of medicinal chemistry 2013;56:8512-20.

124. Fuhrmann DC, Wittig I, Dröse S, Schmid T, Dehne N, Brüne B. Degradation of the mitochondrial complex I assembly factor TMEM126B under chronic hypoxia. Cellular and molecular life sciences 2018;75:3051-67.

125. Turker MZ, Ma K, Wiesner U. Bimodal Morphology Transition Pathway in the Synthesis of Ultrasmall Fluorescent Mesoporous Silica Nanoparticles. The Journal of Physical Chemistry C 2019;123:9582-9.

126. Pourjavadi A, Tehrani ZM. Mesoporous silica nanoparticles with bilayer coating of poly (acrylic acid-co-itaconic acid) and human serum albumin (HSA): A pH-sensitive carrier for gemcitabine delivery. Materials Science and Engineering: C 2016;61:782-90.

127. Manzano M, Vallet-Regí M. Mesoporous Silica Nanoparticles for Drug Delivery. Advanced Functional Materials 2019:1902634.

128. Zulfiqar U, Subhani T, Husain SW. Synthesis and characterization of silica nanoparticles from clay. Journal of Asian Ceramic Societies 2016;4:91-6.

129. Jayalath S, Larsen SC, Grassian VH. Surface adsorption of Nordic aquatic fulvic acid on amine-functionalized and non-functionalized mesoporous silica nanoparticles. Environmental Science: Nano 2018;5:2162-71.

130. Corne G, Lenoble D, Thomann J-S. Negatively Charged Self-Assembling Supported Lipid Bilayer On Mesoporous Silica Nanoparticles, Method Of Synthesis And Use As A Nanovector. Google Patents; 2018.

131. Miguel-Sancho N, Martinez G, Sebastian V, et al. Pumping Metallic Nanoparticles with Spatial Precision within Magnetic Mesoporous Platforms: 3D Characterization and Catalytic Application. ACS applied materials & interfaces 2017;9:41529-36.

132. Chang D, Gao Y, Wang L, et al. Polydopamine-based surface modification of mesoporous silica nanoparticles as pH-sensitive drug delivery vehicles for cancer therapy. Journal of colloid and interface science 2016;463:279-87.

133. Sun J-H, Zhang W, Zhang D-Y, et al. Multifunctional mesoporous silica nanoparticles as efficient transporters of doxorubicin and chlorin e6 for chemo-photodynamic combinatorial cancer therapy. Journal of biomaterials applications 2018;32:1253-64.

134. Meiser VC, Kreysa H, Guntinas-Lichius O, Volk GF. Comparison of in-plane and out-of-plane needle insertion with vs. without needle guidance. European Archives of Oto-Rhino-Laryngology 2016;273:2697-705.

135. Rahmani S, Durand J-O, Charnay C, et al. Synthesis of mesoporous silica nanoparticles and nanorods: Application to doxorubicin delivery. Solid State Sciences 2017;68:25-31.

136. Zhang J, Weng L, Su X, et al. Cisplatin and doxorubicin high-loaded nanodrug based on biocompatible thioether-and ethane-bridged hollow mesoporous organosilica nanoparticles. Journal of colloid and interface science 2018;513:214-21.

137. Federici C, Lugini L, Marino ML, et al. Lansoprazole and carbonic anhydrase IX inhibitors sinergize against human melanoma cells. Journal of enzyme inhibition and medicinal chemistry 2016;31:119-25.

138. Rahman IA, Padavettan V. Synthesis of silica nanoparticles by sol-gel: size-dependent properties, surface modification, and applications in silica-polymer nanocomposites—a review. Journal of Nanomaterials 2012;2012:8.

139. Wu S-H, Mou C-Y, Lin H-P. Synthesis of mesoporous silica nanoparticles. Chemical Society Reviews 2013;42:3862-75.

140. Qiao Z-A, Zhang L, Guo M, Liu Y, Huo Q. Synthesis of mesoporous silica nanoparticles via controlled hydrolysis and condensation of silicon alkoxide. Chemistry of Materials 2009;21:3823-9.

141. Shinde P, Gupta SS, Singh B, Polshettiwar V, Prasad BL. Amphi-functional mesoporous silica nanoparticles for dye separation. Journal of Materials Chemistry A 2017;5:14914-21.

142. Moghaddam SPH, Yazdimamaghani M, Ghandehari H. Glutathione-sensitive hollow mesoporous silica nanoparticles for controlled drug delivery. Journal of controlled release 2018;282:62-75.

143. Quan G, Pan X, Wang Z, et al. Lactosaminated mesoporous silica nanoparticles for asialoglycoprotein receptor targeted anticancer drug delivery. Journal of nanobiotechnology 2015;13:7.

144. Campbell RA, Parker SR, Day JP, Bain CD. External reflection FTIR spectroscopy of the cationic surfactant hexadecyltrimethylammonium bromide (CTAB) on an overflowing cylinder. Langmuir 2004;20:8740-53.

145. Sanaeishoar H, Sabbaghan M, Mohave F. Synthesis and characterization of micro-mesoporous MCM-41 using various ionic liquids as co-templates. Microporous and Mesoporous Materials 2015;217:219-24.

146. Huang X, Li L, Liu T, et al. The shape effect of mesoporous silica nanoparticles on biodistribution, clearance, and biocompatibility in vivo. ACS nano 2011;5:5390-9.

147. Xu P, Guo S, Yu H, Li X. Mesoporous silica nanoparticles (MSNs) for detoxification of hazardous organophorous chemicals. Small 2014;10:2404-12.

148. Pawlikowska-Pawlęga B, Misiak LE, Zarzyka B, Paduch R, Gawron A, Gruszecki WI. FTIR, 1H NMR and EPR spectroscopy studies on the interaction of flavone apigenin with dipalmitoylphosphatidylcholine liposomes. Biochimica et Biophysica Acta (BBA)-Biomembranes 2013;1828:518-27.

149. Mudakavi RJ, Raichur AM, Chakravortty D. Lipid coated mesoporous silica nanoparticles as an oral delivery system for targeting and treatment of intravacuolar Salmonella infections. RSC Advances 2014;4:61160-6.

150. Butler KS, Durfee PN, Theron C, Ashley CE, Carnes EC, Brinker CJ. Protocells: modular mesoporous silica nanoparticle-supported lipid bilayers for drug delivery. Small 2016;12:2173-85.

151. Zhang Y, Zhi Z, Jiang T, Zhang J, Wang Z, Wang S. Spherical mesoporous silica nanoparticles for loading and release of the poorly water-soluble drug telmisartan. J Control Release 2010;145:257-63.

152. Shen J, He Q, Gao Y, Shi J, Li Y. Mesoporous silica nanoparticles loading doxorubicin reverse multidrug resistance: performance and mechanism. Nanoscale 2011;3:4314-22.

153. Peng S, Deng Y, Li W, Chen J, Liu H, Chen Y. Aminated mesoporous silica nanoparticles for the removal of low-concentration malodorous aldehyde gases. Environmental Science: Nano 2018;5:2663-71.

154. Albayati TM, Salih IK, Alazzawi HF. Synthesis and characterization of a modified surface of SBA-15 mesoporous silica for a chloramphenicol drug delivery system. Heliyon 2019;5:e02539.

155. Kai Wana G-FL, Ming-Yao Liua, Li Dua, Zhen-Xing Lianga, *, Panagiotis Tsiakaras. Nitrogen doped ordered mesoporous carbon: synthesis and active sites for electrocatalysis of oxygen reduction reaction 2015:566-71.

156. Pasternak MM, Strohm EM, Berndl ES, Kolios MC. Properties of cells through life and death - an acoustic microscopy investigation. Cell Cycle 2015;14:2891-8.

157. Yang Y, Song W, Wang A, Zhu P, Fei J, Li J. Lipid coated mesoporous silica nanoparticles as photosensitive drug carriers. Phys Chem Chem Phys 2010;12:4418-22.

158. Kastner E, Verma V, Lowry D, Perrie Y. Microfluidic-controlled manufacture of liposomes for the solubilisation of a poorly water soluble drug. International journal of pharmaceutics 2015;485:122-30.

159. Moeller K, Kobler J, Bein T. Colloidal suspensions of nanometer-sized mesoporous silica. Advanced Functional Materials 2007;17:605-12.

160. Baghdan E, Pinnapireddy SR, Strehlow B, Engelhardt KH, Schäfer J, Bakowsky U. Lipid coated chitosan-DNA nanoparticles for enhanced gene delivery. International journal of pharmaceutics 2018;535:473-9.

161. Dubois L, Douma K, Supuran CT, et al. Imaging the hypoxia surrogate marker CA IX requires expression and catalytic activity for binding fluorescent sulfonamide inhibitors. Radiotherapy and oncology 2007;83:367-73.

162. Gieling RG, Babur M, Mamnani L, et al. Antimetastatic effect of sulfamate carbonic anhydrase IX inhibitors in breast carcinoma xenografts. Journal of medicinal chemistry 2012;55:5591-600.

163. Ledaki I, McIntyre A, Wigfield S, et al. Carbonic anhydrase IX induction defines a heterogeneous cancer cell response to hypoxia and mediates stem cell-like properties and sensitivity to HDAC inhibition. Oncotarget 2015;6:19413.

164. Supuran CT. Carbonic anhydrase inhibition and the management of hypoxic tumors. Metabolites 2017;7:48.

165. Alfarouk KO, Stock C-M, Taylor S, et al. Resistance to cancer chemotherapy: failure in drug response from ADME to P-gp. Cancer cell international 2015;15:71.

166. Trédan O, Galmarini CM, Patel K, Tannock IF. Drug resistance and the solid tumor microenvironment. Journal of the National Cancer Institute 2007;99:1441-54.

167. Song X, Liu X, Chi W, et al. Hypoxia-induced resistance to cisplatin and doxorubicin in non-small cell lung cancer is inhibited by silencing of HIF-1α gene. Cancer chemotherapy and pharmacology 2006;58:776-84.

168. Sanna K, Rofstad EK. Hypoxia-induced resistance to doxorubicin and methotrexate in human melanoma cell lines in vitro. International journal of cancer 1994;58:258-62.

169. Li X, Chen D, Le C, et al. Novel mucus-penetrating liposomes as a potential oral drug delivery system: preparation, in vitro characterization, and enhanced cellular uptake. International journal of nanomedicine 2011;6:3151.

170. Janoniene A, Liu Z, Baranauskiene L, et al. A versatile carbonic anhydrase IX targeting ligand-functionalized porous silicon nanoplatform for dual hypoxia cancer therapy and imaging. ACS applied materials & interfaces 2017;9:13976-87.

5.3 Publications

- **Muhammad Umair Amin**, Sajid Ali, Imran Tariq, Muhammad Yasir Ali, Shashank Reddy Pinnapreddy, Christian Wölk, Richard D. Harvey, Gerd Hause, Jana Brüßler, Udo Bakowsky; Ultrasound-Responsive Smart Drug Delivery System of Lipid Coated Mesoporous Silica Nanoparticles. Submitted to ACS Nano

- **Muhammad Umair Amin**, Sajid Ali, Muhammad Yasir Ali, Imran Tariq, Shashank Reddy Pinnapreddy, Udo Bakowsky, and Jana Brüßler; Lipid Coated Mesoporous Silica Nanoparticles for Enhanced Delivery and Cellular Uptake of Doxorubicin. Submitted to International edition of Angewandte Chemie

- **Muhammad Umair Amin**, Sajid Ali, Dominik C. Fuhrmann, Imran Tariq, Muhammad Yasir Ali, Jana Brüßler, Bernhard Brüne, Udo Bakowsky; Lipid Supported Mesoporous Silica Nanoparticles for Co-delivery of Carbonic Anhydrase IX Inhibitor and Doxorubicin to Address Chemoresistance in Hypoxia. Manuscript in preparation

- Sajid Ali, **Muhammad Umair Amin**, Muhammad Yasir Ali, Imran Tariq, Shashank Reddy Pinnapireddy, Lili Duse, Nathalie Goergen, Christian Wölk, Gerd Hause, Jarmila Jedelská, Jens Schäfer, and Udo Bakowsky; Wavelength-dependent Photo-cytotoxicity to ovarian carcinoma using temoporfin loaded tetraether liposomes as efficient drug delivery system. Submitted to European journal of pharmaceutics and biopharmaceutics

- Sajid Ali, **Muhammad Umair Amin**, Imran Tariq, Farhan Sohail, Muhammad Yasir Ali, Shashank Reddy Pinnapireddy, Lili Duse, Jarmila Jedelská, Jens Schäfer, and Udo Bakowsky; Lipid enveloped biodegradable nanoparticles for synergistic delivery of temoporfin and pirarubicin to ovarian carcinoma cells; *in-vitro* and *in-vivo* evaluations. Manuscript in preparation

- Sajid Ali, **Muhammad Umair Amin**, Imran Tariq, Farhan Sohail, Muhammad Yasir Ali, Shashank Reddy Pinnapireddy, Jarmila Jedelská, Jens Schäfer, and Udo Bakowsky; Temoporfin loaded biodegradable polymeric nanoparticles for photodynamic therapy of ovarian carcinoma cells; *in-vitro* and *in-vivo* evaluations. Manuscript in preparation

- Muhammad Yasir Ali, Imran Tariq, Muhammad Farhan Sohail, **Muhammad Umair Amin,** Sajid Ali, Shashank Reddy Pinnapireddy, Asad Ali, Jens Schäfer and Udo Bakowsky; Selective anti-ErbB3 aptamer modified sorafenib microparticles: *In vitro* and *in vivo* toxicity assessment. European journal of pharmaceutics and biopharmaceutics, 145 (2019) 42- 53.

- Imran Tariq, Shashank Reddy Pinnapireddy, Lili Duse, Muhammad Yasir Ali, Sajid Ali, **Muhammad Umair Amin**, Nathalie Goergen, Jarmila Jedelská, Jens Schäfer and Udo Bakowsky; Lipodendriplexes: A promising nanocarrier for enhanced gene delivery with minimal cytotoxicity, European journal of pharmaceutics and biopharmaceutics, 135 (2019) 72- 82.

- Muhammad Yasir Ali, Imran Tariq, Sajid Ali, **Muhammad Umair Amin**, Shashank Reddy Pinnapireddy, Lili Duse, Konrad Engelhardt, Jens Schäfer and Udo Bakowsky; Targeted ErbB3 cancer therapy: A synergistic approach to effectively combat cancer. Submitted to International Journal of Pharmaceutics

- Imran Tariq, Muhammad Yasir Ali, Muhammad Farhan Sohail, **Muhammad Umair Amin**, Sajid Ali, Nadeem Irfan Bukhari, Abida Raza, Shashank Reddy Pinnapireddy,Jens Schäfer and Udo Bakowsky; Lipodendriplexes mediated enhanced systemic delivery and gene expression. Manuscript in preparation.

- Imran Tariq, Muhammad Yasir Ali, Harshavardhan Janga, Sajid Ali, **Muhammad Umair Amin**, Ghazala Ambreen, Uzma Ali, Shashank Reddy Pinnapireddy, Jens Schäfer and Udo Bakowsky; Downregulation of MDR 1 gene contributes to tyrosine kinase inhibitor induced apoptosis and inhibition in tumor metastasis: A gravity to space investigation. Manuscript in preparation

- **Muhammad Yasir Ali**, Imran Tariq, Sajid Ali, Muhammad Umair Amin, Shashank Reddy Pinnapireddy, Lili Duse, Jens Schäfer and Udo Bakowsky; Selective sorafenib-loaded liposomal chemotherapy: An extensive cytotoxicity assessment; Manuscript in preparation.

5.4 Oral and Poster Presentations

- Lipid coated mesoporous silica nanoparticles for enhanced delivery and cellular uptake of doxorubicin – *Oral presentation*
  Muhammad Umair Amin; 12th world drug delivery summit, 24-26 Sep 2018, Chicago, USA

- Design of mesoporous silica nanoparticles as novel drug carrier systems – *Oral presentation (Poster flash)*
  Muhammad Umair Amin; 22nd Annual Meeting of Controlled Release Society, Local Chapter Germany, 01-02 March 2018, Halle, Germany

- Doxorubicin loaded lipid coated mesoporous silica nanoparticles as advance drug delivery system – *poster presentation*
  Muhammad Umair Amin, Sajid Ali, Imran Tariq, Muhammad Yasir Ali, Jana, Brüßler, Udo, Bakowsky; 23rd Annual Meeting of Controlled Release Society, Local Chapter Germany, 07-08 March 2019, Leipzig, Germany

- Design of mesoporous silica nanoparticles as novel drug carrier systems – *Poster presentation* - ***Best Poster Award***
  Muhammad Umair Amin; 22nd Annual Meeting of Controlled Release Society, Local Chapter Germany, 01-02 March 2018, Halle, Germany

5.5 Curriculum Vitae

Personal Information

Name	Muhammad Umair Amin
Date of Birth	21-01-1984
Place of Birth	Gujranwala, Pakistan
Gender	Male
Nationality	Pakistani

Working Experience

March 2013 - To date	Lecturer Department of Pharmacy The University of Lahore, Pakistan
Sep 2013 - May 2014	Lecturer (Visiting Faculty) Riphah Institute of Pharmaceutical Sciences Riphah International University Lahore, Pakistan
Dec 2010 - March 2013	Pharmacist City Pharmacy, Gujranwala, Pakistan
Sep 2009 - Nov 2010	Sales and Marketing Novartis Pharma, Lahore, Pakistan

Education and Training

March 2016-To date	PhD Dep. of Pharmaceutics and Biopharmaceutics University of Marburg, Marburg, Germany
May 2011 - June 2013	Mphil (Pharmaceutics) University College of Pharmacy The University of Punjab, Lahore, Pakistan
March 2004 - July 2009	Pharm-D (Pharmacy) University College of Pharmacy The University of Punjab, Lahore, Pakistan
May 2000 - Aug 2003	Intermediate (Pre-Medical) National Science College, Gujranwala, Pakistan Board of Intermediate and Secondary Education, Gujranwala, Pakistan

March 1993 - Aug 2000	Matric JDIHS, Gujranwala, Pakistan Board of Intermediate and Secondary Education, Gujranwala, Pakistan